The Messenger

No. 149 – September 2012

Progress on SPHERE
Calibrating HARPS with a laser frequency comb
Disentangling early-type galaxies
Planning mm-VLBI with ALMA

50 YEARS 1962–2012

ESO

Astronomical Spectrograph Calibration at the Exo-Earth Detection Limit

Gaspare Lo Curto[1]
Luca Pasquini[1]
Antonio Manescau[1]
Ronald Holzwarth[2,3]
Tilo Steinmetz[3]
Tobias Wilken[3]
Rafael Probst[2]
Thomas Udem[2]
Theodor W. Hänsch[2]
Jonay González Hernández[4,5]
Massimiliano Esposito[4,5]
Rafael Rebolo[4,5]
Bruno Canto Martins[6]
Jose Renan de Medeiros[6]

[1] ESO
[2] Max-Planck-Institut für Quantenoptik, Garching, Germany
[3] Menlo Systems GmbH, Martinsried, Germany
[4] Instituto de Astrofisica de Canarias, La Laguna, Spain
[5] Departamento de Astrofísica, Universidad de La Laguna, Tenerife, Spain
[6] Universidade Federal do Rio Grande de Norte, Natal, Brazil

Following the development of the laser frequency comb which led to the 2005 Nobel Prize in Physics, we began investigating the possibility of using this novel technology for precise and accurate spectrograph calibration. A programme was begun, aimed at demonstrating the capabilities of laser frequency combs (LFC) when coupled to an astronomical spectrograph. In the last three years we have tested an LFC connected to HARPS at the 3.6-metre telescope in La Silla, the most precise spectrograph available. Here we show the very promising results obtained so far, and outline future activities, including the provision of an LFC system for routine operation with HARPS, to be offered to the community in the near future.

The most widely used wavelength reference in astronomical spectroscopy, the thorium–argon (Th-Ar) lamp, can achieve a precision on the determination of individual line positions of several tens of metres per second (m/s). The uncertainty in the wavelength of a spectral line can either be expressed as an absolute wavelength (such as in Å), as a fractional wavelength, e.g. 10^{-7}, or by scaling by the speed of light to express it in m/s. The limitation on Th-Ar wavelength precision is due not only to the measurement process (Palmer Engleman, 1983), but also to the production method (contamination) and aging of the lamps. Even when averaging over a wide spectrum with say, 10 000 lines, measurements are limited to an overall precision of 10^{-9} at best (the achievable precision is furthermore degraded by line blending, and non-uniform density of the Th lines across the spectrum).

This precision in the measurement of the positions of spectral lines is not sufficient for various compelling science cases:

- the measurement of the variation of the fundamental constants, which requires a precision at least as good as the precision with which the constants are determined; for the best known (the proton to electron mass ratio and the fine structure constant) this is ~ 3–4 × 10^{-10} (Beringer et al., 2012);
- the amplitude of the recoil motion imprinted by the Earth on the Sun is ~ 9 cm/s. The radial velocity detection of an extrasolar planet with the mass of the Earth in a 1 AU orbit around its solar-type star therefore requires a measurement precision of about 3 cm/s, or 10^{-10};
- the direct measurement of the expansion rate of the Universe, which can constrain the cosmological parameters that define the metric of the theory of gravity, requires a measurement precision at the level of cm/s (10^{-10}) for over ten years (Liske et al., 2008).

The new class of giant telescopes with greatly increased light-collecting power will naturally ease the photon noise limitation to high precision spectroscopy by a factor of five to ten. A new calibration source is therefore needed, which enables these science cases and capitalises on the great opportunity that giant telescopes open up for high precision spectroscopy. The ideal calibration source would be at least ten times more precise than Th-Ar lamps allow and would have many unblended lines, with approximately the same intensity and equally spaced across the spectrum. The obvious choice is the laser frequency comb.

For the measurement of frequencies, LFCs represent the ultimate level of precision, as they are locked to the energy level of a well-known atomic transition via an atomic clock. They are the most precise time-keeping devices, and the unit of measurement of time in the International System (SI), the second, is defined by the caesium transition via a caesium atomic clock. LFCs have many applications, from metrology and precise time-keeping to laboratory atomic and molecular spectroscopy. Now the period is beginning when LFCs will “look at the sky”.

The demonstrator programme

In 2006 ESO approached the group of Prof. Theodor Hänsch at the Max Planck Institute for Quantum Optics (MPQ), to study the possibility of using an LFC for the calibration of high-resolution astronomical spectrographs. Due to its unsurpassed stability, HARPS at the 3.6-metre telescope in La Silla provided the best candidate to validate the performance of this technique (Mayor et al., 2003). A fruitful collaboration was initiated between ESO, MPQ and Menlo GmbH, a spin-off company from MPQ which markets LFCs, with the goal of demonstrating the feasibility of operating an LFC to calibrate an astronomical spectrograph, thus opening up a new horizon for the current and next generation high-precision, high-resolution spectrographs.

The demonstrator programme started in 2007 (Araujo-Hauck et al., 2007) and concluded in 2011. In this period a prototype LFC dedicated to astronomy (or astro-comb) was developed and refined. The astro-comb was tested in the laboratory; in the infrared (IR) regime on a telescope for the first time (Steinmetz, 2008); to validate technical solutions; and in four campaigns in the visible, with HARPS at the 3.6-metre telescope in La Silla, to test the global performance (Lo Curto et al., 2010; Wilken et al., 2010; Wilken et al., 2012).

An LFC consists of thousands of equally spaced frequencies over a bandwidth of several THz. It is based on the properties of femtosecond (fs) mode-locked lasers. The frequency difference between two neighbouring lines corresponds to

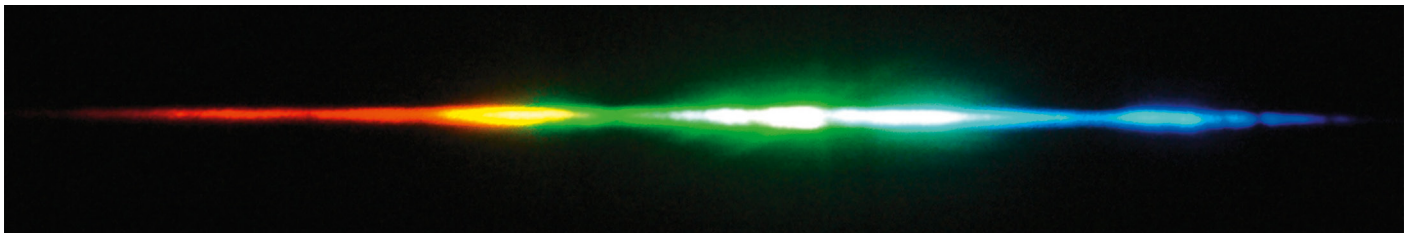

Figure 1. The spectrum of the LFC dispersed by a low-resolution grating and projected on a wall. The individual lines are not resolved and only the continuum is visible: its spectral structure is due to the spectral broadening stage and can be flattened out by a spatial light modulator (SLM).

the repetition frequency (f_{rep}) of the pulsed laser and is therefore constant across the comb spectrum. The entire LFC spectrum can be described by the simple equation $f = f_{off} + n \cdot f_{rep}$ where f_{rep} is the repetition frequency, i.e. the distance in frequency between two adjacent lines, and f_{off} is the "offset frequency" that can be interpreted as a "zero point"; n is a large integer which projects the radio frequencies f_{off} and f_{rep} into the visible domain. Since all frequencies used in the system are radio frequencies, they can be stabilised to an atomic clock using well-established electronic phase-locking techniques. In this way, each optical frequency obtains the accuracy and long-term stability of the atomic clock.

An LFC acts like a gear, transferring the precision of atomic clocks from the microwave regime to the optical. LFCs are the ideal calibrator for astronomical spectrographs if they can cover the spectral bandwidth of the spectrograph with a sufficiently flat spectrum and if their line spacing is adapted to the spectrograph's resolution. While there are several proposed frequency comb systems that will match the criteria for a spectrograph calibrator, our choice has been to use a fibre-laser-based LFC. Fibre lasers are technically mature and turn-key systems that are commercially available. When using Yb-fibre lasers, high-power amplifiers can be employed and the second harmonic of the central wavelength (1030 nm) is in the centre of the desired wavelength range for a spectrograph in the visible. However, the required fibre length limits the round-trip time in the oscillator, and thus the line spacing of the laser (its pulse repetition rate) is currently limited to roughly below 1 GHz.

Although an LFC based on fibre lasers is essentially an off-the-shelf product, its adaptation for use in an instrument like HARPS requires major developments. The basic turn-key LFC systems available on the market today deliver a comb of lines centred at 1025–1050 nm, with a repetition frequency of 250 MHz and generally cover only few nanometres in wavelength. Resolving spectral lines 250 MHz apart in the visible range requires a spectral resolution of more than six million, which is not practical for the typical use of an astronomical spectrograph. An LFC with such a line spacing would appear as a continuum source to instruments such as HARPS or UVES (see Figure 1).

New developments are needed to operate an LFC on an astronomical spectrograph in the visible with a spectral resolution of ~ 10^5:

1) increase the repetition frequency to ~ 18 GHz;
2) double the frequency of the spectrum to have it centred in the visible at ~ 520 nm;
3) broaden the spectrum to increase wavelength coverage.

These are the three steps where most of the efforts of the programme have been focussed.

Towards an LFC for astronomy

High finesse Fabry-Pérot cavities (FPCs) acting as periodic, high-resolution spectral filters can be used to increase the line spacing by transmitting only modes (lines) that are phase-shifted by an integer number of wavelengths and suppressing the intermediate ones. After this first step, the spectrum of the LFC undergoes two nonlinear processes: one for frequency doubling and one for spectral broadening. The challenge is to combine the frequency conversion and the high pulse repetition rate. A high repetition rate corresponds to low pulse energies that are detrimental to nonlinear conversion processes. The approach to overcome this dilemma employs two key components. First, a comb system based on an Yb-fibre laser enables the use of Yb-fibre high-power amplifiers to reduce the problem of low pulse energies. Second, when using specially designed photonic crystal fibres (PCFs), relatively low pulse energies are sufficient to obtain spectral broadening.

Another challenge comes at the FPC filtering stage and arises from the fact that the nonlinear processes (interactions between photons) in the PCF can amplify spectral lines that were intended to be suppressed. We saw this effect during our first test run in La Silla. The solution was to employ more FPC cavities, essentially one of them replicating the suppression of the unwanted modes, and with a higher finesse. Finally in our system we used three FPCs in series to guarantee a sufficient suppression of the intermediate lines. A series of four FPCs was also tested, but no improvements were noticed from the fourth cavity. The line spacing is increased to 18 GHz, which is well resolved by HARPS (the instrument has an intrinsic resolution of ~ 5 GHz).

After the last FPC a fibre amplifier is employed that can deliver up to 10 W to facilitate the subsequent nonlinear processes. The spectral bandwidth after these amplifiers suffers from re-absorption and gain narrowing. The initial 50 nm wide spectrum reduces to a 3 dB bandwidth of only 20 nm after the high-power amplifier. After re-amplification, the frequency of the light is doubled by a second harmonic generator (SHG), and finally injected into the PCF for spectral broadening. The broadening is a highly nonlinear process (four-wave mixing), and so the intensity distribution in the final spectrum can vary. For this reason, in the last test run, a spatial light modulator

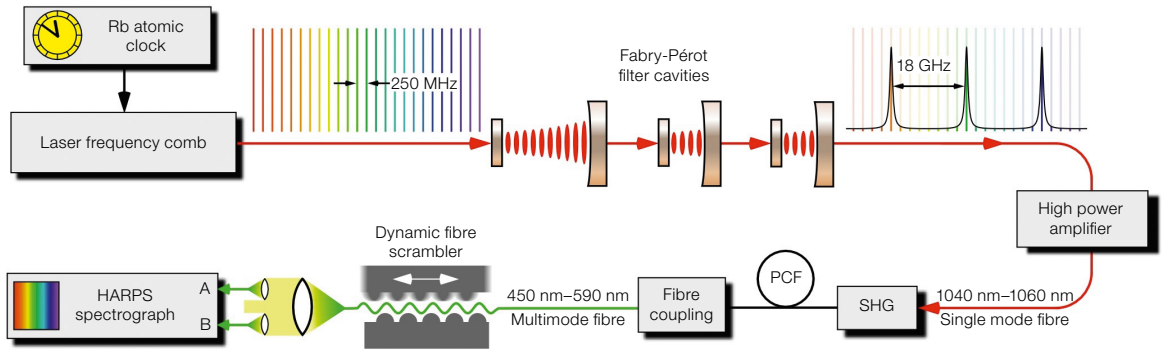

Figure 2. Representation of the HARPS-LFC setup as described in the text. The SLM after the PCF is missing in the figure because it was not always used during data acquisition (see text for details). From Wilken et al., 2012.

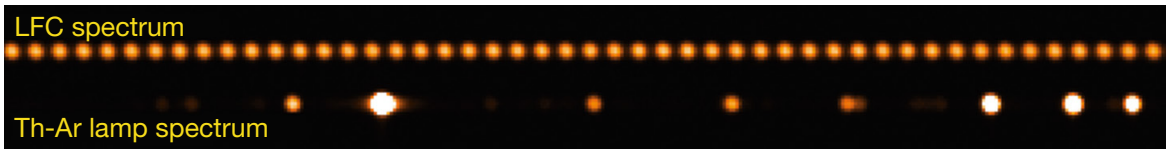

Figure 3. A comparison of a portion of one order of the LFC and the Th-Ar lamp as seen by HARPS.

(SLM) was sometimes inserted as a last stage of the LFC, yielding a flat spectrum envelope at the cost of an attenuation of 12 dB.

Light from the LFC is finally coupled to a multimode fibre that comprises a dynamic mode scrambler. Multimode fibres are mandatory, because starlight cannot yet be coupled efficiently to single mode fibres. The scrambler serves to reduce multi-pass interference effects and the sensitivity to the light injection by averaging over a large number of fibre modes. The light is then coupled, within the HARPS calibration unit, to the two HARPS calibration fibres, which simultaneously illuminate the telescope focal plane, injecting light into the "object" fibre and the "simultaneous reference" fibre. The system is sketched in Figure 2.

Characterising the LFC on HARPS

Some of the advantages of LFCs over Th-Ar lamps are immediately noticeable from Figure 3, where a portion of the order of the two sources is compared. The LFC has a very dense, non-blending line pattern (~ 350 lines per order), which is also very uniform in intensity. In contrast the Th-Ar lamp has fewer lines (~ 100 lines per order), some of which are saturated. The spectra in Figure 3 were obtained using both the object and the simultaneous reference fibres of HARPS, and by illuminating the spectrograph simultaneously with both sources.

The wavelength range of the LFC for HARPS now covers ~ 100 nm, and work is in progress to extend this to at least 200 nm. Owing to the high line density of the LFC spectra, we are now able to better characterise the detectors. For example, Figure 4 shows the effect of the stitching pattern of the CCD fabrication on the wavelength calibration. Every 512 pixels the wavelength solution encounters a discontinuity as the intra-pixel distance is slightly different along the stitching borders. The effect reaches over 60 m/s, well above the attainable stability of HARPS. Although the effect is clearly visible when using the LFC calibration, it goes unnoticed when Th-Ar calibration is used, due to the low number of lines present in the orders and their highly non-uniform distribution. This effect clearly underlines the need for a detailed characterisation of the detector when the highest radial velocity precision and accuracy are aimed for. Such in-depth characterisation can be performed with the use of the LFC, by modifying the parameters that define the spectrum, i.e. the offset frequency and the repetition frequency, effectively scanning the detector and probing all the pixels which lie within the spectral profile.

The characterisation of the stability of the LFC system when coupled to HARPS has been clearly the first priority during the tests. However with only one comb available we have to rely on its intrinsic stability as verified up to now on very many laser physics experiments. We are considering a test with two independent LFCs feeding light to HARPS in the future. Currently we are focussing instead on effects due to mode (mis)matching, coupling and injection. To characterise these, we inject light into both HARPS calibration fibres and illuminate both the object and the simultaneous reference orders (from here onward referred to as channels) in the CCD. We then monitor the relative drifts measured between the two channels, with the assumption that instrumental drifts are subtracted out when looking at the relative variations between them (an assumption which is the basis of the simultaneous reference method).

In Figure 5 the measured drift of all the spectra collected in the two test runs of November 2010 and January 2011 is shown. During the test run we stressed the system in many ways, well beyond what could be considered "standard operation": we completely disassembled the FPC chain and reassembled it again in January to test a fourth FPC; changed several PCFs; inserted and removed neutral density filters; misaligned the injection fibres; introduced polarimetric plates, integrating spheres, etc.... We also switched off the CCD cooling for few minutes. Despite this, each individual series of data shows a relative drift consistent with, or very close to, the estimated photon noise, and the relative drift between the two channels never exceeded 1 m/s, and the root mean square (RMS) of the relative drift was

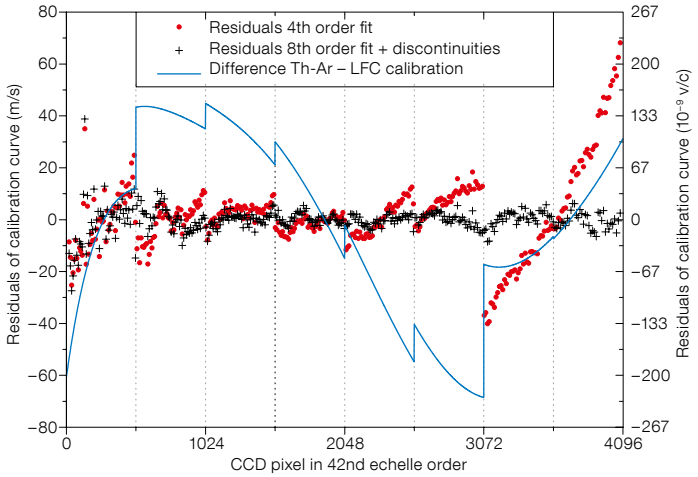

Figure 4. Evidence of the CCD stitching pattern as revealed by the LFC wavelength calibration. Due to the paucity of spectral lines, the Th-Ar calibration was unable to identify this effect. From Wilken et al., 2010.

~ 34 cm/s over the whole run. When the CCD cooling was stopped, and then restarted, we could measure a drift of 13 m/s on the individual channels, but the relative drift between channels was below 40 cm/s peak to valley, an indication that the method of simultaneous reference in HARPS is capable of reducing systematic effects by more than a factor of 30, at least when they originate from the detectors.

Two large deviations in the relative drift between the two channels are seen in the data (Figure 5). These correspond to the series of spectra acquired when an integrating sphere, with a diameter of 5 cm, was used to couple the LFC outgoing fibre to the HARPS calibration fibres. We do not yet understand the cause of this drift, but speculate it could be related to the strong intensity variation (close to two orders of magnitude) or to a different occupation of the modes after the transition through the integrating sphere. Possible alternative explanations point towards detector effects that could distort the instrument profile depending on light intensity, or data reduction effects, also related to a change of the instrument profile for very faint signals. Work is still being done to understand these measurements, but it must be stressed that this is well beyond what happens under standard operating conditions.

When looking at sequences of data during which we did not intervene to modify the system (orange and violet vertical stripes in Figure 5), the stability was seen to be superb. As in almost all series, the RMS of the relative drift between the two channels is consistent with the photon noise of ~ 7 cm/s. In order to decrease the contribution of the photon noise, we added an increasing number of exposures and computed the Allan (or two-sample) deviation (Figure 6). This estimator is capable of distinguishing statistical noise processes from systematics, e.g., drifts. In Figure 6 we see that the orange and violet points, corresponding to two quiet LFC series, follow well the curve of the estimated (not fitted) photon noise, up to a level of ~ 2.5 cm/s, where the data flatten. At this point systematics limit the stability of the system. Short-term (~ 2 hours) repeatability of the LFC+HARPS system is at the level of 2.5 cm/s. Although we cannot say the same for the long-term stability due to the various drifts exemplified in Figure 5, we stress once more that these instabilities in the long term were most likely generated from our interventions in the system. In Figure 6 we display a similar measurement for Th-Ar calibration, and the limitation of Th-Ar lamps with respect to the LFC is clearly visible.

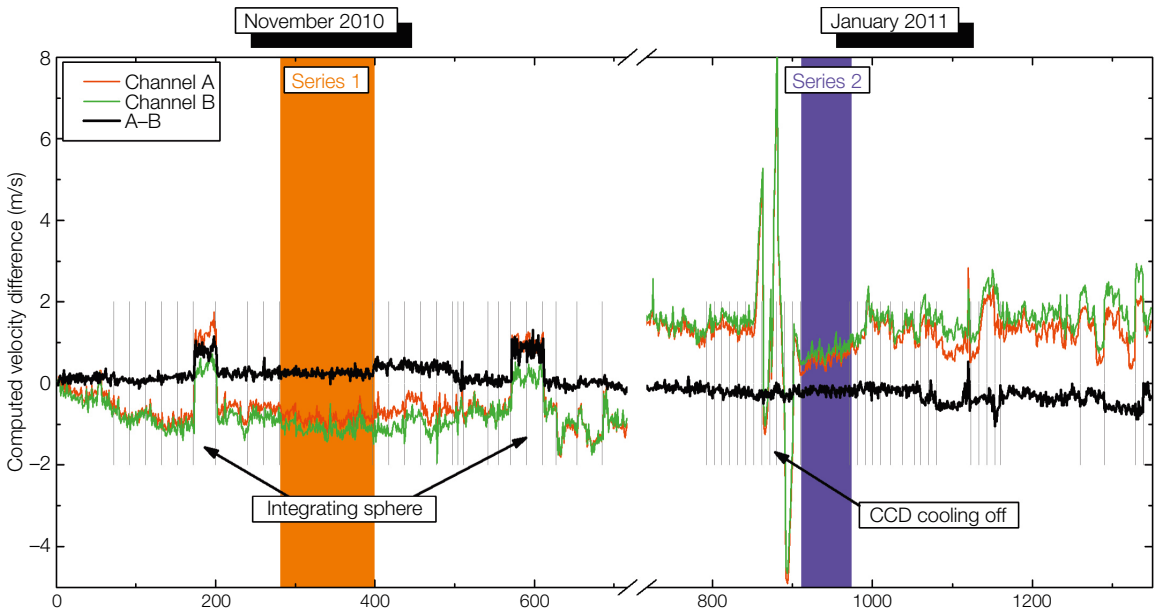

Figure 5. Drift of the two spectrograph channels for all the LFC data collected between November 2010 and January 2011 (almost 1300 spectra) is shown. The drift of the individual channels is measured with respect to an arbitrarily chosen spectrum. The relative drift between them is shown in black. The orange and violet vertical stripes indicate two long series (> 200 spectra in total) during which time the system was left unperturbed. From Wilken et al., 2012.

During our test runs in La Silla we monitored the radial velocity variation of the solar-type star HD 75289, known to host a Jupiter-mass planet with a period of 3.5 days. Using the LFC for wavelength calibration and simultaneous reference, we could reconstruct the orbit of the exoplanet. The measurements calibrated with the LFC nicely agree with previous data and the deviations from the fit could be due to stellar activity or pulsations. To our knowledge this is the first time that the orbit of an exoplanet has been reconstructed using LFC calibrations.

During the four years of the programme the LFC system has improved much, not only in its performance, but also in robustness and operational stability. The laboratory test and the campaigns with HARPS have achieved successful results, which have consolidated the concept of the system. The achieved repeatability of 2.5 cm/s is sufficient to detect an Earth-like planet in a one-year orbit around a star like our Sun.

Laser frequency comb for HARPS

After the successful completion of the demonstrator programme, beginning in February 2012, in partnership with the Instituto de Astrofisica de Canarias and the Universidade Federal do Rio Grande de Norte, we started a project aimed at the acquisition of a turn-key LFC system for HARPS. The system will be offered to the astronomical community after successful commissioning at the telescope. This project is not only directed towards improvement of HARPS, but also towards future instruments like ESPRESSO. The goals of this programme are to:

- gain experience in the use of the LFC, study its long-term behaviour and its reliability in operations, optimise the reduction tools to achieve the best performance with the LFC, with a view to its use on VLT and E-ELT instrumentation;
- bridge the gap between HARPS and ESPRESSO and acquire the potential of detecting a population of super-Earths in the habitable zone of solar-type stars;
- improve HARPS precision, which in turn will improve our capability for finding low-mass planets, further the understanding of stellar activity and refine the observation strategy for ESPRESSO planet searches.

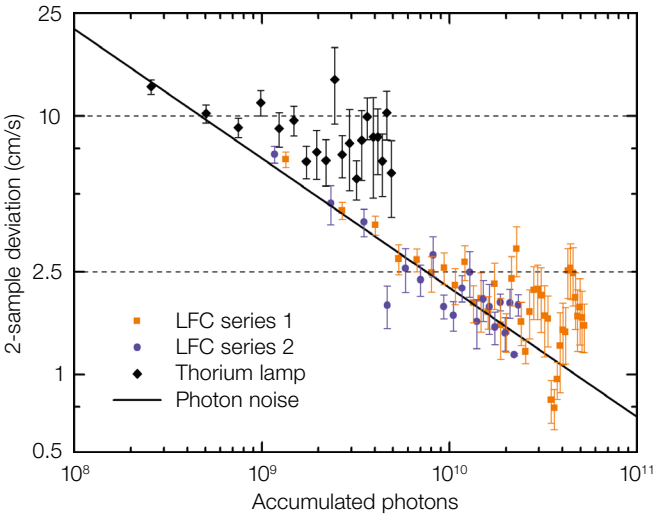

Figure 6. Two-sample variance of the LFC and the Th-Ar calibration. The black solid line is an estimation of the photon noise. The dashed horizontal lines at 10 cm/s and 2.5 cm/s indicate, for the Th-Ar and the LFC simultaneously, the level at which the data no longer follow the estimated noise and systematic effects become important. From Wilken et al., 2012.

The radial velocity (RV) precision of HARPS is estimated to be around 60 cm/s (Lovis et al. 2006). Knowledge of the instrument has permitted the instrumental causes that limit the RV precision to be identified: the light injection system and scrambling, the wavelength calibration system and, to a lesser extent, the temperature variations of the detector. After commissioning a new injection system in 2009, which improved the image stability at the fibre entrance, the Th-Ar wavelength calibration system is the strongest limiting factor to the long-term RV precision of HARPS. With the LFC, which has been shown to have a stability as good as a few cm/s with HARPS, the instrument is capable of reaching long-term RV precision below 30 cm/s, giving access to the detection of Earth-mass planets in close-in orbits, tracing out the path towards the detection of Earth twins. This RV precision is midway between the current HARPS performance and the 10 cm/s precision expected for ESPRESSO at the VLT, planned to start operations in about four years. The LFC calibration system will be one of the key components of ESPRESSO.

The step of moving from a laboratory prototype to a device to be operated at the telescope on an existing instrument will move us to the production phase, and will drive the development of an operational comb for the next high-precision radial velocity instruments for the VLT and the E-ELT. The experience collected with the HARPS LFC will be invaluable for ESPRESSO and beyond.

While delivering top RV precision data with HARPS, this project would permit an understanding of the long-term systematics (if any), early optimisation of comb operations and of the reduction software before ESPRESSO goes online and well in advance of the preliminary design of any high resolution spectrograph for the E-ELT.

Acknowledgements

We wish to thank Gerado Avila from ESO for preparing the injection and the scrambling unit, and Francesco Pepe, Christophe Lovis and Bruno Chazelas from the Geneva Observatory for their help with the reduction software and their advice.

References

Araujo-Hauck, C. et al. 2007, The Messenger, 129, 24
Beringer, J. et al. 2012, Phys. Rev., D86, 010001
Liske, J. et al. 2008, MNRAS, 386, 1192
Lo Curto, G. et al. 2010, Proc. SPIE, 7735, 77350Z
Lovis, C. et al. 2006, Nature, 441, 305
Mayor, M. et al. 2003, The Messenger, 114, 20
Murphy, M. et al. 2007, MNRAS, 380, 839
Palmer, B. & Engleman, R. 1983, *Atlas of the Thorium spectrum*, Los Alamos National Laboratory
Steinmetz, T. et al. 2008, Science, 321, 1335
Wilken, T. et al. 2010, Proc. SPIE, 7735, 77350T
Wilken, T. et al. 2010, MNRAS, 405, L16
Wilken, T. et al. 2012, Nature, 485, 611W

ESO VISTA Public Surveys — A Status Overview

Magda Arnaboldi[1]
Marina Rejkuba[1]
Jörg Retzlaff[1]
Nausicaa Delmotte[1]
Reinhard Hanuschik[1]
Michael Hilker[1]
Wolfgang Hümmel[1]
Gaitee Hussain[1]
Valentin Ivanov[1]
Alberto Micol[1]
Mark Neeser[1]
Monika Petr-Gotzens[1]
Thomas Szeifert[1]
Fernando Comeron[1]
Francesca Primas[1]
Martino Romaniello[1]

[1] ESO

The ESO policies for public surveys include regular monitoring and reviews of the progress of the surveys to ensure their legacy value and scientific competitiveness. The review process is carried out on the basis of reports by the ESO survey team and the survey PIs submitted to the relevant Public Survey Panel (PSP) — the VISTA PSP in this case. A summary of the time allocation to VISTA surveys, the service mode observations and the current progress after two years of telescope operation is provided. Furthermore the content of the data products delivery by the survey teams to the ESO Science Archive Facility is described.

Phase 1 — time allocation to surveys

Scheduling of the VISTA Public Surveys (PS) is done in line with the VISTA PSP recommendation that every effort should be made to complete the surveys within five years. Realistic expectations on what can be executed in the next semester are also taken into account, based on experience gained from the previous semester(s) of VISTA operation. The time allocation to surveys is based on the updated observing request by the PS principal investigators (PIs) and takes into account the carryover time needed to complete the observations submitted in the previous period. Figure 1 provides an overview of the time allocation to the six VISTA PSs from the extended period 85 to period 89 (P85–P89).

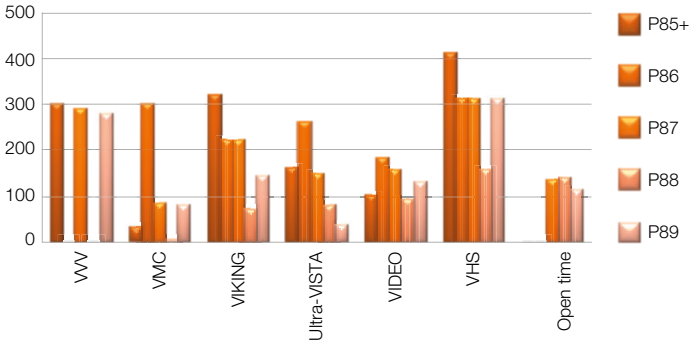

Figure 1. Overview of the VISTA time allocation in hours. P85+ included dry runs which were executed before the official start of VISTA operations.

The implementation of the PSP recommendation on time to survey completion implied a revision of the standard VLT model of scheduling observing time in service mode because the VISTA public survey programmes are all essentially at the highest priority of execution. As an added complexity, normal programmes were scheduled alongside public surveys and Chilean programmes from P87. Because the former have top priority and essentially cover all observing conditions, normal (open time) programmes must also be assigned a similar priority if they are to be executed at the telescope. Starting from P88, normal programme observations are not carried over regardless of their ranking, to avoid extra carryovers hindering the progress of the surveys. To limit the impact of open programmes on the progress of the VISTA PS the following policy has been implemented since P89: open time proposals can access restricted right ascension ranges, but should carefully justify the scientific goals and why these scientific goals are not achievable through the scheduled PS.

Phase 2 — service mode observations for public surveys

VISTA public surveys are ambitious programmes which entail very large allocations of time, of order of 1800 to 3400 hours, with consistent observing conditions. For a summary of the scientific goals of the VISTA public surveys, their area coverage and photometric characteristics, see Arnaboldi et al. (2007). An overview of VISTA and of its wide-field imager VIRCAM is provided by Emerson et al. (2006). Observation preparation and submission for public surveys is done on a half-yearly basis, following the standard ESO service mode procedures. The PIs of VISTA public surveys and their teams submit Observation Blocks (OBs) — the standard basic observing units. The deeper surveys (Ultra-VISTA, VIDEO, VIKING and VMC) have typically ~ 1-hour-long OBs, while the wide surveys (VHS and VVV) have OBs lasting between 5 and 30 minutes. The survey with the largest number of submitted OBs is VVV: because of the multi-epoch observations the total number of OBs prepared and executed will be of order 30 000. Figure 2 shows the number of hours of execution of OBs each month for all VISTA surveys. The time charged for each OB execution is only counted for successfully completed observations and Figure 2 shows the completed OB hours that are computed by the observation preparation software (P2PP3). While in the first year of the operations there was still some fine-tuning of the operational procedures and overheads, now the overheads computed by version 3 of the Phase 2 Proposal Preparation system (P2PP3) are very similar to the actual time needed to execute the observations.

The histogram in Figure 2 shows the effect of technical interventions on the speed of execution of the public survey OBs, with the main impact falling in the period 3 April 2011 to 4 May 2011, which coincided with the recoating of the primary (M1) and secondary (M2) mirrors with aluminium due to fast degradation of the original silver coating, and an extended recovery and maintenance of M1.

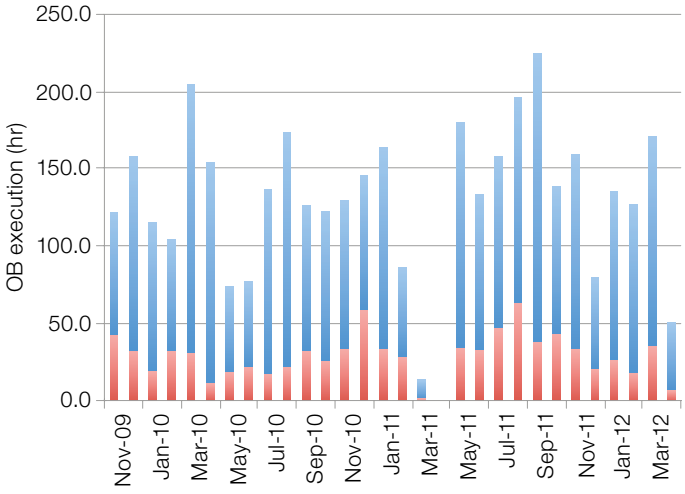

Figure 2. Histogram of the number of hours of execution of OBs each month for all VISTA surveys up to 1 April 2012. Quality control grade A is assigned to OBs completed fully within requested constraints (i.e. sky transparency, image quality, airmass, Moon illumination, etc.), while grade B is assigned to those OBs for which one of the constraints is violated up to ~ 10%.

In order to enable the survey teams to prepare large numbers of similar OBs and for ESO user support and science operations to verify and execute them in the most efficient manner, new tools have been developed (Arnaboldi et al., 2008). We list them briefly:

The Survey Area Definition Tool (SADT) was developed by the VISTA consortium (led by J. Emerson) and delivered as part of the United Kingdom in-kind contribution to joining ESO. The main role of the SADT is to efficiently mosaic the survey area and to identify the necessary active optics and guide stars for each tile. The SADT has been further improved following the experience gained during VISTA science verification, dry runs, and the first period of observations (P85+). The latest improvement was to introduce the 2MASS catalogue transformation to *J*-band magnitudes, which is now used for guiding and active optics on VISTA. This is important, as it was noticed that other catalogues suffered from low resolution, containing binary stars or galaxies, and some defects (e.g., containing spurious sources due to scratches on the plates from which these surveys were derived) which caused execution time losses due to the choice of unsuitable guide and/or active optics stars.

Phase 2 preparation tool for surveys (P2PP3) and Observing Tool (OT) for public survey support have resulted from the evolution of the main ESO observation preparation and execution tools. The PS teams prepare the observations using P2PP3 which takes as input the survey area definition file generated with SADT. In this way hundreds of similar OBs that adopt the same observing strategy and point to different areas in the sky are generated automatically, thus preventing typing errors and saving time. In addition to an interface with the SADT, this tool also allows the survey PIs to define the survey observing strategy via scheduling containers. These concepts can be easily encoded in an automatic ranking algorithm that suggests to the observers which OB is to be selected out of many thousands of similar survey OBs. The OT is used on Paranal for selecting the observations to be executed; it has the VISTA-specific ranking algorithm (Bierwirth et al., 2010) as well as reporting functionality.

Survey Monitoring and Visualisation Tool (SVMT) is a new tool developed to facilitate the Phase 2 review of thousands of survey OBs and to enable monitoring of the survey observations. The main functionalities are the display of the survey areas and the OB status for selected areas or survey runs, and the visualisation of the distribution on-sky for the submitted survey data products. Basic statistical functionalities have been implemented, such as calculation of the survey area and accumulated exposure times for which the observations have been completed or the data products submitted. This tool is used by the User Support Department and Archive Science Group, for the purpose of Phase 2 and Phase 3 reviews, respectively, and for overall survey progress monitoring by the ESO Survey Team (EST).

VISTA public survey completion rates

Here we present the current fraction of completeness for each VISTA PS and the expected time to completion, based on the current efficiency of execution. The absolute completion rate is based on theoretical OB execution times as computed by the P2PP execution time module and the time requested by the PI of each survey for the total duration of the project, as described in the Survey Management Plan (SMP). The absolute completeness fraction is given by the ratio of the completed OB time divided by the time requested in the SMPs. The completion rates are calculated for the observations up to the end of Period 88 (end of March 2012), hence they cover the first four periods of VISTA operations. In these four periods, the effective telescope time is about 1.75 years, as there were three months of technical downtime (mirror coating, M1 intervention and technical downtime to correct the focal plane tilt). These technical interventions affected mostly the VVV and Ultra-VISTA projects, as they took place in those months when either the Milky Way Bulge or the COSMOS fields are visible.

The absolute completion rates of the surveys at the end of P88 are listed in Table 1. These can be used to extrapolate the time necessary to complete the VISTA public surveys, assuming that the observations continue at a similar pace. From these assumptions, the VHS survey can be completed in about five years, while VVV, Ultra-VISTA, VIDEO and VMC are all expected to take more than seven years. These numbers are lower limits as the requested observing time in the SMPs was computed using overhead values that later proved to be underestimates. As the survey projects progress, and once one of the approved surveys is completed, the speed of completion is expected to increase for the other surveys. The VIKING survey was set to the lowest priority in P89 (October 2011–March 2012), as this survey currently fails to comply with the Phase 3 policies of data products submission for the ESO public surveys. Additional time allocation for the public surveys is pending the completed delivery of the agreed data products.

Table 1. Overview of the absolute completeness of the VISTA public surveys after 1.75 years of VISTA observing time (effective).

Period	VVV	VMC	VIKING	Ultra-VISTA	VIDEO	VHS
01.04.2010–30.03.2012	24 %	22 %	32 %	29 %	25 %	38 %

VISTA science operations

The VISTA telescope and its near-infrared camera VIRCAM are in normal operation: science data are being taken, and delivered to the users. Currently, the typical technical downtime is 2–3 %, to be compared with 10–12 % of weather downtime. During the commissioning of VISTA and VIRCAM, the overheads for telescope pointing, guiding and camera setup turned out to be ~ 30 % larger than the overheads estimated by the VISTA consortium. Several actions were then implemented to reduce the various sources of overhead. Furthermore, the telescope efficiency is about 10 % lower than expected because the original silver mirror coating was replaced with aluminium in April 2011, due to the fast degradation of the earlier coating. In Table 2 we provide the zero-point measurements in early operations with silver coating (dating from October 2009), the last measurements for silver (from March 2010) and the zero point with the new aluminium coating (measurements from July 2011).

Table 2. Photometric zero-point measurements (Vega magnitudes) in early operations (October 2009) with silver coating, last silver coating values (taken March 2010) and with the new aluminium coating (July 2011).

Filter	October 2009	March 2010	July 2011
Ks	23.03	22.88	22.96
H	23.87	23.61	23.76
J	23.78	23.43	23.66
Y	23.45	22.97	23.33
Z	23.82	23.22	23.58

During current standard operations, typical VIRCAM/VISTA technical downtime is due either to the M2 unit or active optics (AO) and autoguiding (AG) related problems. The AO and AG problems are partially caused by the incompleteness of the catalogues used by SADT to select guiding stars. The catalogue issue was improved by replacing the Guide Star Catalogue 2 (GSC2) optical catalogue with the 2MASS near-infrared catalogue, and by extending the latter catalogue to include synthetic optical magnitudes. The high elongation of the measured point spread function (PSF) detected during early telescope operations is now mostly under control and resolved. Occasionally elliptical images are recorded, typically due to azimuth axis oscillations that appear at seldom and irregular intervals.

Several optimisation steps were introduced into the instrument and telescope operation to increase the efficiency of observations: relaxing the declination tolerance of the AO correction and parallelising the instrument and telescope setups to decrease the overheads. Finally, the calibration plan was further revised, giving an extra 40 minutes per night for survey OB execution. Further hardware improvements are not realistic; software developments and further improvement of operations procedures may effectively improve progress speed, but only by a few percent.

The ESO policies for public surveys entail that raw data become public as soon as they are ingested in the ESO Science Archive Facility (SAF). Following the Memorandum of Understanding for VISTA, the Cambridge Survey Unit (CASU) receives a copy of all the raw data collected by VISTA for public surveys and normal programmes. PIs of VISTA public surveys do not automatically receive a copy of the raw data, but can access the pipeline data products either from CASU or the Wide Field Astronomy Unit (WFAU) archive in Edinburgh. Raw data are delivered regularly upon request to the Ultra-VISTA team.

Phase 3 – data products from public surveys

The raw data collected at the survey telescopes for the different projects amounts to about 1.5 TB per month, which, in turn, are condensed into a few terabytes of data products each year. Because of the legacy value of the public survey data products, ESO's policy is to ensure their long-term archival storage and public accessibility in order to promote their wide scientific use by the astronomical community at large, beyond those scientific goals initially identified by the survey teams. In order to bring this about, ESO has set in place a whole new process, called Phase 3, which represents the final step in the execution of ESO large programmes and public surveys.

The new Phase 3 infrastructure was deployed on 10 March 2011; it supports the reception, validation and publication of data products from the public survey projects and large programmes to the ESO Science Archive Facility; for a description of the Phase 3 tools and the infrastructure see Arnaboldi et al. (2011). Data products must be consistent with the data standards documented by the Archive Science Group at ESO. These data standards are required to characterise the level of data reduction and calibration, to track provenance, which allows ESO to monitor survey progress, and finally to support the query for specific data products via the ESO archive interfaces. In the context of the Phase 3 process, the data products returned by the survey teams are regularly monitored with respect to the actually executed observations. The timeline defining the requested delivery dates by type of data product is given by the Phase 3 policies.

For the VISTA data, a number of product types have been identified: images, weight maps and source lists. As high-level data products, the resulting source catalogues from the PS projects represent particularly important resources. The catalogues are different from the source lists, which are per-tile products and can be downloaded as entire FITS tables. The catalogue contents will be searchable via a dedicated query interface in the ESO SAF, which should become available in the second half of 2012. Basic functionalities will be supported to allow the archive user to carry out searches by position as well as by non-positional source parameters for sources in any area of the sky visible

Table 3. Overview of the ESO Phase 3 data releases resulting from the VISTA public surveys.

Survey	Submission Date	Date of Observations	Release Content	Filter	Sky Coverage (sq.deg)	Type of Data Products	Total Volume	Total Number of Files	Publication Date
VVV	03.05.2011	Feb 2010–Sep 2010	Contiguous patch of Bulge and Disc region including multi-epoch data in *Ks*	*ZYJHKs*	~ 520 (348 tiles)	Tiles Single-band source lists	1.5 TB	7980	25.07.2011
VIDEO	03.05.2011	Nov 2009–Feb 2010	XMM-LSS field	*YJHKs*	1.5	Tiles Single-band source lists	24 GB	291	25.07.2011
VMC	08.09. 2011	Nov 2009–Nov 2010	Two tiles in the LMC: one overlapping 30 Doradus and the other the South Ecliptic Pole region	*YJKs*	3	Stacked tiles and pawprints Single-band and band-merged source lists	8.1 GB	1256	25.09.2011
VHS	15.09.2011	Nov 2009–Sep 2010	VHS DES – 120 s in *JHK* VHS ATLAS – 60 s in *YJHK* VHS GPS – 60 s in *JK*	*YJHKs*	~ 1910	Tiles Pawprints Single-band source lists	3.9 TB	96474	17.10.2011
Ultra-VISTA	06.10.2011–30.01.2012	Dec 2009–Apr 2010	Deep imaging of the COSMOS field	*YJHKs*, NB118	1.5	Stacked images, SExtractor catalogues including *w*-selected multi-band catalogue	87 GB	19	15.02.2012
VIKING	10.10.2011	*Phase 3 data submission to be closed by PI*			–	–	19 GB	6276	–

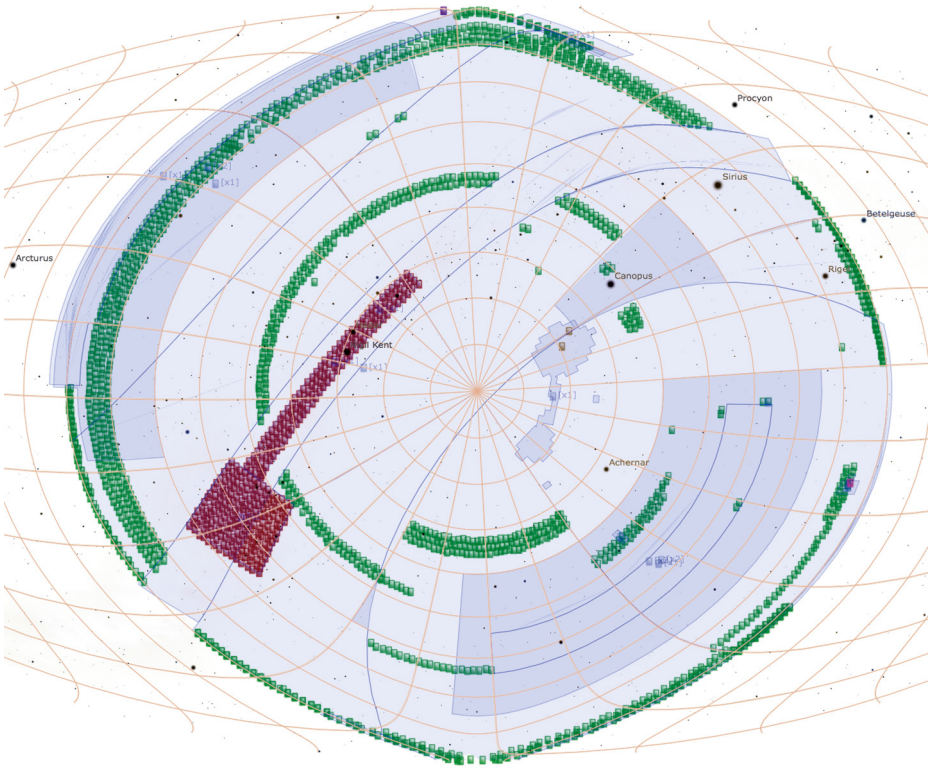

from the La Silla Paranal Observatory, for further scientific selection and investigation on the user's computer.

Table 3 provides an overview of the ESO Phase 3 data releases resulting from the VISTA public surveys and Figure 3 shows a map with the sky coverage. A detailed description of the data releases is available[1]. These release pages are based on the information provided by the PIs and give an overview of the observations, a description of the data reduction and calibration, additional release notes illustrating the scientific quality of the data and any additional useful information regarding the content of the release. The data products from each VISTA public survey are available via the query form[2] or by following the link at the bottom of each release description page.

Figure 3. The VISTA public survey data products released through the Phase 3 process in 2011/2012 cover almost 2500 square degrees of the southern hemisphere. Colour coding: VHS–green, VVV–red, VMC–yellow, VIDEO–pink, UltraVISTA–purple. Entire survey footprints are shown in light blue.

The first public data release from the VISTA public surveys took place in December 2011. Since then, more than five thousand files and 2.0 TB of VISTA data products have been downloaded from the ESO SAF by the community. The most requested and downloaded data product type is the source list (in FITS table format).

Conclusions

VISTA survey operations have now reached a steady state and nearly 80 % of the night-time on VISTA is used to successfully execute survey observations. The VISTA public survey teams are actively carrying out their observations and achieving their scientific goals: as documented by the nine ESO press releases based on VISTA data since January 2010 and the 23 refereed papers from ESO public surveys thus far. In order to increase community awareness of the scientific research opportunities from the VISTA public surveys, ESO is organising a workshop on 15–18 October 2012 entitled "Science from the next generation imaging and spectroscopic surveys"[3]. The astronomical community is invited to access the opportunities provided by the large wealth of data products delivered by the public surveys and to use them to explore science goals beyond those originally identified by the VISTA PS teams.

References

Arnaboldi, M. et al. 2011, The Messenger, 144, 17
Arnaboldi, M. et al. 2008, The Messenger, 134, 42
Arnaboldi, M. et al. 2007, The Messenger, 127, 28
Bierwirth, T. et al. 2010, SPIE, 7737, 19
Emerson, J., McPherson, A. & Sutherland, W. 2006, The Messenger, 126, 41

Links

[1] Description of the Phase 3 data release: http://www.eso.org/sci/observing/phase3/data_releases.html
[2] Query form for data products from each VISTA public survey: http://archive.eso.org/wdb/wdb/adp/phase3_vircam/form
[3] Homepage of the workshop "Science from the next generation imaging and spectroscopic surveys": http://www.eso.org/sci/meetings/2012/surveys2012.html

ESO/INAF-VST

This large field colour image of the nearby edge-on spiral galaxy NGC 253 was composed from VLT Survey Telescope (VST) images in *g*-, *r*- and *i*-bands. NGC 253 is a member of the Sculptor group at a distance of about 3.5 Mpc and as the nearest starburst galaxy shows signs of disc disruption and outflowing ionised gas. The dust absorption, well seen in this image, obscures the central starburst and possibly an active galactic nucleus. More details are available in Release eso1152.

On the Photometric Calibration of FORS2 and the Sloan Digital Sky Survey

Daniel Bramich[1]
Sabine Moehler[1]
Lodovico Coccato[1]
Wolfram Freudling[1]
Cesar Enrique Garcia-Dabó[1]
Palle Møller[1]
Ivo Saviane[1]

[1] ESO

An accurate absolute calibration of photometric data to place them on a standard magnitude scale is very important for many science goals. Absolute calibration requires the observation of photometric standard stars and analysis of the observations with an appropriate photometric model including all relevant effects. In the FORS Absolute Photometry (FAP) project, we have developed a standard star observing strategy and modelling procedure that enables calibration of science target photometry to better than 3 % accuracy on photometrically stable nights given sufficient signal-to-noise. In the application of this photometric modelling to large photometric databases, we have investigated the Sloan Digital Sky Survey (SDSS) and found systematic trends in the published photometric data. The amplitudes of these trends are similar to the reported typical precision (~ 1 % and ~ 2 %) of the SDSS photometry in the *griz*- and *u*-bands, respectively.

The general photometric calibration problem

Calibration of science target photometry consists of fitting an appropriate photometric model (e.g., zero-point, extinction and colour coefficients, etc.) to the calibration data (standard star observations) and then using the photometric model parameters to derive the photometric corrections that should be applied to the science observations. Sometimes it is convenient to split the calibration problem into an absolute calibration (i.e. knowledge of fluxes in physical units such as J m^{-2} s^{-1}) and a relative calibration (where all observations are calibrated to the same instrumental flux scale). This splitting is necessary since an accurate absolute calibration is substantially more challenging to achieve than a precise relative calibration due to the inherent difficulties in minimising the systematic uncertainties between the spectral energy distribution of appropriate (and usually very bright) photometric standards and the natural photometric system of the observations.

FORS2 photometry

With the Very Large Telescope (VLT) FORS2 instrument, we aim to provide the user with the possibility, given sufficient science target signal-to-noise (S/N), of performing an absolute calibration of their photometry to an accuracy of better than 3 % on photometrically stable nights. This is a challenging problem both in terms of collecting appropriate standard star observations as well as with regards to modelling the standard star photometry.

The photometric model should not only account for a photometric zero-point, nightly extinction coefficients and colour terms to convert from the standard filter wavebands to the instrumental wavebands, but should also potentially include terms to model the static and rotating residual flatfield patterns (Freudling et al., 2007; Moehler et al., 2010). The latter effect was found to be caused by the linear atmospheric dispersion compensator (LADC) and was worst for the LADC used with the now retired FORS1 instrument. The LADC used with FORS2, however, shows mainly a gradient (of amplitude 1.5 % peak-to-valley) instead of a complicated pattern. The necessity for a photometric model to account for all these effects leads to requirements for non-trivial modelling software. Furthermore, the standard star observations need to be designed to provide plenty of photometric measurements over sufficient ranges in airmass, time, colour, spatial coordinates and rotator angles during photometrically stable nights.

Simulated FORS2 observations

To understand how to provide calibrations that allow better than 3 % absolute photometric accuracy with FORS2, we performed extensive simulations and modelling of standard star observations in order to identify the minimum requirements for a certain photometric precision. To each simulation realisation, we fitted a photometric model that analyses a large number of nights of data simultaneously. For this purpose, we developed a general IDL program[1] to perform photometric modelling, including both absolute and relative photometric calibrations. This software allows the user to fit any linear photometric model (i.e. any sum of photometric terms) to a set of magnitude measurements. The main results from our modelling of the simulated data are the following:

1) To achieve ~ 1 % precision for the photometric zero-point, two standard star images per night should be obtained at airmasses of ~ 1.1 and 1.8, ensuring a range in airmass of ~ 0.6–0.7, and at least 18 photometric nights should be included in the photometric model to be fitted. This result is based on the assumption that the extinction coefficient is stable for the time period over which the standard star images are observed on any one night.
2) Observations coupled with modelling that satisfies the constraints described above should enable the atmospheric extinction coefficient to be determined to a precision of ~ 6–8 %.
3) The FAP project goal, to allow the user to reach an absolute photometric accuracy of 3 % during photometric nights, may be achieved by following the constraints described above, which lead to the ability to reach absolute photometric accuracies of 1.4–1.8 % (given sufficient science target S/N).
4) Once two standard star images at airmasses of ~ 1.1 and 1.8 have been obtained, further images at intermediate airmasses have little impact on the precision of the monitoring of the photometric zero-point and the extinction coefficient for the night in question, but will be needed to monitor the photometric stability of the night.

Comparing the requirements defined by these simulations to the calibration plan we found that:

a) The standard star fields for each month did not provide calibrating stars with a sufficiently wide and homogeneous range of colours.
b) The calibration plan needs to include standard star observations at both

high and low airmass to allow a correct judgement of the photometric quality at the start of the night (as opposed to an observation of just one standard star field near zenith).

c) In order to judge the photometric quality based on a single observation, the extinction derived assuming a well-determined instrumental zero-point should be used, as opposed to deriving a zero-point from an average extinction (which shows a correlation with airmass if the true extinction differs from the average extinction).

New calibration plan

Triggered by these findings, we changed the FORS2 imaging calibration plan. At the beginning of every night without visible clouds, one standard star field near zenith is observed. If the extinction coefficient derived from this observation (using the latest best estimate of the zero-point) is consistent with the extinction coefficient limits for a photometric night, then a second standard star field at high airmass is observed immediately afterwards to verify the stability of the extinction coefficient. If both observations yield the same extinction coefficient, then the night is declared to be photometric. If science data requiring photometric conditions are observed in service mode, then additional standard stars have to be taken at the middle and at the end of the night to allow monitoring of the photometric stability of the night.

The standard star fields are observed with offsets in position and rotation angle to allow the presence of static and rotating residual flatfield patterns to be investigated. After problems experienced with some of the Stetson standard star fields (Stetson, 2000) due to a lack of stars, we carefully selected a new set of Stetson fields that primarily satisfy the airmass constraints in the new calibration plan, and that are further optimised for the number of standard stars that are observed along with the colour range that is achieved.

The new FORS2 calibration plan (including the new standard star fields) was put into operation on 24 October 2011, and compliance was carefully monitored. The new calibration plan is now followed in about 75 % of the nights where it is applicable (i.e. potentially photometric nights). Most of the potentially photometric nights during which it is not fully followed are nights in which FORS2 is used for only part of the night.

Fit of photometric model for FORS2

With the new calibration plan in place, a sufficiently large dataset is routinely collected to fit our photometric model. The FORS2 pipeline provides two recipes for that purpose, called **fors_zeropoint** and **fors_photometry**. The former identifies standard stars with catalogued magnitudes in each frame, and performs aperture photometry. The latter fits our model to the data of several nights, and computes, in addition to a number of nuisance parameters (*viz*. model parameters which need fitting but whose values we are not interested in, which in this case are the true instrumental object magnitudes), a single zero-point for these nights and an extinction coefficient for each night.

To obtain reliable results, several improvements had to be made to the recipes, the parameters to run those recipes, and the data distributed with the recipes[2]. Specifically, the following changes were made:

1) We found that the automatic identification of standard stars by the FORS2 pipeline recipe **fors_zeropoint** was not robust, sometimes resulting in misidentifications that can cause incorrect extinction coefficients to be derived. We replaced the original pattern-matching algorithm used in this recipe with a robust algorithm that identifies the shift between the standard stars in the catalogue and the detected objects in the image by building up a histogram of all possible shifts between the standard stars and the detected objects and finding the histogram peak (which is very pronounced for ≥ 4 standard stars in the field). Although this algorithm can only cope with very small rotations (≤ 0.3 deg), this is not a problem because rotations in the FORS2 world coordinate system (WCS) are extremely rare.
2) Up until December 2011, the September 2007 version of the Stetson catalogue of standard stars was used by the FORS2 pipeline. A newer version is available (December 2010[3]) which contains *BVRI* photometry of a larger number of stars in fields that are part of the calibration plan and increases the coverage in very sparse fields by up to a factor of three. Hence we adopted this newer standard star catalogue.
3) The FORS2 pipeline recipe **fors_zeropoint** uses SExtractor (Bertin & Arnouts, 1996) to perform the background subtraction and measure the standard star flux. The settings used as default values were optimised for the Landolt catalogue (Landolt, 1992) that was originally used and which contains a few bright, isolated stars, whose catalogued magnitudes were measured with classical aperture photometry. The detection threshold in **fors_zeropoint** was therefore set rather high and a global background subtraction was used. The aperture size was set to 14 arcseconds in diameter, corresponding to the aperture used by Landolt.
The Stetson catalogue, on the other hand, reports magnitudes derived using adaptive aperture photometry, i.e. the aperture size increases until it encounters the next star. In addition, many of the Stetson fields are quite densely populated, so that a global approximation of the background is problematic. The higher star density also makes it advisable to lower the detection threshold to enable SExtractor to also correct for stars detected inside the aperture. We therefore lowered the detection threshold in **fors_zeropoint** from 3 σ to 1.5 σ and decreased the aperture size to 10 arcseconds in diameter. In addition we switched from global to local background fitting. These changes reduced the scatter in the derived photometric zero-points from individual stars within one image by more than a factor of two on average.

We experimented with the number of nights needed to obtain reliable fits of our model. We found that a minimum of seven fully photometric nights were needed. We therefore adopted the follow-

ing procedure to collect the data for each model fit. For each night, we chose a range of dates that is large enough to include at least seven fully photometric nights around that night. During periods with few fully photometric nights, this means that a date range of up to 60 nights needed to be included in the analysis. The number of seven photometric nights is a compromise between the increase in accuracy with an increasing number of photometric nights and temporal resolution of the parameters. In Figure 1 we show a comparison between the results of a fit that used a fixed window of 28 nights, not including the above pipeline improvements, and a fit using the current procedure. It can be seen that the zero-points change by less than about 5 % over a range of 100 nights.

We believe that the photometric parameters obtained with the procedure as outlined above are accurate enough to photometrically calibrate science data if a night is photometric. However, the user should be aware that the new calibration plan is not sufficient in itself for establishing that a night is photometric. There is a finite risk that a non-photometric night has not been recognised as such by the classification performed at Paranal. It is therefore advisable, that for science observations requiring photometric conditions, the user requests further standard star observations during the night. A procedure to submit standard star observing blocks without having to specify which standard star field is to be observed is currently under preparation. Another tool to judge the quality of a given night is the MeteoMonitor tool[4]. This tool should be consulted if the data of any given night are to be used for photometry.

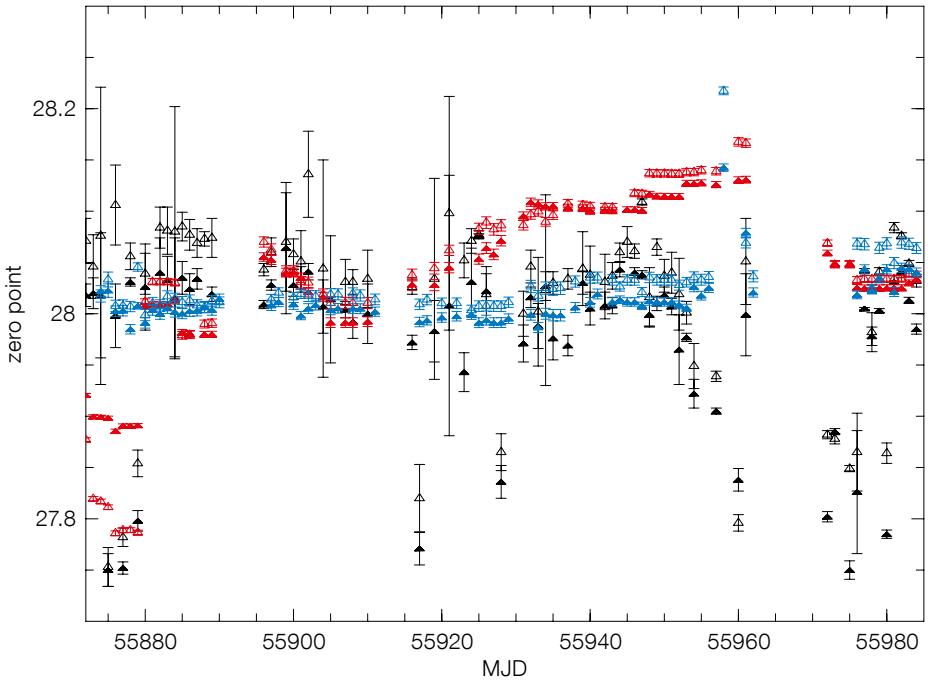

Figure 1. Three estimates of nightly photometric zero-points for FORS2 over 100 nights. The black points are computed using averaged extinctions as done for quality control. The red points are computed using our photometric model but without the improvements to the pipeline as described in the text. The blue points are our best current estimates. The two detectors in FORS2 are distinguished by open and filled points. It can be seen that by fitting a photometric model, zero-points can be obtained with an accuracy of a few percent. The fairly stable difference in zero-point between the two chips is clearly visible.

SDSS photometry

Our modelling of historical FORS2 photometric data revealed subtle effects, such as a rotating illumination pattern that can be corrected to improve the photometric accuracy. This raises the question of whether other large photometric datasets suffer from biases that can be revealed, modelled and corrected with our methodology. Arguably the most productive wide-field multi-waveband survey is the Sloan Digital Sky Survey (SDSS).

The large size of the SDSS survey makes it challenging to search for biases. Since our software is capable of handling such a large dataset, we decided to use it for an investigation of the SDSS photometry.

The SDSS (York et al., 2000) provides photometry (including widely used aperture and point spread function [PSF] magnitudes) in the *ugriz*-bands for objects down to ~ 22.5 mag and covering ~ 14555 square degrees. Padmanabhan et al. (2008) developed a photometric calibration model for SDSS data, similar to the model that we developed for FORS2, but with many more (~ 2000) calibration parameters of interest and ~ 10^7 nuisance parameters to be solved for, that results in a relative photometric calibration that is good to ~ 1 % in the *griz*-bands (~ 2 % in the *u*-band).

The repeat observations from the SDSS allow us to test our photometric modelling procedures using a dataset that includes many objects with unknown true magnitudes. So we decided to apply our methodology to investigate any systematic trends that might still be present in the SDSS photometric data after the Padmanabhan calibration effort. To this end, we downloaded all of the SDSS photometric data down to 19 mag in each waveband and analysed the repeat observations that satisfy certain quality constraints. We considered the aperture (7.43 arcseconds) and PSF magnitude measurements, and we looked for trends as a function of image and observation properties, such as detector column and row, PSF full width at half maximum (FWHM), sub-pixel coordinates, etc.

In the upper panel of Figure 2, we show how measured *u*-band aperture magnitudes systematically change as a function of PSF FWHM for a single detector in the SDSS camera, and we note that the changes increase in amplitude for fainter objects. Similar trends are found in the other bands and they are strongest in the *z*-band. We find that the trends range from ~ 7–15 millimag in each band for objects brighter than 16 mag, to

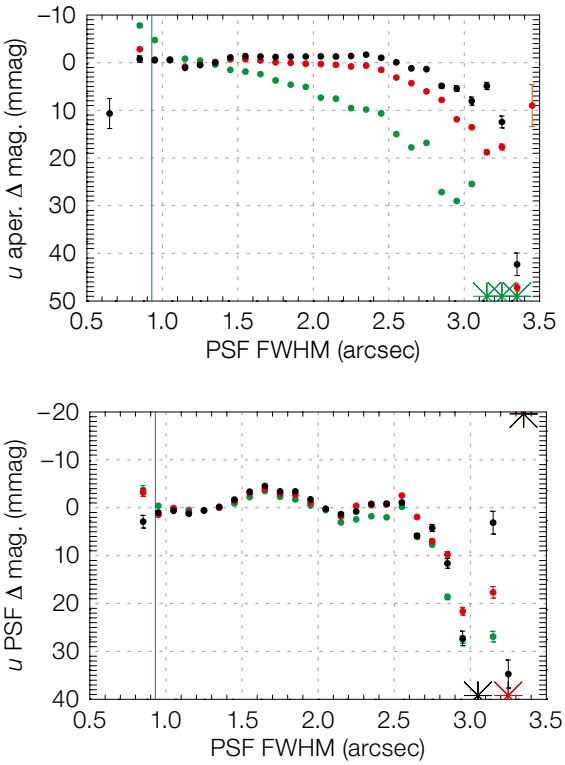

Figure 2. Upper: Systematic trends in the *u*-band aperture magnitude measurements as a function of PSF FWHM and object brightness for one of the detectors in the SDSS camera. The black, red and green points correspond to aperture magnitude measurements brighter than 16 mag, in the range 16–18 mag and fainter than 18 mag, respectively. Asterisks represent magnitude offsets that fall outside of the plot range. Lower: Same as the upper panel for the *u*-band PSF magnitude measurements from the same detector in the SDSS camera. In both plots the vertical blue line represents the critical sampling for the SDSS camera.

~ 30–60 millimag and ~ 100–170 millimag, in the *ugri*- and *z*-bands, respectively, for objects fainter than 18 mag.

In the lower panel of Figure 2, we present a similar plot for the *u*-band PSF magnitudes for the same detector in the SDSS camera. The systematic trends for the PSF magnitudes as a function of PSF FWHM are similar in amplitude to those for the aperture magnitudes but they are also more complicated and seem to "oscillate" as the PSF FWHM increases (the *ug*-bands show the clearest examples).

The full details of our analysis of the SDSS data are presented in Bramich & Freudling (2012) where we also investigate systematic trends as a function of other parameters such as subpixel coordinates, and we speculate as to the causes of some of the trends that we have found.

Acknowledgements

We thank Wolfgang Hummel for his helpful comments.

References

Bertin, E. & Arnouts, S. 1996, A&AS, 117, 393
Bramich, D. M. & Freudling, W. 2012, MNRAS, 424, 1584
Freudling, W. et al. 2007, The Messenger, 128, 13
Landolt, A. 1992, AJ, 104, 340
Moehler, S. et al. 2010, PASP, 122, 93
Padmanabhan, N. et al. 2008, ApJ, 674, 1217
Stetson, P. B. 2000, PASP, 112, 925
York, D. G. et al. 2000, AJ, 120, 1579

Links

[1] The IDL photometric modelling program is available from dbramich@eso.org on request
[2] All improvements to the pipeline recipes are available in version 4.9.11 of the FORS pipeline at: www.eso.org/sci/software/pipelines/fors/fors-pipe-recipes.hmtl
[3] New version of the Stetson photometric catalogue: http://www2.cadc-ccda.hia-iha.nrc-cn
[4] Paranal MeteoMonitor: http://archive.eso.org/asm/ambient-server

ESO/Manu Mejias

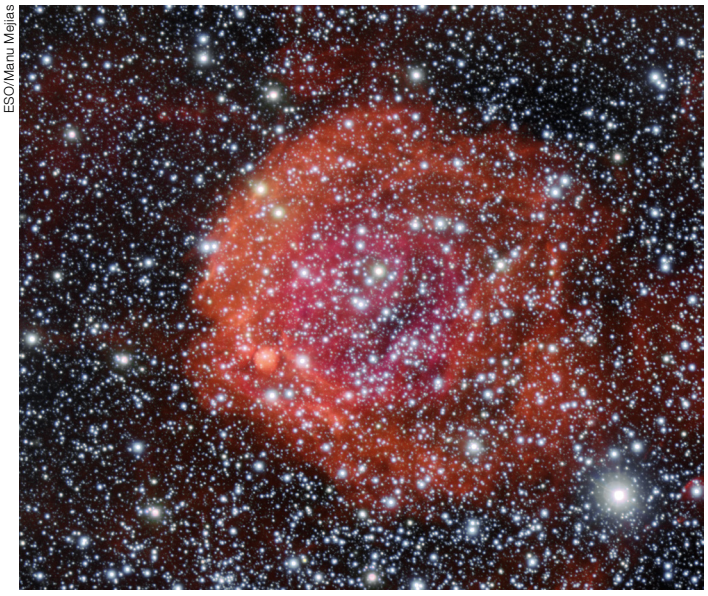

Colour image of the young open cluster NGC 371 in the Small Magellanic Cloud obtained with FORS1. Images in three emission lines – two of helium (He I 5876 Å and He II 4686 Å) and one of hydrogen (Hα) – were combined and emphasise the extended Hα emission produced by ionising photons from the hot O and B type stars in the cluster. See eso1111 for more details.

Provisional Acceptance of KMOS

Suzanne Ramsay[1]
on behalf of the KMOS team

[1] ESO

The near-infrared, multi-integral-field unit spectrograph, KMOS, has passed an important milestone. The provisional acceptance of this instrument by ESO in summer 2012 was the first step towards the commissioning of this new Very Large Telescope facility on the VLT Unit Telescope 1 (UT1) at the end of November 2012.

KMOS has been designed, built and tested by a consortium consisting of Durham University, the Max-Planck-Institut für extraterrestrische Physik (MPE), Universitäts Sternwarte München (USM), Oxford University and the UK Astronomy Technology Centre (Sharples et al., 2005). This unique spectrometer covers the wavelength range from 0.8–2.45 µm with five gratings. The *IZ*-, *YJ*-, *H*- and *K*- bands can each be observed in one setting at resolving powers between 3000 and 4000. A lower resolving power mode allows the *H*- and *K*- windows to be covered simultaneously. Spatially resolved information on 24 sources can be obtained with a single pointing. Cryogenic arms position pick-off mirrors over a 7.2 arcminute field at the focal plane of the UT1 Nasmyth focus, relaying 2.8 × 2.8 arcsecond fields to integral field units. The spatial sampling on sky is 0.2 × 0.2 arcecseconds. KMOS has been designed for the scientific goals of understanding the evolution and mass assembly of galaxies at moderate redshift, galaxies at extremely high redshift, reionisation and galactic stellar populations.

Before provisional acceptance was awarded, extensive testing was carried out in the integration laboratory at the UK Astronomy Technology Centre (see Sharples et al., 2010). ESO instituted a rigorous Provisional Acceptance Europe (PAE) process for this second generation instrument. Over the first six months of this year, ESO staff from Paranal and Garching worked with the consortium to witness and carry out tests that verified the performance in all areas, from safety conformance to scientific performance. The instrument on a flexure rig is shown in Figure 1.

With these tests successfully completed, the instrument has been released for delivery to Paranal. The cable rotator (on the right of the figure) needed to support the KMOS electronics is too large for air freight, and so was sent by sea in advance of the rest of the instrument. During the months of September and October KMOS will be reintegrated and tested in the Paranal Assembly, Integration and Test facility before being installed on the Nasmyth platform. First light is planned for the end of November, followed by commissioning periods to confirm the instrument performance on-sky and to ensure that the system is fully integrated into the Paranal Observatory. Astronomers can look forward to a first call for proposals with KMOS in March 2013 (Period 92).

References

Sharples, R. et al. 2005, The Messenger, 122, 5
Sharples, R. et al. 2010, The Messenger, 139, 24

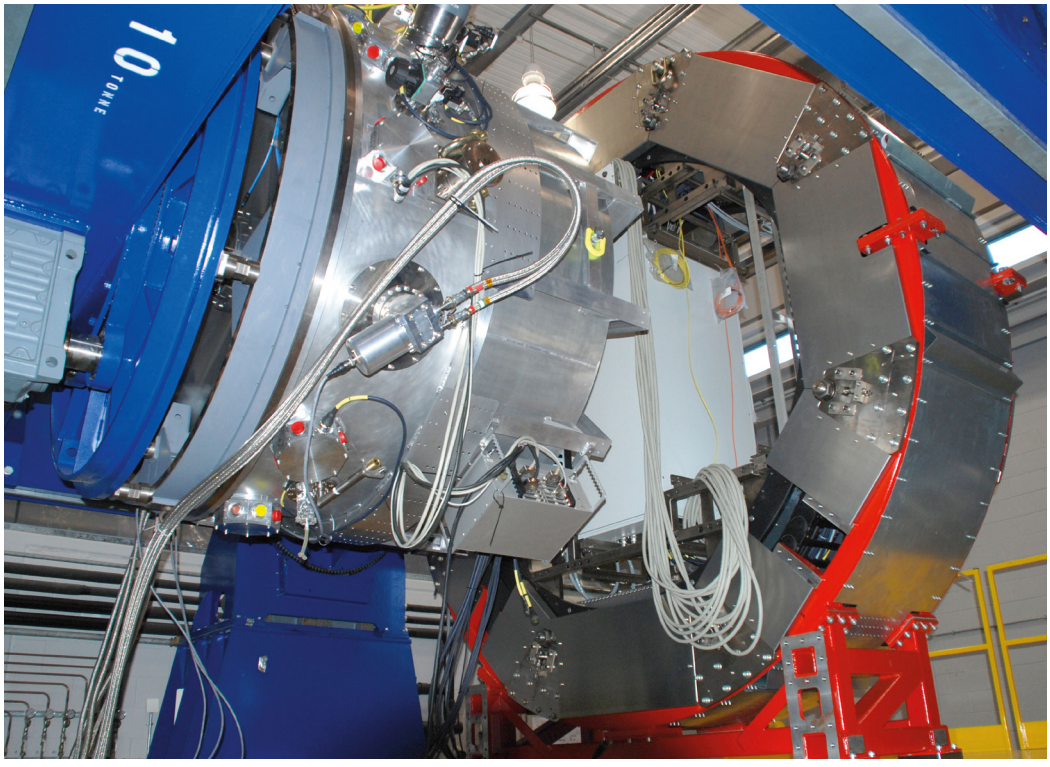

Figure 1. KMOS is shown on the flexure test rig in the integration hall at the UK Astronomy Technology Centre.

Gearing up the SPHERE

Markus Kasper[1]
Jean-Luc Beuzit[2]
Markus Feldt[3]
Kjetil Dohlen[4]
David Mouillet[2]
Pascal Puget[2]
Francois Wildi[5]
Lyu Abe[6]
Andrea Baruffolo[7]
Pierre Baudoz[8]
Andreas Bazzon[9]
Anthony Boccaletti[8]
Roland Brast[1]
Tristan Buey[8]
Olivier Chesneau[6]
Riccardo Claudi[7]
Anne Costille[2]
Alain Delboulbé[2]
Silvano Desidera[7]
Carsten Dominik[12]
Reinhold Dorn[1]
Mark Downing[1]
Philippe Feautrier[2]
Enrico Fedrigo[1]
Thierry Fusco[11]
Julien Girard[1]
Enrico Giro[7]
Laurence Gluck[2]
Frederic Gonte[1]
Domingo Gojak[1]
Raffaele Gratton[7]
Thomas Henning[3]
Norbert Hubin[1]
Anne-Marie Lagrange[2]
Maud Langlois[4]
David Le Mignant[4]
Jean-Louis Lizon[1]
Paul Lilley[1]
Fabrice Madec[4]
Yves Magnard[2]
Patrice Martinez[2]
Dimitri Mawet[1]
Dino Mesa[7]
Ole Möller-Nilsson[3]
Thibaut Moulin[2]
Claire Moutou[4]
Jared O'Neal[1]
Aleksei Pavlov[3]
Denis Perret[8]
Cyril Petit[11]
Dan Popovic[1]
Johan Pragt[12]
Patrick Rabou[2]
Sylvain Rochat[2]
Ronald Roelfsema[12]
Bernardo Salasnich[7]
Jean-François Sauvage[11]
Hans Martin Schmid[9]
Nicolas Schuhler[1]
Arnaud Sevin[8]
Ralf Siebenmorgen[1]
Christian Soenke[1]
Eric Stadler[2]
Marcos Suarez[1]
Massimo Turatto[7]
Stéphane Udry[5]
Arthur Vigan[4]
Gérard Zins[2]

[1] ESO
[2] Institut de Planétologie et d'Astrophysique de Grenoble, France
[3] Max-Planck-Institut für Astronomie, Heidelberg, Germany
[4] Laboratoire d'Astrophysique de Marseille, France
[5] Observatoire de Genève, Switzerland
[6] Laboratoire Lagrange, Nice, France
[7] INAF – Osservatorio Astronomico di Padova, Italy
[8] Laboratoire d'Etudes Spatiales et d'Instrumentation en Astrophysique, Paris, France
[9] Eidgenössische Technische Hochschule Zürich, Switzerland
[10] University of Amsterdam, the Netherlands
[11] Office National d'Etudes et de Recherches Aérospatiales, Châtillon, France
[12] Stichting ASTRonomisch Onderzoek in Nederland, the Netherlands

Direct imaging and spectral characterisation of exoplanets is one of the most exciting, but also one of the most challenging areas, in modern astronomy. The challenge is to overcome the very large contrast between the host star and its planet seen at very small angular separations. This article reports on the progress made in the construction of the second generation VLT instrument SPHERE, the Spectro-Polarimetric High-contrast Exoplanet REsearch instrument. SPHERE is expected to be commissioned on the VLT in 2013.

Direct imaging is presently the most promising technique to efficiently reduce the photon noise generated by the host star, by suppressing its light intensity while retaining the light from the exoplanet. It is mandatory to obtain spectral or polarimetric data of faint (contrast lower than about 10^{-6}) exoplanets. Direct imaging offers important complementary information to radial velocity studies of exoplanets, such as resolving the sin *i* ambiguity intrinsic to the radial velocity method, and allows for dynamic mass measurements of individual exoplanets. It can provide additional diagnostic data, e.g., through polarimetry, and greatly improves observing efficiency through the ability to confirm a detection in a couple of nights rather than following an orbit, which may take years.

In August 2007, the contract for the construction of SPHERE was signed with a consortium of 11 institutes from five European countries: IPAG (PI institute, Grenoble, France); MPIA (Co-PI institute, Heidelberg, Germany), LAM (Marseille, France), LESIA (Paris, France), Lagrange (Nice, France), Osservatorio Astronomico di Padova (Italy), Observatoire de Genève (Geneva, Switzerland), ETHZ (Zurich, Switzerland), University of Amsterdam (the Netherlands), ASTRON (Dwingeloo, the Netherlands), and ONERA (Châtillon, France). Signing the contract was quickly followed by the preliminary design review in September 2007 and the final design review in December 2008. The assembly, integration and testing of subsystems at the various integration sites took almost three years, ending in autumn 2011,W and was concluded by a series of assembly readiness reviews. Since the end of 2011, SPHERE has been undergoing integration and testing at IPAG in Grenoble. The fully assembled instrument is now entering the final test phase and rapidly approaching Preliminary Acceptance Europe (PAE).

SPHERE (see Beuzit et al. [2006] for an overview) will provide high imaging contrast by combining extreme adaptive optics (XAO), coronagraphy, accurate calibration of non-common path instrumental aberrations and post-observational data calibration through various differential methods. The instrument is integrated on a large optical table which will occupy the Nasmyth platform A of the VLT Unit Telescope 3. The optical table

contains all the common-path optics including the XAO module and infrastructure such as the calibration source module. An enclosure will provide thermal inertia and stability and will also reduce local turbulence. Three scientific instruments are attached to this main bench: a differential near-infrared imaging camera and spectrograph (IRDIS, InfraRed Dual Imaging Spectrograph); a near-infrared low spectral resolution Integral Field Spectrograph (IFS); and a visible imaging differential polarimeter (ZIMPOL, Zurich Imaging Polarimeter).

Figure 1 illustrates the specified and simulated contrast performance of SPHERE for the different scientific instruments. The differential imaging methods rely either on spectroscopic features (IRDIS) or a certain degree of polarised flux (ZIMPOL) in order to provide the expected contrast performance. The simulations were performed for very bright stars, so the main limitations are residual differential aberrations rather than photon noise. The IFS data are assumed to be calibrated by spectral deconvolution (Mesa et al., 2011). Field rotation and potential further contrast improvements by angular differential imaging techniques were not taken into account. Such techniques are expected to make ZIMPOL compliant with its contrast requirements.

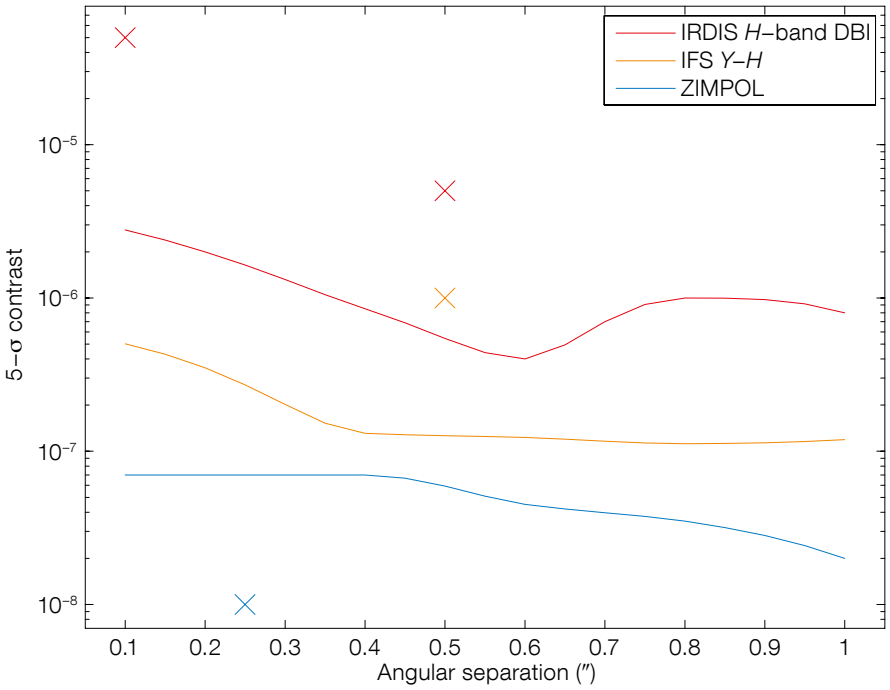

Figure 1. The contrast performance of SPHERE for its scientific instruments is shown as obtained from simulations (solid lines) before applying angular differential imaging techniques. The specified contrast performance of the different instruments is shown by crosses.

Concept and features

SPHERE is built around the XAO system, SAXO (SPHERE Adaptive optics for eXoplanet Observation), which is designed as a standard single conjugate adaptive optics (AO) unit with many degrees of freedom. SAXO incorporates the high-order deformable mirror (HODM) with 1377 actuators on a 41 × 41 grid covering the aperture; a high temporal correction bandwidth of about 100 Hz is provided by ESO's deep depletion L3-CCD wavefront sensor camera and extremely low latency SPARTA real-time computer. As two of the dominant terms in the error budget (fitting error and temporal bandwidth error) are strongly reduced this way, SAXO provides a high Strehl ratio in the near-infrared (NIR) maximising the flux intensity in the point spread function (PSF) core and hence the exoplanet signal. The correction quality is still good enough for diffraction-limited images in the optical part of the spectrum.

The HODM can suppress residual wavefront aberrations up to its correction radius θ_{AO} given by the ratio of the assumed wavelength of the observation divided by twice the inter-actuator spacing projected back to the telescope aperture ($\lambda/2D$). For a wavelength of 1.6 µm and an actuator spacing of 0.2 metres, $\theta_{AO} \approx 0.8$ arcseconds. The intensity of the stellar coronagraphic PSF halo is proportional to the power spectrum of residual aberrations, and their spatial frequency defines the angular separation from the PSF centre at which the light is scattered.

Since exoplanets are to be found at small angular separations, typically well below 0.5 arcseconds, a very efficient and precise correction of low spatial frequency aberrations, i.e., the low-order modes, is required to achieve a high-contrast (dark hole) close to the PSF centre, and is thus a prime objective of SAXO. Its spatially filtered Shack–Hartmann wavefront sensor (SHWFS) with 40 × 40 subapertures of 6 × 6 pixels each is a suitable and well-established technology to achieve this goal. Very small low spatial frequency wavefront errors, even in the presence of vibrations, are achieved by efficient tip-tilt correction through linear quadratic Gaussian (LQG) control to a level of about one milliarcsecond root mean square (RMS). Figure 2 shows IRDIS images recorded in *H*-band without a coronagraph. The optically simulated seeing has a median value of 0.85 arcseconds, and the Strehl ratio derived from the corrected image was 94 %.

The AO-corrected PSF is dominated by the Airy pattern of the telescope aperture and shows a ring structure modulated and sprinkled by quasi-static speckles from residual instrument aberrations with intensity up to 10^{-3} of the peak intensity at small angular separations. This Airy pattern is then removed by a coronagraph, and SPHERE provides a multitude of state-of-the-art coronagraphs such as the apodised Lyot coronagraph or the four-quadrant phase masks with inner working angles approaching the theoretical limit of one (λ/D), e.g., Martinez et al. (2010). Since stellar coronagraphy is a quickly evolving research field, future evolutions can be implemented through exchangeable masks both in the coronagraphic focus and in its entrance and

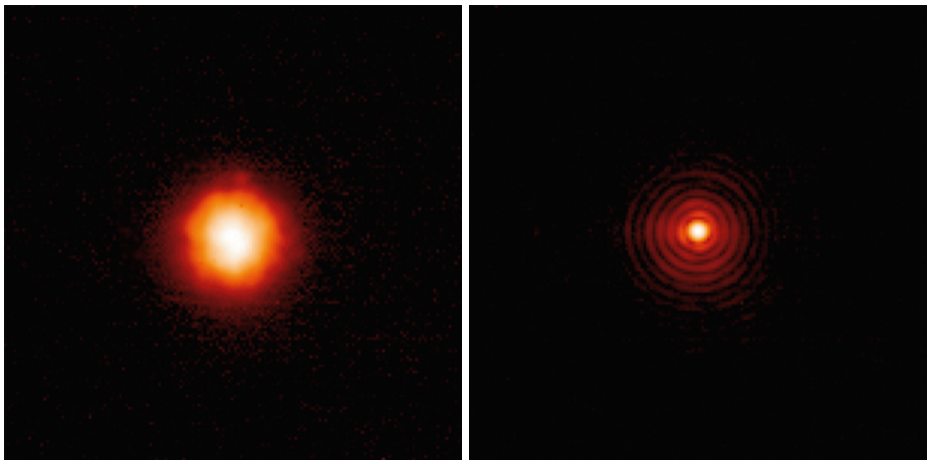

Figure 2. The SPHERE SAXO *H*-band point spread function is illustrated with the AO loop open (left, uncorrected image) and with the AO loop closed (right, corrected image).

exit pupil planes. Finally, residual instrumental aberrations will be measured by an evolved phase diversity technique and suppressed to a level of only a few nanometres rms by the deformable mirror (DM). Figure 3 shows an *H*-band PSF which has been corrected for the instrumental aberrations and has a derived Strehl ratio of 99%, consistent with a residual wavefront error of just a few tens of nanometres RMS.

The three scientific instruments will be fed by the XAO/coronagraphy system and implement the means for post-observational data calibration techniques. The main parameters of these instruments are summarised:

IRDIS covers a spectral range from 0.95–2.32 µm with an image scale of 12.25 milliarcseconds (mas) for Nyquist sampling at 950 nm. The field of view is permanently split into two channels of 11 by 12.5 arcseconds each, both for direct and dual imaging. The differential aberrations between the two channels, introduced by the beam splitter and the individual mirrors, focusing lenses and filters, have been carefully minimised to 7–10 nm rms total. Both channels are projected onto the same Hawaii 2RG NIR detector. Long-slit spectroscopy at resolving powers of 50 and 500 is provided, as well as a dual polarimetric imaging mode.

The IFS covers the spectral range 0.96–1.66 µm again with an image scale of 12.25 mas. The 1.73 by 1.73 arcsecond field of view is sampled by a two-sided lenslet array, and each of the spatial pixels (spaxels) is dispersed by either one of two Amici prisms providing spectral resolutions of about 110 and 70 for the two bandpass modes *Y–J* and *Y–H* respectively.

ZIMPOL covers the spectral range 600–900 nm with an image scale of 7 mas for correct sampling at 600 nm wavelength. The instantaneous field of view of 3.58 by 3.58 arcseconds is increased to almost 8 arcseconds in diameter through dithering by internal field selectors. The beam is split into two arms by a polarising beam splitter, each arm with its own detector. Differential polarimetry in each of the arms is implemented by a ferro-liquid crystal (FLC) modulator that is synchronised with a row modulation of the CCD (every second row is blind thanks to a lenslet array that is mounted directly onto the detector, see Figure 4), such that each CCD image contains interlaced images of perpendicular linear polarisation states. Filter sets common and separate to the two arms as well as a number of calibration devices complete the list of functions.

A set of three main observing modes defines how the light is split between the scientific instruments. IRDIFS is the survey mode which will be used for a large fraction of the time. In its main configuration, it combines IRDIS dual imaging in the *H*-band with IFS imaging spectroscopy in the *Y–J* bands with pupil stabilised coronagraphy. Other configurations

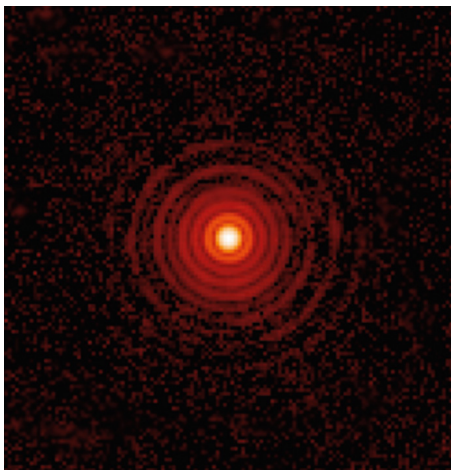

Figure 3. The SPHERE *H*-band point spread function, corrected from residual aberrations, is shown.

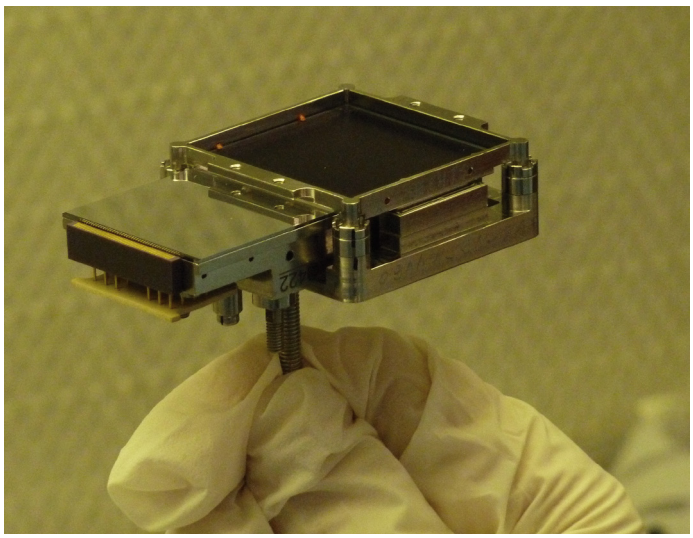

Figure 4. The SPHERE ZIMPOL CCD with the cylindrical lenslet array mounted on the detector is shown.

include *K*-band IRDIS and *Y–H* band IFS splitting as well as field stabilisation. IRDIS alone can be used to exploit its various modes for more generic NACO-like (*viz*. high resolution AO imaging) science, while ZIMPOL alone will provide high precision differential and absolute polarimetry as well as classical diffraction-limited imaging at optical wavelengths. No mode supports simultaneous NIR and optical observations.

Current status

SPHERE with all its subsystems has fully been integrated at IPAG in Grenoble. Figure 5 shows the status in early 2012, when the XAO wavefront sensor arm was still not populated, and the main bench was still exposed to the laboratory environment. In the meantime the main enclosure has been installed, and a thermal tent now surrounds SPHERE. Figure 6 shows a detailed view of the SPHERE optical bench with various subsystems and important components indicated. A detailed status update of the project has recently been presented by Beuzit et al. (2012).

The instrument software as well as data reduction and handling software are complete and are used for test data acquisition through template operation and for data analysis by the pipeline. Functional testing has been successful, and SPHERE is now entering the end-to-end performance evaluation with optically simulated turbulence. Major activities that are still to be completed are the thermal testing of the complete instrument over its specified temperature range between 0°C and 20°C, and the installation and testing of the vacuum cryogenic system, which has many similarities with the one that has been developed for MUSE.

There are, however, some pending issues which impact on the instrument performance and which will be resolved only in the longer term. The most prominent one is the HODM, which suffers from two main limitations: i) a strongly temperature-dependent shape-at-rest (about 1 µm peak-to-valley cylindrical wavefront deformation per degree Celsius); and ii) an electrical interface incompliance for

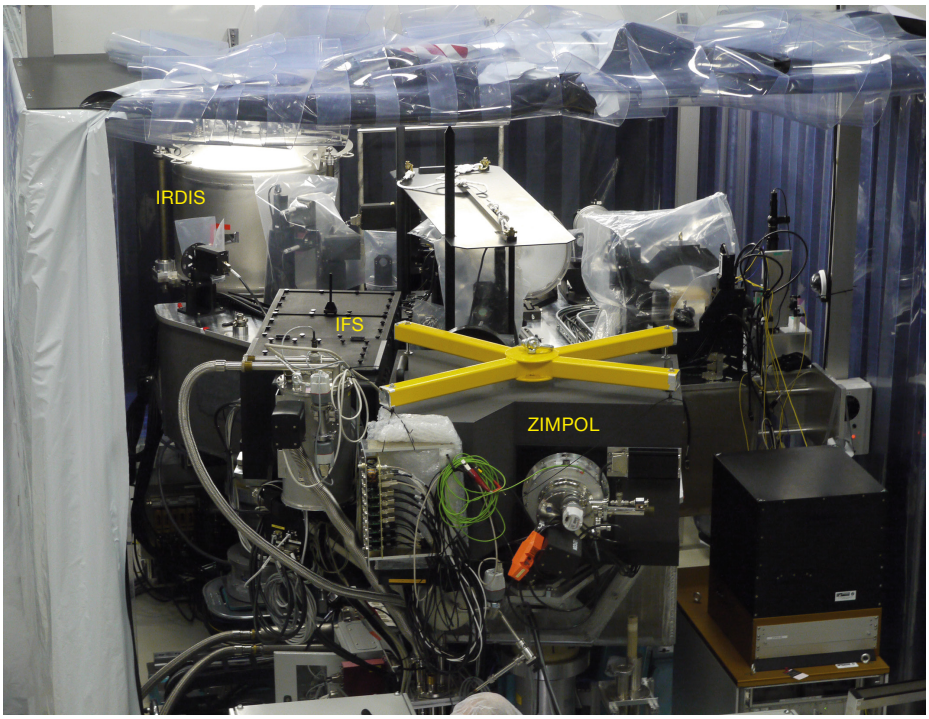

Figure 5. SPHERE in the assembly laboaratory at IPAG with all instruments integrated into the common path.

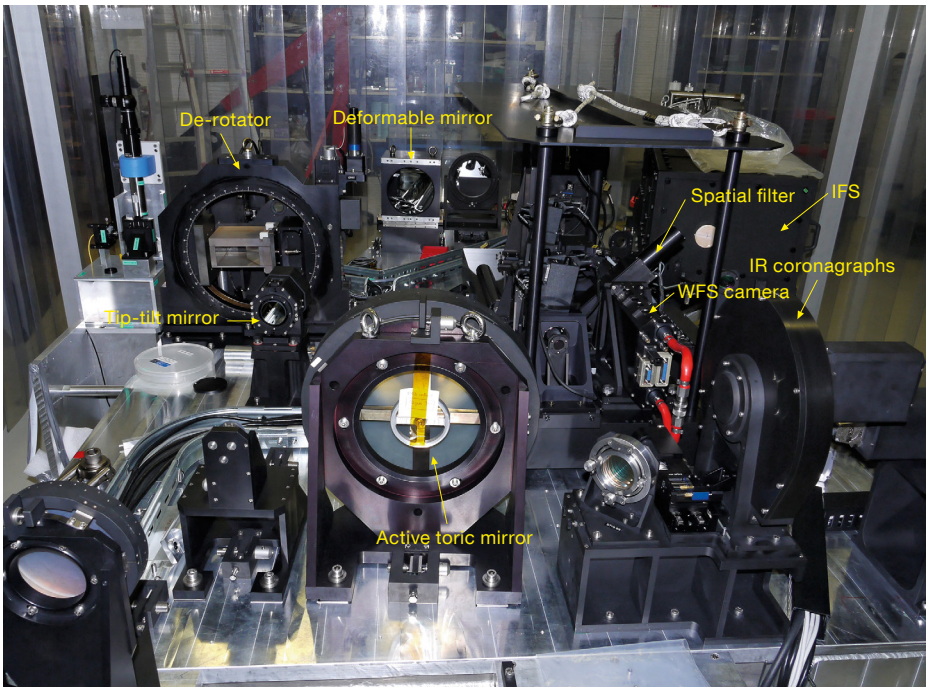

Figure 6. Detailed view of the SPHERE optical bench is shown with the main subsystems indicated. The active toric mirror, used to compensate for the HODM temperature-dependent shape-at-rest, is clearly visible in the centre foreground.

a number of actuators (currently four actuators are dead, and several tens of actuators respond more slowly than specified, but still on a timescale of a millisecond). In order to overcome these problems, the production of a replacement, HODM2, was launched in 2010. Several modifications to the design ensure that all SPHERE specifications are fulfilled. Unfortunately, a number of manufacturing problems have occurred that have delayed the delivery of HODM2 until October 2013. Because the cylindrical shape-at-rest of the HODM can be offloaded to a toric mirror (a mirror with a spherical surface with added astigmatism from Zernike terms of third and fifth order) in the common path, and the actuator deficiencies mainly introduce increased photon noise which can be mitigated by longer exposure times, SPHERE will use HODM1 for its acceptance and integration testing (AIT) and, depending on the achieved performance, even for installation and commissioning at the VLT.

Another concern is the degradation of the protected silver coatings of several common path and infrastructure (CPI) mirrors. These are being closely monitored and may require a re-coating at some stage, probably during the period of shipment to Paranal Observatory. Finally, the detector motion stage (DMS) of IRDIS has been found to be out of specification, with one axis not working properly and not achieving the required amplitude. The DMS is supposed to move the detector by small amounts to cope with bad pixels and improve the flat field accuracy, which are both important, but, at least for AIT, not necessarily vital objectives. A replacement DMS is currently in production and should be ready for installation at the VLT.

Releasing SPHERE

The instrument's preliminary acceptance in Europe is planned for early spring 2013, immediately followed by shipment to the Paranal Observatory and on-site integration in late spring 2013. With this schedule, first light is expected in summer 2013 during the first commissioning period. Further commissioning periods will be carried out later in 2013 during which the instrument will be operated, characterised and validated in all possible observing modes. Further objectives of the commissioning period include instrument operation through the standard procedures and the implementation of the data reduction pipeline as well as the determination of operational efficiency. After the commissioning period, science verification will be carried out involving scientists from the ESO community to demonstrate SPHERE's scientifc potential and to experiment with the data reduction tools available at this time.

A workshop dedicated to SPHERE and its future use is planned for late summer 2013; the date will be confirmed depending on a successful start of commissioning, possibly followed by a delta call for proposals. This workshop will include a dedicated session on ground-based high contrast imaging with SPHERE and cover observing proposal preparation and data reduction.

It is foreseen to release SPHERE to the community during Period 92, and to include SPHERE in the Period 93 (April–September 2014) regular call for proposals for the first time. Starting early 2014, European astronomers will be able to carry out spectacular programmes dedicated to the detection and characterisation of exoplanets with an unprecedented accuracy.

References

Beuzit, J.-L. et al. 2006, The Messenger, 125, 29
Beuzit, J.-L. et al. 2012, Proc. SPIE, 8446
Martinez, P., Aller-Carpentier, E. & Kasper, M. 2010, The Messenger, 140, 10
Mesa, D. et al. 2011, A&A, 529, 131

ESO/University of Oxford/L. N. Fletcher/T. Barry

Two thermal infrared images of Saturn (centre and right) taken with VISIR, and an amateur visible-light image (left) by Trevor Barry for orientation, are shown. The images were taken on 19 January 2011 and show the mature phase of the northern spring hemisphere storm. The centre image (18.7 μm) reveals the structures in Saturn's lower atmosphere including the storm clouds and its central cooler vortex; the right image (8.6 μm) is sensitive to much higher altitudes in the stratosphere, where emission flanking the central cool region over the storm is observed. See Release eso1116 for more details.

Acknowledgement: ESO Imaging Survey

Colour image of the Galactic globular cluster M4 (NGC 6121) taken with the Wide Field Imager (WFI) attached to the MPG/ESO 2.2-metre telescope. M4 is the closest globular cluster (distance 2.2 kpc) and cluster stars occupy the whole WFI field. The image was formed by combining *B*-, *V*- and *I*-band exposures and more details can be found in Release 1235.

New Surprises in Old Stellar Clusters

Ivo Saviane[1]
Enrico V. Held[2]
Gary S. Da Costa[3]
Veronica Sommariva[4]
Marco Gullieuszik[2]
Beatriz Barbuy[5]
Sergio Ortolani[6]

[1] ESO
[2] INAF – Osservatorio Astronomico di Padova, Italy
3 Australian National University, Mt. Stromlo Observatory, Australia
[4] INAF – Osservatorio Astrofisico di Arcetri, Italy
[5] University of Sao Paulo, Brazil
[6] University of Padova, Italy

Galactic globular clusters have a long and distinguished history as conspicuous providers of simple populations where models of low-mass stars can be tested. However their simplicity has been challenged several times and a few peculiar objects have been identified. Only recently has the case for extended star formation histories become really compelling, with the unprecedented quantity and quality of data from Hubble Space Telescope imagers and multiplexing spectrographs on large telescopes. With ages close to that of the Universe, globular clusters can also help us uncover the earliest phases in the formation of the Milky Way. In both areas, one of the major challenges is to have an abundance ranking of all clusters based on the same metallicity index, and for as many stars as possible inside each cluster; a homogeneous metallicity compilation is only available for about half of all globular clusters. A few years ago we began a project to help close this gap and we report on a few surprising results that are emerging.

In his book *Reflecting Telescope Optics* Ray Wilson (Wilson, 2004) writes that the 60-inch telescope on Mt. Wilson was, in its time, "arguably the greatest relative advance in astronomical observing potential ever achieved [together with W. Herschel's 20-foot focus telescope]", made possible by the technical genius of George Ritchey. The telescope had its first light on 8 December 1908, and eight years later it was used by Harlow Shapley to publish the first paper of his series "Studies Based On The Colors And Magnitudes In Stellar Clusters". In the introduction, he recalled that, "No serious attempts have been made to determine accurate magnitudes, chiefly because of the lack of dependable magnitude scales for the fainter stars." Such attempts could finally be made thanks to the availability of that superb telescope, which could collect photometric data of such distant objects as Galactic globular clusters (GCs).

Among the motivations to undertake his work, Shapley quoted the possibility of solving the problem of "the order of stellar evolution; that is, the probable character of the progression of spectral type (color) with age". Almost one hundred years later, this motivation still underlies a large fraction of stellar cluster studies. In particular globular clusters have been, and still are, crucial in testing theories of low-mass stellar evolution, because their stars were born in a single episode, thus representing the simplest conceivable population. Or at least this has been the common wisdom for many years. But as observations and data analysis techniques have improved, this view has started to change. This change has been helped in part by our work, as we illustrate here, after setting things in context.

A few historical notes

The practice of using GCs to test the resolving and light-collecting power of new telescopes and instrumentation continued until well after Shapley, and these beautiful objects are still often featured in press releases today when new facilities are inaugurated. So it is not surprising that just a handful of years after its first light in 1948, the 200-inch telescope at Palomar was used by Arp, Baum & Sandage (1953) to resolve the faint stars defining the turnoff feature in the colour–magnitude (CM) diagram of M92. It was a breakthrough that suggested the connection between the main sequence in the CM diagram of young clusters, and the later evolutionary phases seen in globular cluster diagrams.

The theoretical interpretation of such diagrams came almost immediately with the work of Hoyle and Schwarzschild, who, in 1955, were able to calculate a stellar age of 6.2 Gyr by comparing the track of a 1.1 $M_{\odot}$ star to the CM diagram of the clusters M92 and M3. To be able to perform the analytic calculations, some simplifications had to be introduced, so the

Figure 1. The fuzzy object above the ESO 3.6-metre telescope (and the NTT in the foregound) is Omega Centauri, the most massive globular cluster in the Milky Way. This object was perhaps the nucleus of a dwarf galaxy that was disrupted several Gyr ago.

track was only in qualitative agreement with the observations. However computers soon became powerful enough to allow numerical calculations, which were pioneered by Icko Iben and collaborators. Iben & Rood (1970) were able to follow the evolution of metal-poor stars for objects of different mass, metallicity, and helium abundance, thus yielding isochrones that could be compared quantitatively to observed CM diagrams. The comparison exercise was immediately performed by Sandage (1970) with four globular clusters, and his investigation set the foundations for the classic research lines that extend into our times.

Based on the colour and luminosity of the clusters' turnoffs, Sandage established an average age of 11.5 Gyr, and cluster-to-cluster age differences formally not greater than ~ 2% (although photometric errors allowed an age spread as large as one Gyr). The data were not in conflict with contemporary estimates of the Hubble time, and they were also consistent with the rapid-collapse (~ 10^8 yr) formation of the Milky Way halo, as proposed by Eggen, Lynden-Bell & Sandage (1962). Globular clusters had thus acquired a prominent role both for cosmology and for theories of galaxy formation. The new perspective also brought questions about cluster and star formation in the primordial Universe, and about survival mechanisms against internal and external disruption processes.

A uniform database of metallicities

The determination of absolute ages requires knowledge of cluster distances, which are difficult to obtain because of the paucity in the solar vicinity of population II standard candles that can be calibrated via parallax. Relative ages are comparatively easier to obtain, and therefore many studies after Sandage tried to uncover the age distribution of Galactic globular clusters, with mixed results. The situation was reviewed by Stetson, van den Bergh & Bolte (1996), who concluded that "as of the current date the state of the field is still somewhat muddled", but also hoped that "data now being collected by numerous groups in various sub-disciplines may resolve the remaining controversy within a few years". The controversy arose in considerations of whether there was an age spread, or a majority of coeval clusters plus a few younger ones with possible extragalactic origin. To settle the question, a large, homogeneous and high quality photometric database of CM diagrams was needed, a task that was becoming possible at that time thanks to the introduction of charge coupled devices (CCDs) as detectors into astronomical instrumentation.

With these detectors, errors better than 0.01 magnitudes could be achieved at the cluster turnoff, which opened the way to comparing the position of that feature — relative to the red giant branch or the horizontal branch — in many different clusters, with sufficient accuracy to detect age differences of the order of 0.5 Gyr. Because of the small format of those early CCD chips, the fast, post-turnoff phases of stellar evolution (the horizontal branch in particular) could not be well sampled, so the photometric colour of the turnoff relative to the giant branch became the easiest parameter to be measured. The combination of all these ideas was behind the Rosenberg et al. (1999) study, which was based on a homogeneous photometric database for 35 clusters, assembled with the 91-centimetre Dutch telescope at La Silla and the 1-metre Johannes Kapteyn Telescope (JKT) at La Palma. The conclusion was that most globular clusters were formed in a single epoch, but a few objects were clearly formed at later stages. Meanwhile Ortolani et al. (1995) had also found that the Bulge is coeval with the oldest Halo clusters. This is consistent with recent simulations of the formation of the Galaxy which find that up to 80 % of the Milky Way could have been formed *in situ* (e.g., de Rossi et al., 2009).

Notwithstanding the success of relative age studies, they still suffer from one major problem: in addition to its age, the luminosity and colour of a star at the turnoff depend on its metallicity, so a key input to relative age studies is a metallicity compilation that is also homogeneous. Rosenberg et al. (1999) could take their [Fe/H] values from Rutledge et al. (1997), which was based on homogeneous measurements of the equivalent widths (EW) of the Ca II infrared triplet lines. The photometric data were collected in the *V*- and *I*-bands because it had been shown empirically that the *V*–*I* colour difference is much less sensitive to [Fe/H] than the *B*–*V* one (Saviane et al., 1997). However homogeneous [Fe/H] values are available for only a fraction of clusters, a fact that was one of the main motivations for our project.

The current state of [Fe/H] data is summarised in Figure 2 and in Table 1. The largest homogeneous spectroscopic sample of individual stars is still that of Rutledge et al. (1997) and if we add the clusters of Saviane et al. (2012) then we find that ~ 55% of objects have a metallicity measurement based on the same index (the "reduced" equivalent width of the Ca II infrared triplet). We then have to move to integrated-light spectroscopy, to the samples of ZW84 and AZ88 (see Table 1). They are based on the equivalent widths of various metallic lines (Ca II K line, *G*-band and Mg I triplet), and of the Ca II infrared triplet, respectively. After excluding objects in common with the

Table 1. Major metallicity compilations. For each reference, NP and NC are the number of programme clusters, and the number of clusters with [Fe/H] homogenised on the same scale. The fifth column lists whether (r)esolved stars or (i)ntegrated light was studied.

Reference	Acronym	NP	NC	i/r	Method
Searle, L. & Zinn, R. 1978, ApJ, 225, 357	SZ78	19	–	r	Mean of reddening-free magnitudes for seven bands
Zinn, R. 1980, ApJS, 42, 19	Z80	79	84	i	Reddening-independent colour quotient Q_{39}
Zinn, R. & West, M. J. 1984, ApJS, 55, 45	ZW84	60	121	i	EW of Ca II K line, *G*-band, Mg I triplet
Armandroff, T. E. & Zinn, R. 1988, AJ, 96, 92	AZ88	27	–	i	EW of Ca II infrared (IR) lines
Rutledge, G. A. et al. 1997, PASP, 109, 907	RHS97	52	70	r	EW of Ca II IR lines
Carretta, E. et al. 2009, A&A, 508, 695	C09	19	133	r	EW of Fe lines in medium-resolution spectra
Harris, W. E. 2010, arXiv, 1012.3224	H10	157	–	–	Average of literature

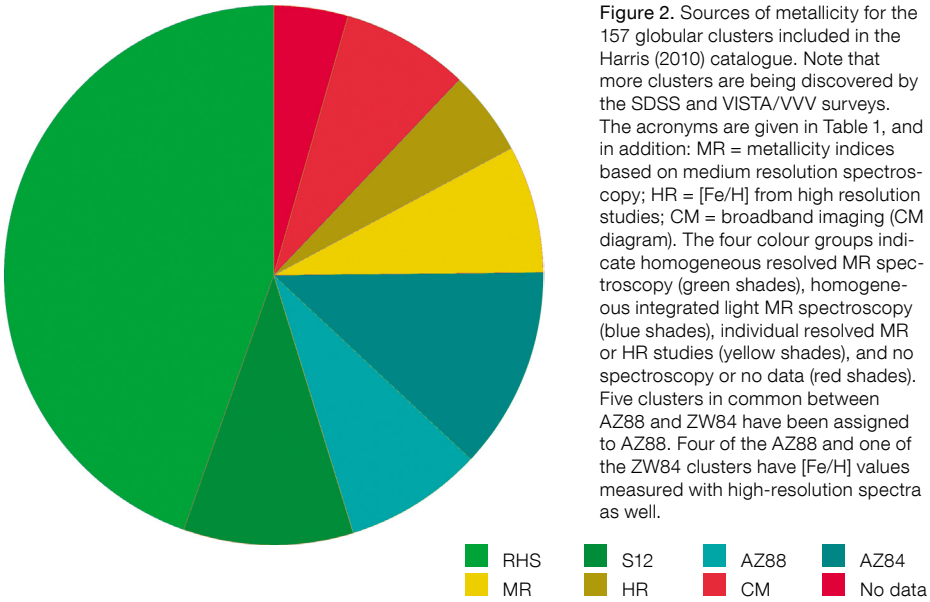

Figure 2. Sources of metallicity for the 157 globular clusters included in the Harris (2010) catalogue. Note that more clusters are being discovered by the SDSS and VISTA/VVV surveys. The acronyms are given in Table 1, and in addition: MR = metallicity indices based on medium resolution spectroscopy; HR = [Fe/H] from high resolution studies; CM = broadband imaging (CM diagram). The four colour groups indicate homogeneous resolved MR spectroscopy (green shades), homogeneous integrated light MR spectroscopy (blue shades), individual resolved MR or HR studies (yellow shades), and no spectroscopy or no data (red shades). Five clusters in common between AZ88 and ZW84 have been assigned to AZ88. Four of the AZ88 and one of the ZW84 clusters have [Fe/H] values measured with high-resolution spectra as well.

cited studies, these two datasets comprise 8 % and 12 % of clusters, respectively. No other homogeneous datasets exist: 12 % of clusters have medium or high-resolution spectroscopic data of resolved stars from a variety of sources, and for another ~ 8 % the metallicity estimate comes from their CM diagram. Finally there are a handful of objects for which no [Fe/H] data exist.

Rutledge et al. (1997) obtained their spectra with the modest 2.5-metre Dupont telescope at Las Campanas, so homogeneous [Fe/H] data are missing mostly for outer halo or heavily extincted clusters. As relative age studies include more and more outer halo objects, we are forced to take metallicities from a variety of sources. For example Marín-Franch et al. (2009) based their study on the largest homogeneous photometric sample of Galactic globular clusters (64 objects), but for as many as 25 % of them they had to estimate [Fe/H] from the Zinn & West (1984) compilation of the reddening-independent Q_{39} photometric index. To summarise, for almost half of GCs, the metallicity values are based on data that are either not spectroscopic, not homogeneous or not of individual stars. Furthermore, even when all these conditions are satisfied, the number of stars measured might be too small to look for metallicity dispersions, precisely the area where globular clusters started to show the first surprises.

When the first CM diagrams of main sequence stars based on CCD imaging appeared, they showed a virtually zero-width locus, confirming the visual impression of a smooth, single-age stellar population. However as more and more data accumulated, things started to look less simple. In particular, abundance variations have been found for light elements in all clusters that have been searched so far (see the very recent review of Gratton et al. [2012]). In addition, a spread in one or more of iron-peak, n-capture, and α elements has also been found for ω Cen, M54, M22, NGC 1851, NGC 2419, Terzan 5 and NGC 5824. This is particularly interesting because it is direct evidence for extended star formation in these clusters. In three of these seven objects the spread was discovered or confirmed from our FORS2 project.

Improving the situation

In May 2006 we had two observing nights assigned to us at the VLT, to collect medium-resolution FORS2 spectra for globular clusters whose distance modulus is too large for high-resolution studies, either because of distance or high extinction. The weather did not help us very much, so of the 49 planned targets we could observe only twenty, plus eight calibrators. To increase observing efficiency we used the multi-object capability of FORS2: the maximum slit density can be reached with the mask exchange unit, however the lengthy operations of mask manufacture and insertion meant that only a few objects per night could have been observed. Therefore we opted for the configurable slits solution, and left the masks for the most compact objects.

All data were reduced with the FORS2 pipeline (Izzo et al., 2010) which delivers wavelength-calibrated, sky-subtracted spectra in an extremely efficient manner; organising the data took more time than reducing them. On the other hand because of the high crowding typical of globular clusters, often more than one star per slit was extracted, so a major part of the work was to cross-check the identification of the ~ 600 spectra. Cluster members were identified as objects with both radial velocity and reduced equivalent widths not deviating significantly from the average, taking into account that uncertainties in our mean velocities are of order 5–6 km/s. The fraction of stars that were eventually confirmed as members varies significantly from cluster to cluster, with a median value of 53 % and being always better than 20 %. Especially for bulge clusters where field contamination is high, the catalogues of member stars for follow-up high-resolution studies is another useful byproduct of our work.

The equivalent widths of calcium lines in red giant stars depend on the Ca abundance and also on their luminosity, so this dependency was removed by adding a linear term in $V–V_{HB}$ and obtaining the "reduced" equivalent width. A calibration relation from such reduced equivalent widths to the scale (Carretta et al., 2009) was then obtained, with 14 clusters having well-determined [Fe/H] values by high-resolution studies. It was then applied to convert the reduced equivalent widths of programme clusters into metallicity values. These new [Fe/H] values are significantly different from literature values for about half of our programme clusters, as graphically illustrated by Figure 3, which shows a type of diagram first introduced by Zinn (1993). Our new average abundances are lower than literature values for six clusters (Pyxis, Terzan 3, HP1, NGC 7006, NGC 6569 and

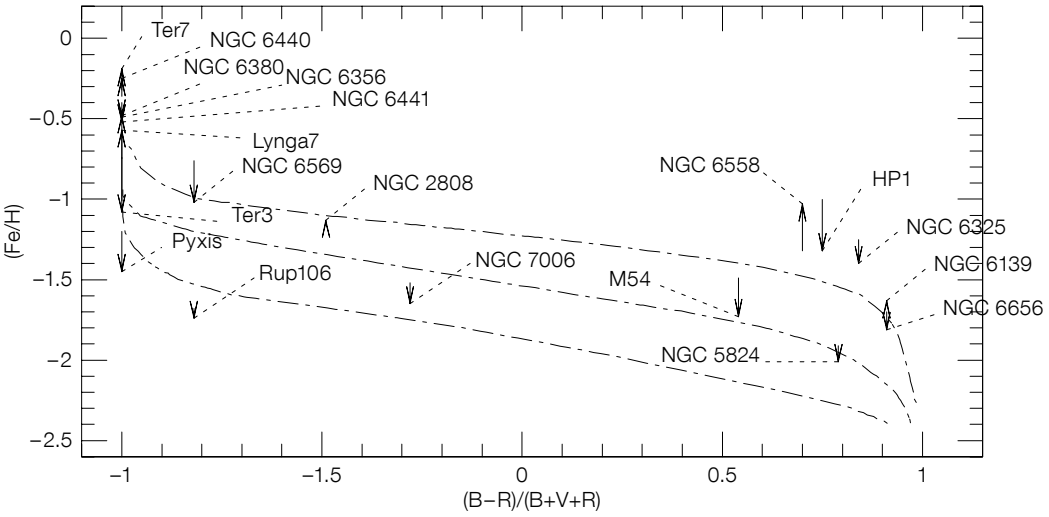

Figure 3. The metallicity of our programme clusters on the Carretta et al. (2009) scale is plotted here against horizontal branch (HB) type. Isochrones are from Rey et al. (2001), and are separated by 1.1 Gyr, with age decreasing from top to bottom. The oldest isochrone gives the age of clusters at $R < 8$ kpc (Rey et al., 2001). The arrows connect the position of the cluster, if [Fe/H] from Harris (2010) is used, to the position given by our metallicity value.

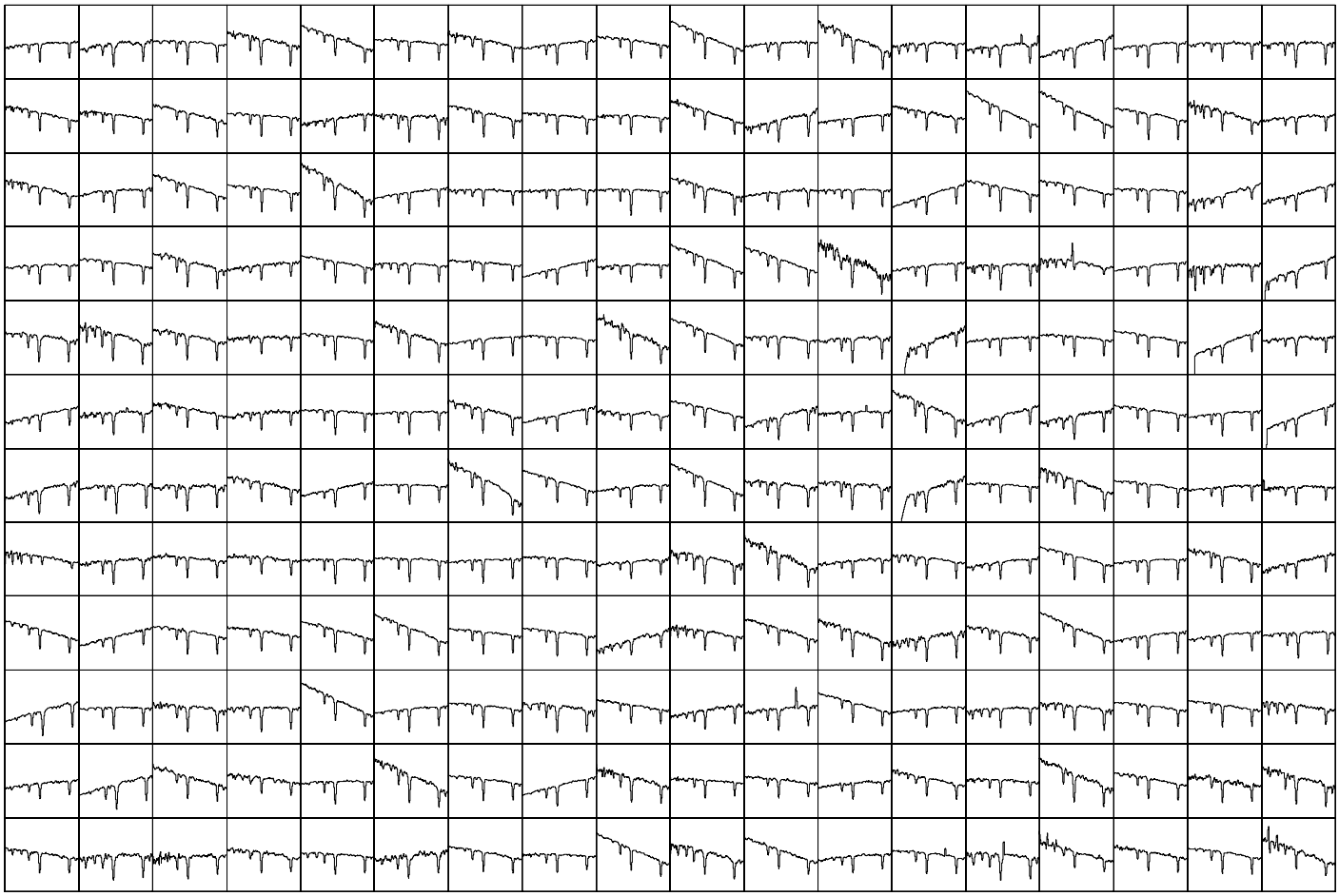

Figure 4. The 216 useful spectra of NGC 5824 and foreground stars taken with FORS2 in the calcium triplet region (840–870 nm). The three most prominent lines belong to the Ca II ion, with wavelengths of 849.8, 854.2 and 866.2 nm.

NGC 6715), so to retain their horizontal branch (HB) morphology they must be younger. The higher abundances of Lynga 7, NGC 6558 and NGC 6380 suggest instead older ages. Zinn had introduced the diagram of Figure 3 to see whether the age distribution of Galactic clusters would support the extended halo formation proposed by Searle & Zinn (1978). In this scenario, our [Fe/H] revision would bring more clusters into the "young halo" class, however the HB morphology depends also on the mass loss along the red giant branch (RGB) and the helium abundance, so the conclusion will have to be confirmed with precise turnoff photometry.

The second finding of our project is that, for three clusters, the dispersion of reduced equivalent widths is larger than the measurement error. We thus confirmed the [Fe/H] dispersion of M54 and discovered a metallicity dispersion in M22 (in parallel with Marino et al. [2009]) and probably in NGC 5824. The metallicity distribution of M22 (NGC 6656) has been discussed in Da Costa et al. (2009), where it was found to range from –2.2 to –1.2 dex, and to share many properties with those of ω Cen, including a fast rise to a peak and a broad tail to higher abundances. M22 could be well characterised because three FORS2 masks were dedicated to this cluster (41 member stars), while the small number of stars did not allow us to perform a similar detailed analysis for NGC 5824; we could only estimate a value ≈ 0.11–0.14 dex for its dispersion. However with observations carried out both at Gemini and at the VLT in period 87, we were able to collect spectra for a couple of hundred stars, of which more than a hundred were confirmed as cluster members. The data analysis is in progress, but the new data seem to confirm the presence of a metallicity spread. Figure 4 shows a montage of all useful spectra extracted with the FORS2 pipeline.

Outlook

The discovery of metallicity dispersions was greatly advanced by the advent of multiplexing spectrographs at 8–10-metre class telescopes, but the other important breakthrough in globular cluster research could only have been achieved with the Hubble Space Telescope (HST). By measuring stellar magnitudes on archival Wide Field Planetary Camera 2 (WFPC2) images with his specialised software, Anderson (2002) discovered that the main sequence of ω Cen is split in two. Multiple stellar populations were subsequently discovered in many other clusters, including those having metallicity dispersions. The latter are also among the most massive in the Galaxy, and some of them appear to be associated with stellar streams: M54 (M_V = –10.0) is clearly the nuclear star cluster of the Sagittarius dwarf galaxy, which is currently being tidally disrupted by the Milky Way, and NGC 1851 (M_V = –8.3) is surrounded by an extensive stellar halo that may have resulted from the destruction of the dwarf galaxy in which the cluster was once embedded (Olszewski et al., 2009).

Theoreticians have been able to simulate ω Cen as the nuclear remnant of a disrupted dwarf galaxy (Bekki & Freeman, 2003) and Newberg et al. (2009) have suggested that NGC 5824 (M_V = –8.8) may be associated with the newly discovered Cetus Polar Stream (CPS). The nuclear cluster scenario is quite appealing because it would offer an explanation for the peculiarities illustrated above. If a cluster is located in a deep potential well inside a dwarf galaxy, it might be able to retain or to accrete gas, thus forming multiple generations of stars or developing chemical anomalies. It is also interesting to note that both M54 and NGC 5824 lie on the same young isochrone in Figure 3, and that stars in the nuclei of early-type dwarf galaxies tend to be younger than the underlying population (e.g., Monaco et al. 2009; Paudel et al., 2011). It should be added that metallicity spreads might be explained by other mechanisms (e.g., merging clusters with different [Fe/H]), and for these we refer to Gratton et al. (2012).

In a bigger picture, finding evidence of disrupting satellites in the Galactic Halo has great significance for the current Lambda Cold Dark Matter galaxy formation paradigm. In this scheme, the Galaxy is built up through the merger and accretion of lower mass systems, predominantly at early epochs. Indeed, while the spatial and kinematic signatures of this process have been erased in the inner parts of the Galaxy, in its halo where dynamical times are long, several stellar streams have been identified in the past. There is however still an order of magnitude discrepancy between the large number of predicted satellites in the Milky Way and the observed ones. Any addition of a new remnant is therefore important to confirm the paradigm.

Under the working hypothesis that clusters with metallicity spreads signpost halo substructures, we have been assigned more than 13 hours of additional FORS2 time in period 89 to extend our sample, and potentially to find still more unknown examples of these peculiar stellar systems.

Acknowledgements

The completion of this project was significantly fostered by visits of two members of the collaboration to Padova and ESO. We warmly thank the ESO Director General Discretionary Fund for supporting them.

References

Anderson, J. 2002, ASP Conf. Series, 265, eds. F. van Leeuwen, J. D. Hughes, G. Piotto, 87
Arp, H. C., Baum, W. A. & Sandage, A. R. 1953, AJ, 58, 4
Bekki, K. & Freeman, K. C. 2003, MNRAS, 346, L11
Da Costa, G. S. et al. 2009, ApJ, 705, 1481
de Rossi, M. E. et al. 2009, MNRAS, 395, 210
Eggen, O. J., Lynden-Bell, D. & Sandage, A. R. 1962, ApJ, 136, 748
Gratton, R. G., Carretta, E. & Bragaglia, A. 2012, A&A Rev., 20, 50
Izzo, C. et al. 2010, Proc. SPIE, 7737, 773729
Marín-Franch, A. et al. 2009, ApJ, 694, 1498
Marino, A. F. et al. 2009, A&A, 505, 1099
Monaco, L. et al. 2009, A&A, 502, L9
Newberg, H. J., Yanny, B. & Willett, B. A. 2009, ApJ, 700, L61
Olszewski, E. W. et al. 2009, AJ, 138, 1570
Ortolani, S. et al. 1995, Nature, 377, 701
Paudel, S., Lisker, T. & Kuntschner, H. 2011, MNRAS, 413, 1764
Rey, S.-C. et al. 2001, AJ, 122, 3219
Rosenberg, A. et al. 1999, AJ, 118, 2306
Sandage, A. 1970, ApJ, 162, 841
Saviane, I. et al. 2012, A&A, 540, A27
Saviane, I., Rosenberg, A. & Piotto, G. 1997, in *Stellar Ecology: Advances in Stellar Evolution*, eds. R. T. Rood & A. Renzini, 65
Searle, L. & Zinn, R. 1978, ApJ, 225, 357
Stetson, P. B., van den Bergh, S. & Bolte, M. 1996, PASP, 108, 560
Wilson, R. N. 2004, *Reflecting Telescope Optics I. Basic Design Theory and its Historical Development*, 2nd edn. (Springer)

Stellar Populations of Bulges in Galaxies with Low Surface-brightness Discs

Lorenzo Morelli[1,2]
Enrico Maria Corsini[1,2]
Alessandro Pizzella[1,2]
Elena Dalla Bontà[1,2]
Lodovico Coccato[3]
Jairo Méndez-Abreu[4,5]
Mary Cesetti[1,2]

[1] Dipartimento di Fisica e Astronomia, Università di Padova, Italy
[2] INAF–Osservatorio Astronomico di Padova, Italy
[3] ESO
[4] Instituto Astrofísico de Canarias, La Laguna, Spain
[5] Departamento de Astrofísica, Universidad de La Laguna, Spain

The radial profiles of the age, metallicity and α/Fe enhancement of the stellar populations in the bulge-dominated region for a sample of eight spiral galaxies with low surface-brightness stellar discs and bulges are presented. Almost all the sample bulges are characterised by young stellar populations, solar α/Fe enhancements and metallicities spanning from high to sub-solar values. No significant gradient in age and α/Fe enhancement is measured, whereas a negative metallicity gradient is found in a few cases. The stellar populations of the bulges hosted by low surface-brightness discs share many properties with those of high surface-brightness galaxies and are therefore likely to have common formation scenarios and evolution histories.

Galaxies with a central face-on surface brightness fainter than 22.6 mag per square arcsecond in the *B*-band are classified as low surface-brightness (LSB) systems. Although LSB galaxies are more difficult to identify than high-surface brightness (HSB) galaxies, they are not a niche phenomenon in galactic astrophysics. They constitute up to 50 % of the disc galaxy population and, consequently, they represent one of the major baryonic repositories in the Universe. LSB galaxies are characterised by different morphologies (ranging from dwarf irregulars to giant spirals) and they cover a wide range of colours which suggests that they can follow a variety of evolutionary paths (Bothun et al., 1997).

The typical gas surface density of LSB discs is below the critical threshold necessary for star formation, despite the fact that they have a higher content of neutral hydrogen than their HSB counterparts (Galaz et al., 2006). This inability to condense atomic gas into molecular gas results in a very low star formation rate and in a significantly slower evolution of the galaxy. Although most LSB galaxies are bulgeless, there are also galaxies with an LSB disc and a significant bulge component. It is not known whether these bulges are similar to those of HSB galaxies and whether their properties depend on the LSB nature of their host discs.

Invaluable pieces of information that help us to understand the processes of formation and evolution of bulges in LSB galaxies are imprinted in their stellar populations. The central values and radial profiles of age, metallicity and α/Fe enhancement of the stellar component can be used to test the predictions of theoretical models, as has already been done for the bulges of HSB galaxies (Sánchez-Blázquez et al., 2006; Annibali et al., 2007).

Gas dissipation toward the galaxy centre, with subsequent star formation and galactic winds, produces a gradient in the radial profile of metallicity. Therefore, a metallicity gradient is expected in bulges formed by monolithic collapse (Kobayashi, 2004), while the metallicity gradient is expected to be very shallow (or even absent) in bulges built by merging (Bekki & Shioya, 1999). Mergers of gas-poor galaxies mix up the galactic stars, erasing the pre-existing population gradients, and only rarely is the metallicity gradient enhanced by the secondary events of star formation, which eventually occur in mergers of gas-rich objects. If this latter occurs, a clear signature can be observed in the age radial profile for several Gyr (Hopkins et al., 2009). The predictions for bulges assembled through long timescale processes, such as the dissipationless secular evolution of the disc component, are more controversial. According to this scenario, the bulge is formed by the redistribution of disc stars and the gradients that are eventually produced in the progenitor disc could either be amplified, because the resulting bulge has a smaller scalelength than the disc, or could be erased as a consequence of disc heating (Moorthy & Holtzman, 2006).

We present a detailed photometric and spectroscopic study of a sample of eight bulges in LSB discs recently published by Morelli et al. (2012). The analysis of the spectral absorption lines has allowed us to derive the age and metallicity of the stellar populations and to estimate the efficiency and timescale of the last episode of star formation in order to distinguish between the early rapid assembly and late slow growth of the bulge.

Sample selection, surface photometry and long-slit spectroscopy

All the galaxies in this study were selected to be spiral galaxies with a bulge and an LSB disc. The final sample is comprised of eight LSB spiral galaxies, with morphological types ranging from Sa to Sm, including some barred galaxies. The LSB nature of their discs has been confirmed by a detailed photometric decomposition. With this aim, we derived the photometric parameters of the bulge and disc by applying a detailed decomposition of the surface brightness of the galaxy. We adopted the galaxy surface photometric 2D (GASP2D) code by Méndez-Abreu et al. (2008, see Figure 1). The structural parameters of the galaxies were derived assuming the galaxy surface-brightness distribution to be the sum of the contributions of a bulge, a disc and, if necessary, a bar. We fitted iteratively the model of the surface brightness to the pixels of the galaxy image using a nonlinear least squares minimisation.

The photometric and spectroscopic observations were carried out with the Very Large Telescope (VLT) during several runs between 2001 and 2008 with FORS2. For each galaxy the images were obtained with the R_special+76 filter and long-slit spectra on the major and minor axes were usually taken using the

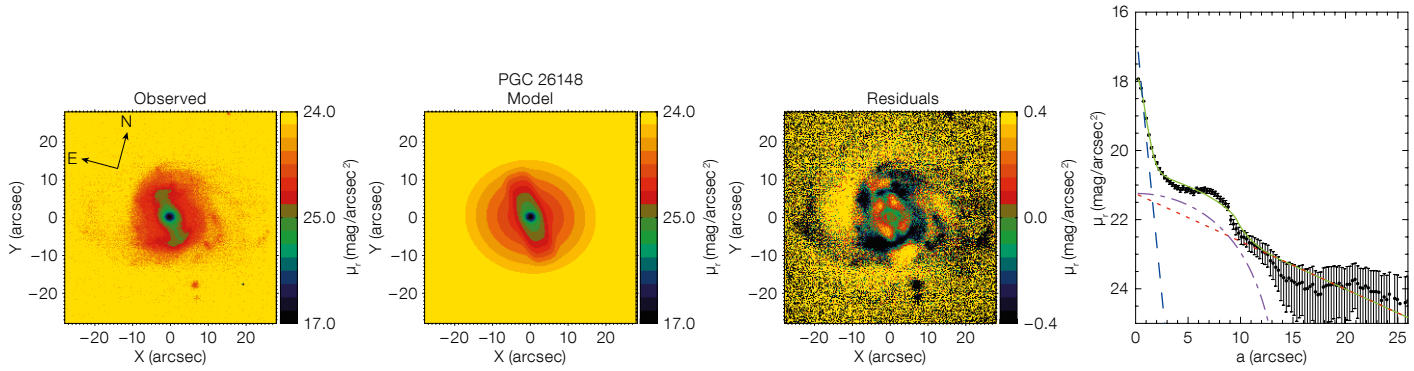

Figure 1. Two-dimensional photometric decomposition of PGC 26148. The FORS2 *r*-band image, best-fitting image, residual (i.e. observed-model) image and surface-brightness radial profile are shown (panels from left to right). The righthand panel shows the ellipse-averaged radial profile of the surface brightness measured from FORS2 (dotted line) and model image (green solid line). The dashed blue, dash-dotted purple, and dotted red lines represent the intrinsic surface-brightness radial profiles of the bulge, bar and disc, respectively.

grism GRIS_1400V+18 in combination with a 0.7-arcsecond slit that guarantees an instrumental velocity resolution of 33 km/s at 5000 Å.

The stellar kinematics were measured from the galaxy absorption features present in the wavelength range centred on the Hβ and Mg I lines by applying the gas and absorption line fitting (GANDALF; Sarzi et al., 2006) IDL package, adapted for dealing with the FORS2 spectra. The Mg, Fe and Hβ line-strength indices were measured from the flux-calibrated spectra of the eight sample galaxies following Morelli et al. (2004). We also measured the average iron index <Fe> = (Fe5270 + Fe5335)/2 and the combined magnesium–iron index [MgFe]' = $[Mg_b\ (0.72 \times Fe5270 + 0.28 \times Fe5335)]^{1/2}$ (Thomas et al., 2003). To account for the contamination of the Hβ line-strength index by the Hβ emission line, the Hβ index was measured from the galaxy spectrum after subtracting the contribution of the Hβ emission line.

Properties of the stellar populations in the central regions

The models of Thomas et al. (2003) predict the values of the line strength Lick indices for a single stellar population as a function of the age, metallicity and [α/Fe] ratio. The central values of the velocity dispersion, Mg_b, Mg_2, Hβ, <Fe>, and [MgFe]' were obtained by a weighted mean of all the measured data points within an aperture of radius 0.3 r_e for all the available spectra. From the central

Figure 2. Distribution of the central values of the Hβ and [MgFe]' indices (left panel) and the <Fe> and Mgb indices (right panel) measured over an aperture of 0.3 r_e for the sample galaxies. The lines indicate the models of Thomas et al. (2003). In the left panel, the age–metallicity grids are plotted with two different α/Fe enhancements: [α/Fe] = 0.0 dex (solid lines) and [α/Fe] = 0.5 dex (dashed lines). In the right panel, the [α/Fe] ratio–metallicity grids are plotted with two different ages: 2 Gyr (solid lines) and 6 Gyr (dashed lines). The green points are the values obtained for three LSB galaxies by Bergmann et al. (2003).

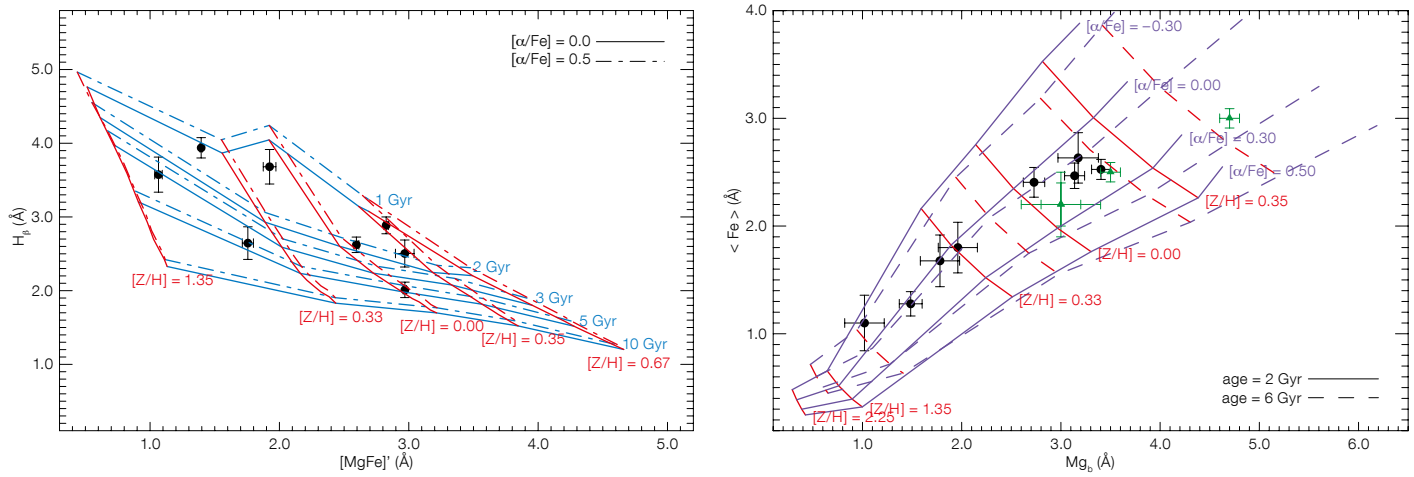

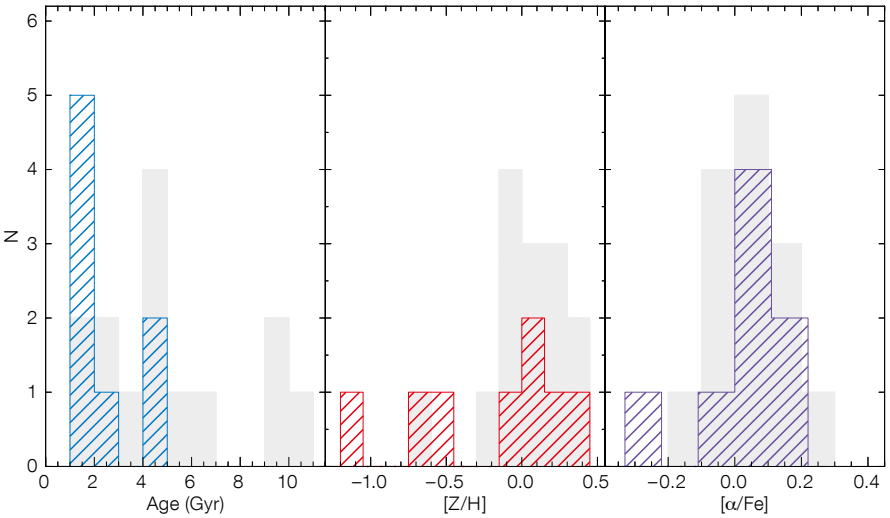

Figure 3. Distribution of the mean age (lefthand panel), total metallicity (central panel), and total α/Fe enhancement (righthand panel) for the stellar populations of the bulges of the sample galaxies. The distributions of the same quantities obtained by Morelli et al. (2008) for the bulges of HSB discs are plotted in grey for comparison.

values of the Lick indices we derived the mean age, total metallicity and total α/Fe enhancement of the stellar population in the central region of the bulge of the sample galaxies (see Figure 2).

The bulges are characterised by a very young stellar population, with a distribution of ages peaking at a value of 1.5 Gyr. They are characterised by ongoing star formation, confirming previous studies of a few LSB galaxies (Bergmann et al., 2003). The metallicity of the sample bulges spans a large range of values from high values ([Z/H] = 0.30 dex) to sub-solar metallicity ([Z/H] = –1.0 dex). Most display solar α/Fe enhancements. These properties closely resemble the properties of the bulges hosted in HSB galaxies (Figure 3) and they suggest a formation mechanism with a dissipative collapse with a short star formation timescale.

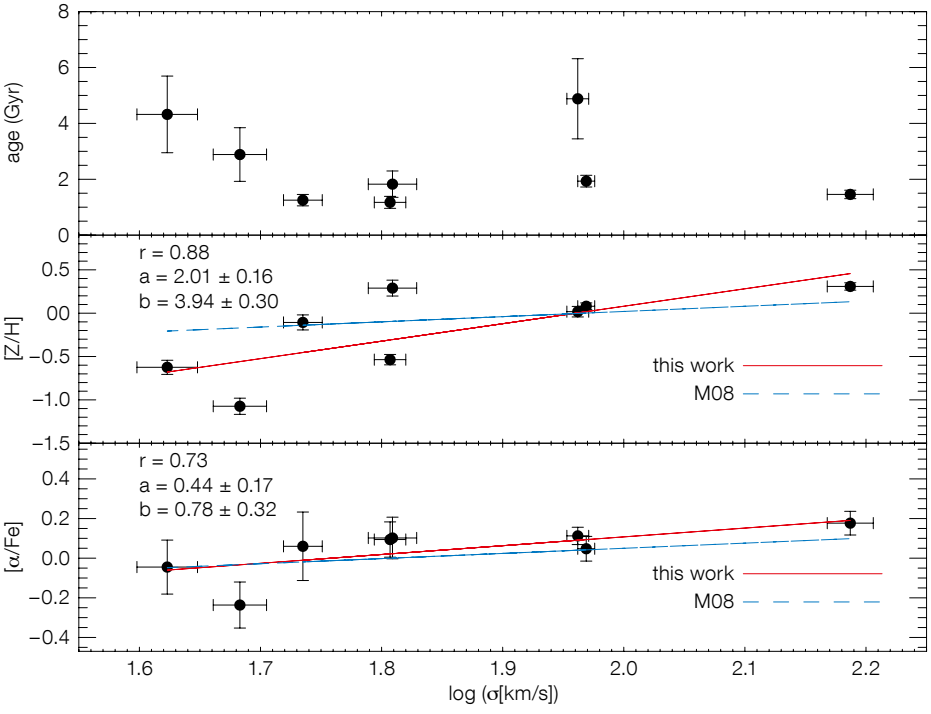

Figure 4. Mean age (upper panel), total metallicity (middle panel), and total α/Fe enhancement (lower panel) of the stellar populations of the bulges of the sample galaxies as a function of the central velocity dispersion. In each panel, the red solid and blue dashed lines represent the linear regression through the data points and the correlation found by Morelli et al. (2008) for the bulges of HSB galaxies, respectively. The Pearson correlation coefficient (*r*) and the coefficients of the linear fit are given.

For galaxies with sub-solar values of α/Fe enhancement, other mechanisms of bulge formation, such as the redistribution of disc material, because of the presence of a bar, or environmental effects need to be considered. The case of the bulge of ESO-LV 4880490 is particularly intriguing. The bulge of this barred galaxy has an intermediate age (3 Gyr), low metallicity, ([Z/H] = –1.07 dex) and sub-solar α/Fe ratio ([α/Fe] = –0.24 dex). These properties are consistent with a slow build-up within a scenario of secular evolution driven by the bar.

The correlation between the galaxy morphological type and the properties of the bulge stellar population is indicative of the possible interplay between the evolution of the bulge and disc. Thomas & Davies (2006) did not observe any correlation between the age and metallicity of the stellar population and galaxy morphology of the bulge, whereas Ganda et al. (2007) and Morelli et al. (2008) found a mild correlation, with early-type galaxies (S0–S0a) being older and more metal-rich than spiral galaxies (Sa–Sc). Because the above relationships are mostly driven by early-type galaxies, which are lacking in our sample, we do not observe any correlation between the galaxy morphological type (Sab–Sm) and the age, metallicity and α/Fe enhancement of our bulges. Nevertheless, we can exclude a strong interplay between the bulge and disc components.

In early-type galaxies and in the bulges of HSB galaxies the metallicity and α/Fe enhancement are well correlated with the central velocity dispersion. We find that

also for LSB galaxies the metallicity and α/Fe enhancement correlate with velocity dispersion (Figure 4) and this correlation is consistent with the results obtained in Morelli et al. (2008).

These relations are explained by chemo-dynamical models and cosmological hydrodynamic simulations of ellipticals and bulges as the result of a mass-dependent star formation efficiency. Low-mass galaxies have a lower efficiency in converting gas-phase metals into new stars, and this gives rise to a prolonged period of star formation and to lower α/Fe ratios. Our results suggest that this is also true for the bulges of LSB galaxies. We conclude that the most massive bulges of our sample galaxies are more metal-rich, and that they are characterised by shorter star formation timescales.

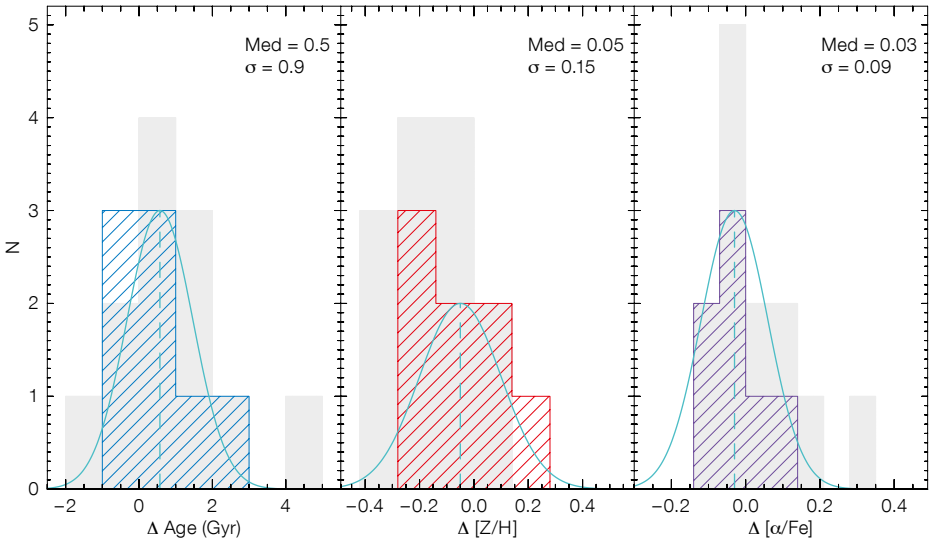

Figure 5. Distribution of the gradients of age (lefthand panel), metallicity (central panel), and α/Fe enhancement (righthand panel) for the sample bulges. The dashed line represents the median of the distribution and its value is reported. The solid line represents a Gaussian centred on the median value of the distribution, with σ reported. The distribution of the same quantities obtained by Morelli et al. (2008) for the bulges of HSB discs is shown in grey for comparison.

Properties of the stellar populations in the bulge region

The contamination of the bulge light by the contribution coming from the underlying disc stellar component is a well-known problem that deserves particular care. To reduce the impact of this effect in the derived stellar population properties as much as possible, we evaluated the gradient inside r_{bd}, the radius where the bulge and disc give the same contribution to the total surface brightness (Morelli et al., 2008). This did not completely remove the contaminations, but it always ensured a similar degree of contamination when comparing the gradients of different galaxies. For each galaxy, we have derived the Mg_2, Hβ, and <Fe> line-strength indices at the radius r_{bd}.

The corresponding ages, metallicities and α/Fe enhancements were derived by using the stellar population models of Thomas et al. (2003), as for the central values. The gradients of the properties of the bulge stellar population were derived from the values of age, metallicity and α/Fe enhancement in the radial range out to r_{bd}. All the sample bulges show no age gradient within the error bars, except for ESO-LV 2060140 and PGC 26148, which are characterised by a shallow gradient. In spite of the peak at Δ([Z/H]) = –0.15, the median of the number distribution of the metallicity gradients is consistent with Δ([Z/H]) = 0 (see Figure 5, middle panel). Also, the number distribution of the gradients of α/Fe enhancements has a median Δ[α/Fe] = 0 (Figure 5, righthand panel). In all the observed distributions, most of the deviations from the median values can be explained as a result only of the errors in the estimates of the gradients. The absence of significant age and α/Fe gradients is in agreement with the earlier findings for early-type galaxies and bulges of unbarred and barred HSB galaxies. However, negative gradients of metallicity are observed in the radial profiles of many early-type galaxies and in the bulges of HSB galaxies.

In the models, the presence of a negative metallicity gradient predicts a formation scenario of the bulges in LSB galaxies via dissipative collapse, when a strong interplay between the star formation timescale and gas flows is taken into account in order to explain the absence of any α/Fe gradient (Pipino et al., 2008). However, pure dissipative collapse cannot explain the formation of all the sample bulges; other phenomena, such as mergers or acquisition events, need to be invoked to account for the formation of those bulges that do not show any metallicity gradient. The metallicity gradients are plotted as a function of the metallicity in the galaxy centre in the lefthand panel of Figure 6. Only the bulges of LSB galaxies with higher metallicity (–0.1 < [Z/H] < 0.4) are consistent with the correlation found by Morelli et al. (2008) for the bulges in HSB galaxies and early-type galaxies, respectively. This is not the case for the few remaining bulges with a very low central metallicity value (–1.1 < [Z/H] < –0.5). If confirmed with more firm statistics, such a result would favour the importance of dissipative collapse in the assembly of bulges (Arimoto & Yoshii, 1987).

No correlation has been found between the central value and gradient of α/Fe enhancement (see the righthand panel of Figure 6). This is in agreement with earlier findings for early-type galaxies and spiral galaxies, and it is expected because of the absence of gradients in the α/Fe radial profiles of the sample galaxies.

The common nature of bulges in LSB and HSB galaxies

We have highlighted the fact that bulges hosted by LSB galaxies share many structural and chemical properties with the bulges of HSB galaxies. Such a similarity suggests that they possibly had common formation scenarios and evolu-

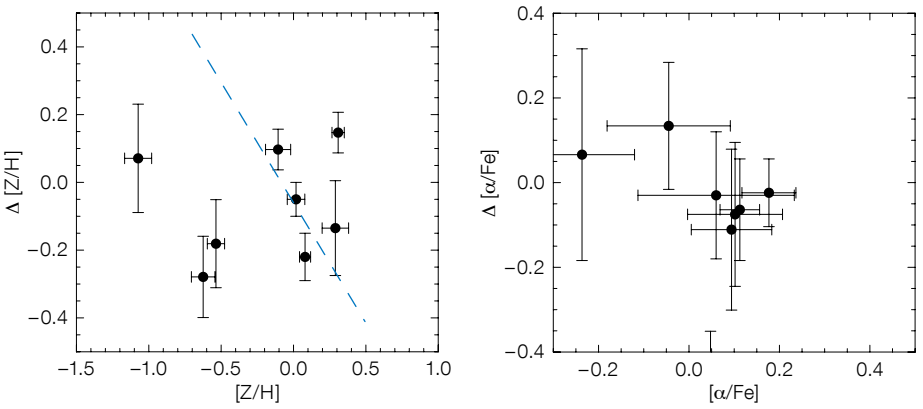

Figure 6. Gradient and central value of metallicity (lefthand panel) and α/Fe enhancement (righthand panel) for the sample bulges. In the lefthand panel, the dashed blue line represents the linear regression obtained for the bulges of HSB galaxies by Morelli et al. (2008).

tion histories. Our findings are in agreement with, and also extend, the previous results inferred by McGaugh, Schombert & Bothun (1995) and Beijersbergen et al. (1999), who compared the photometric properties of the bulges of LSB and HSB galaxies, and by Coccato et al. (2008), who performed a detailed analysis of the kinematical and mass distribution properties of the bulge of the LSB galaxy ESO 323-G064. The fact that bulges hosted in galaxies with very different discs are remarkably similar, rules out significant interplay between the bulge and disc components and provides further support for earlier findings (Thomas & Davies, 2006; Morelli et al., 2008). In order to provide a definite confirmation, this prediction requires a detailed comparison between the properties of the stellar populations of both bulges and discs in LSB galaxies.

References

Annibali, F. et al. 2007, A&A, 463, 455
Arimoto, N. & Yoshii, Y. 1987, A&A, 173, 23
Beijersbergen, M., de Blok, W. J. G. & van der Hulst, J. M. 1999, A&A, 351, 903
Bekki, K. & Shioya, Y. 1999, ApJ, 513, 108
Bergmann, M. P., Jørgensen, I. & Hill, G. J. 2003, AJ, 125, 116
Bothun, G., Impey, C. & McGaugh, S. 1997, PASP, 109, 745
Coccato, L. et al. 2008, A&A, 490, 589
Galaz, G. et al. 2006, AJ, 131, 2035
Ganda, K. et al. 2007, MNRAS, 380, 506
Hopkins, P. F. et al. 2009, ApJS, 181, 135
McGaugh, S. S. et al. 1995, AJ, 109, 2019
Méndez-Abreu, J. et al. 2008, A&A, 478, 353
Moorthy, B. K. & Holtzman, J. A. 2006, MNRAS, 371, 583
Morelli, L. et al. 2004, MNRAS, 354, 753
Morelli, L. et al. 2008, MNRAS, 389, 341
Morelli, L. et al. 2012, MNRAS, 423, 962
Pipino, A., D'Ercole, A. & Matteucci, F. 2008, A&A, 484, 679
Sánchez-Blázquez, P. et al. 2006, A&A, 457, 809
Sarzi, M. et al. 2006, MNRAS, 366, 1151
Thomas, D., Maraston, C. & Bender, R. 2003, MNRAS, 339, 897
Thomas, D. & Davies, R. L. 2006, MNRAS, 366, 510

ESO and Joe DePasquale

MPG/ESO 2.2-metre telescope and Wide Field Imager colour picture of the isolated spiral galaxy NGC 3621. Broadband (*B* and *V*) and narrowband emission line ([O III] and H-alpha) images were combined and highlight the H II regions and young stars in the spiral arms. NGC 3621 appears to have no bulge and yet its centre harbours an active nucleus; the distance, determined from photometry of Cepheid variable stars, is about 6.2 Mpc. More information can be found in Release 1104.

On the Inside of Massive Galaxies: The Sloan Lens ACS Survey and Combining Gravitational Lensing with Stellar Dynamics and Stellar Population Analysis

Léon Koopmans[1]
Oliver Czoske[2]

[1] Kapteyn Astronomical Institute, Groningen, the Netherlands
[2] Institut für Astrophysik, Universität Wien, Austria

Our understanding of the structure and formation of early-type galaxies (ETGs) is rapidly evolving, but our inability to disentangle stellar mass from dark matter often prevents direct comparison of galaxy formation models with observations without making strong assumptions, such as for the initial mass function (IMF) or dark matter mass fraction and density profile. As an example, the increase in mass-to-light ratio (M/L) along the Fundamental Plane could be partly due to changes in the structure of the ETGs, but also to a change in the ratio of dark versus stellar mass and even to a change in the stellar M/L with galaxy velocity dispersion (by a steepening of the IMF). We report on ongoing efforts to disentangle the structure of early-type galaxies using gravitational lensing, two-dimensional kinematics and stellar population analysis making use of high-resolution images from HST, integral field spectroscopy from VIMOS, and UVB/VIS spectra from X-shooter.

Background

Understanding the internal structure of massive galaxies, the present-day end-products of galaxy formation, as well as their evolution over cosmic time is important for understanding galaxy formation and the physical processes that shape galaxies.

One of the roadblocks in these studies has been the (often) unknown contribution of dark matter to the mass distribution of galaxies. Historically, galaxy dynamics has been the main diagnostic to determine how matter is distributed in galaxies, but even in the local Universe it has been difficult to disentangle the contributions and relative distributions of baryonic matter (stars and gas) and dark matter; the reason being the notorious mass-anisotropy degeneracy inherent in dynamical analyses. This has led to many claims of the presence or absence of dark matter in early-type galaxies (ETGs), although some were based on assumptions that were hard to justify (e.g., orbital (an)isotropy).

In recent years, substantial progress has been made to remedy these issues, in particular using integral field spectroscopy to map the kinematics of galaxies (velocities and velocity dispersions) in two dimensions (e.g., ATLAS^{3D}; COMA). However, studies remain confined to the relatively nearby Universe, where ETGs can be studied in greater detail and out to larger galactic radii than at larger cosmological distances. Studying the cosmological evolution of galaxy structure remains out of reach using kinematic/dynamic techniques alone, at least until the recently approved European Extremely Large Telescope (E-ELT) and its equivalents in the US are completed in ten years time.

At cosmological distances (say $z \gtrsim 0.1$), massive galaxies may act as gravitational lenses on background sources at higher redshifts. Modelling the shape of strongly gravitationally lensed sources has become a powerful new tool to investigate the structure of the lens galaxies. While the total mass within the Einstein radius (typically 5–10 kpc at cosmological distances) can be measured extremely accurately (to a few percent), lensing analysis alone also suffers from degeneracies, notably the mass-sheet degeneracy, that prevent unambiguous determination of the mass profile. In order to break these degeneracies, additional information or a combination of information from several independent methods is required.

Over the past decade, new techniques have been developed that systematically combine strong gravitational lensing with galaxy dynamics to break the mass-sheet and mass-anisotropy degeneracies (see e.g., Koopmans & Treu, 2002; Treu & Koopmans, 2004). The constraints from the two methods are complementary, making their combination particularly powerful in studying galaxy structure. The combination of a lensing analysis with even a single stellar velocity dispersion measurement allows the total mass-density slope at the Einstein radius to be measured with an accuracy of typically better than 5% out to redshifts of $z \sim 1$ (Koopmans & Treu, 2002; Treu & Koopmans, 2002). The reason is that the mass enclosed by the Einstein radius is accurately determined from the lensing constraints, significantly reducing its degeneracy with the orbital anisotropy.

To further and self-consistently combine these methodologies beyond the early techniques, where the only lensing constraint used was the mass of the ETG, Barnabè & Koopmans (2007) developed fully grid-based lensing and two-integral dynamical models that can describe the combined two-dimensional datasets (i.e. the lensed images along with velocity and velocity dispersion fields) without the usual assumption of spherical symmetry or Jeans modelling. The combined lensing/dynamics analysis yields the total mass distribution. The final piece of information to disentangle the relative contributions of dark and stellar matter in galaxies is stellar population modelling of the galaxy spectrum, which yields the mass-to-light ratio of the stars and information on the initial mass function (IMF), enabling the light distribution to be converted to the stellar mass distribution.

Powerful techniques require equally good data and much of the effort going into the development of the methods has been driven by the powerful instrumentation on 8–10-metre-class telescopes. On the VLT, the VIMOS integral field unit (IFU) instrument has provided two-dimensional kinematic data of a large sample of strong lens systems. More recently, X-shooter has provided exquisite spectral data whose broad wavelength coverage is ideal for detailed stellar population analysis.

In this article we describe some results from the Sloan Lens ACS Survey (SLACS; see Figure 1), in particular focusing on the critical contributions of VIMOS and X-shooter toward breaking degeneracies in the mass models of ETGs, disentangling the stellar and dark matter density profiles and quantifying these as function of galaxy mass and redshift.

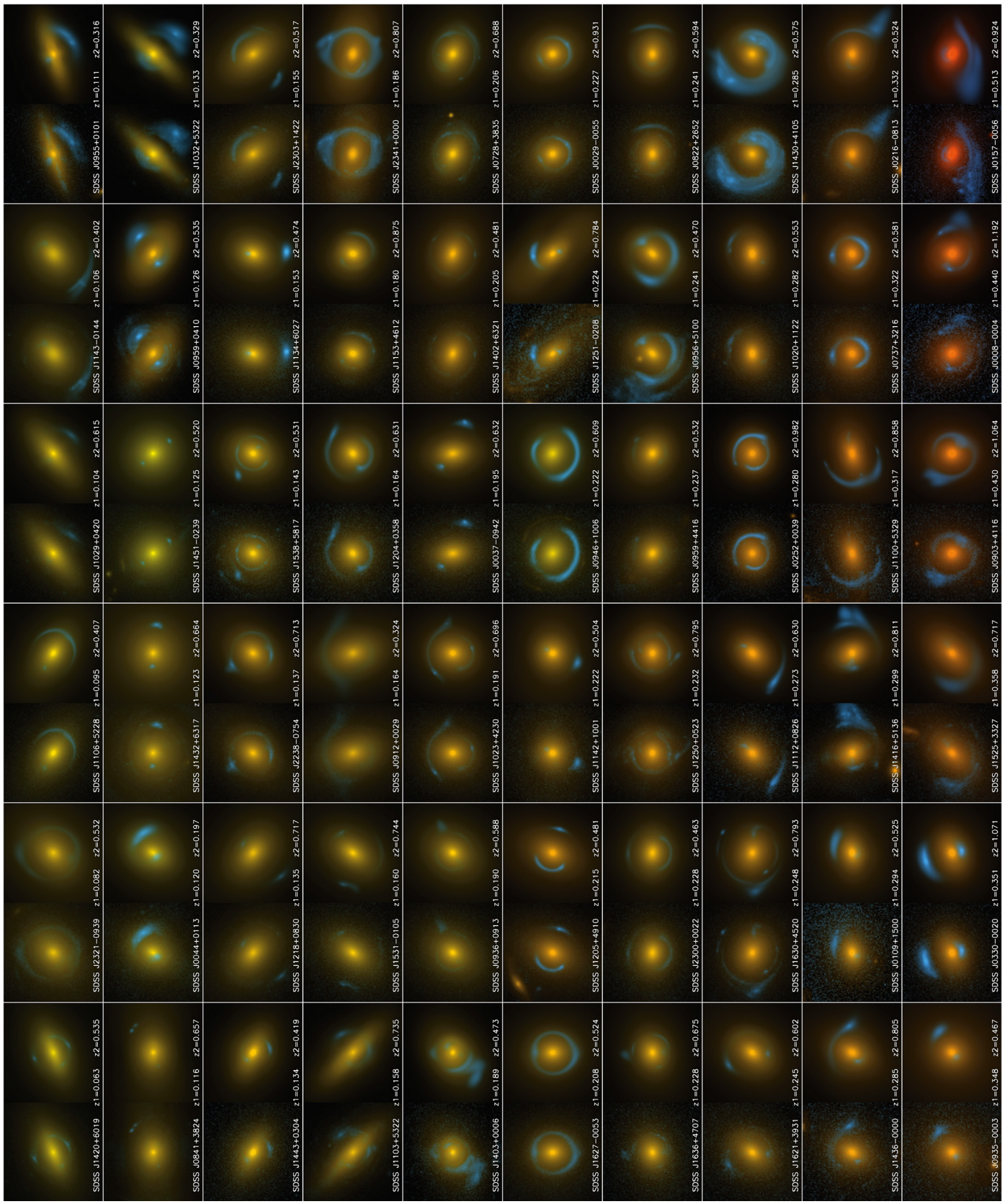
SDSS J1420+6019 z1=0.063 z2=0.535
SDSS J2321−0939 z1=0.082 z2=0.532
SDSS J1106+5228 z1=0.095 z2=0.407
SDSS J1029+0420 z1=0.104 z2=0.615
SDSS J1143−0144 z1=0.106 z2=0.402
SDSS J0955+0101 z1=0.111 z2=0.316
SDSS J0841+3824 z1=0.116 z2=0.657
SDSS J0044+0113 z1=0.120 z2=0.197
SDSS J1432+6317 z1=0.123 z2=0.664
SDSS J1451−0239 z1=0.125 z2=0.520
SDSS J0959+0410 z1=0.126 z2=0.535
SDSS J1032+5322 z1=0.133 z2=0.329
SDSS J1443+0304 z1=0.134 z2=0.419
SDSS J1218+0830 z1=0.135 z2=0.717
SDSS J2238−0754 z1=0.137 z2=0.713
SDSS J1538+5817 z1=0.143 z2=0.531
SDSS J1134+6027 z1=0.153 z2=0.474
SDSS J2303+1422 z1=0.155 z2=0.517
SDSS J1103+5322 z1=0.158 z2=0.735
SDSS J1531−0105 z1=0.160 z2=0.744
SDSS J0912+0029 z1=0.164 z2=0.324
SDSS J1204+0358 z1=0.164 z2=0.631
SDSS J1153+4612 z1=0.180 z2=0.875
SDSS J2341+0000 z1=0.186 z2=0.807
SDSS J1403+0006 z1=0.189 z2=0.473
SDSS J0936+0913 z1=0.190 z2=0.588
SDSS J1023+4230 z1=0.191 z2=0.696
SDSS J0037−0942 z1=0.195 z2=0.632
SDSS J1402+6321 z1=0.205 z2=0.481
SDSS J0728+3835 z1=0.206 z2=0.688
SDSS J1627−0053 z1=0.208 z2=0.524
SDSS J1205+4910 z1=0.215 z2=0.481
SDSS J1142+1001 z1=0.222 z2=0.504
SDSS J0946+1006 z1=0.222 z2=0.609
SDSS J1251−0208 z1=0.224 z2=0.784
SDSS J0029−0055 z1=0.227 z2=0.931
SDSS J1636+4707 z1=0.228 z2=0.675
SDSS J2300+0022 z1=0.228 z2=0.463
SDSS J1250+0523 z1=0.232 z2=0.795
SDSS J0959+4416 z1=0.237 z2=0.532
SDSS J0956+5100 z1=0.241 z2=0.470
SDSS J0822+2652 z1=0.241 z2=0.594
SDSS J1621+3931 z1=0.245 z2=0.602
SDSS J1630+4520 z1=0.248 z2=0.793
SDSS J1112+0826 z1=0.273 z2=0.630
SDSS J0252+0039 z1=0.280 z2=0.982
SDSS J1020+1122 z1=0.282 z2=0.553
SDSS J1430+4105 z1=0.285 z2=0.575
SDSS J1436−0000 z1=0.285 z2=0.805
SDSS J0109+1500 z1=0.294 z2=0.525
SDSS J1416+5136 z1=0.299 z2=0.811
SDSS J1100+5329 z1=0.317 z2=0.858
SDSS J0737+3216 z1=0.322 z2=0.581
SDSS J0216−0813 z1=0.332 z2=0.524
SDSS J0935−0003 z1=0.348 z2=0.467
SDSS J0330−0020 z1=0.351 z2=1.071
SDSS J1525+3327 z1=0.358 z2=0.717
SDSS J0903+4116 z1=0.430 z2=1.064
SDSS J0008−0004 z1=0.440 z2=1.192
SDSS J0157−0056 z1=0.513 z2=0.924

Figure 1 (opposite page). A subsample of 60 SLACS lens systems. For each system, the left panel shows a multi-colour HST image and the right panel shows a reconstruction from the best-fitting lens model.

Finding suitable lenses: the Sloan Lens ACS Survey

Progress in strong gravitational lensing has often been driven by new instrumentation, allowing detailed study of these typically arcsecond-scale systems. The advent of space-based observatories, in particular the Hubble Space Telescope (HST), has allowed optical and infrared images with ~ 0.1 arcsecond resolution, revolutionising the field. Recently, adaptive optics (AO) observations have enabled ground-based telescopes to compete again or even overtake space-based imaging (see e.g., the SHARP projects; Lagattuta et al., 2012; Vegetti et al., 2012). For spectroscopy, 8–10-metre-class telescopes are without competition. IFU observations with the Very Large Telescope (VLT) in particular have made it possible to obtain detailed maps of the kinematic fields of lens ETGs, as we will show.

Gravitational lenses are rare — only a few hundred are known across the entire sky. Early lens searches targeted potentially lensed background sources, and consequently the properties of the lenses were rather heterogeneous. This changed with the advent of the Sloan Digital Sky Survey (SDSS) which took spectra of many millions of targets, among them many ETGs that could act as gravitational lenses. Based on an earlier idea of Warren et al. (1996), the Sloan Lens ACS (SLACS) collaboration (Bolton et al., 2006) searched systematically through the spectra of ETGs in the SDSS database for signs of emission lines coming from a higher redshift. In these cases the 3-arcsecond SDSS fibres ensure a close alignment between a massive ETG and a high-redshift source within 1.5 arcseconds from the ETG. Because the Einstein radius of these systems is often similar to the fibre radius, many of them are excellent strong gravitational lens candidates.

Two more advantages of such a spectroscopic lens search are that the redshifts of the lens and source will both be known without further follow-up, and, in the case of SDSS, a measurement of the stellar velocity dispersion of the ETGs comes for free from these spectra. Given the redshift and the velocity dispersion of the ETG, a simple estimate of the Einstein radius can be made. Nearly 100 % of the candidates with an Einstein radius exceeding that of the fibre turned out to be genuine lenses and the overall success rate of the HST follow-up programme exceeded 50 %. Extensive follow-up with HST has yielded nearly 100 strong gravitational lens systems with multicolour *V*-, *I*- and *H*-band observations, complete redshift information and stellar velocity dispersions for all systems. A recently completed HST snapshot programme has yielded another ~50 lens systems with somewhat lower stellar velocity dispersions. This programme has collected the most complete and uniform galaxy-scale lens sample to date (Figure 1) with most lenses being luminous red galaxies (LRGs).

Initial results from combined gravitational lens (mass inside the Einstein radius) and kinematic data (velocity dispersion inside the SDSS fibre) turned out to be a powerful constraint on the total density profile (stars plus dark matter) and showed that these ETGs have mass slopes very similar to isothermal spheres (i.e. flat circular velocity curves) and similar to those of spiral galaxies. No evolution with redshift and no correlation with galaxy mass was found in the density profiles, although recent observations may have shown some minor evolution (Bolton et al., 2012). In addition, and probably just as interesting, was the related work on the Fundamental Plane by Bolton et al. (2007), who showed that if one replaces the surface brightness within one effective radius (R_{eff}) by the surface mass density derived from lensing and dynamical models, then the tilt of the Fundamental Plane changes to that derived from the virial theorem. This finding demonstrates that these galaxies are homologous (see e.g., Koopmans et al., 2009) and that the tilt is mostly due to a change in the dark matter content of these galaxies.

Two-dimensional kinematic fields: VLT-VIMOS

To further push the lensing and kinematic analysis and to assess the effects of anisotropy and the non-spherical nature of ETGs in greater detail, a single velocity dispersion measurement is not sufficient. Integral field spectroscopy of 17 SLACS lenses (of which 16 were ETGs) was obtained with the VIMOS IFU on the VLT in 2006–2008, as part of a VLT Large Programme (see Figure 2). Fitting of the spectra with stellar templates yielded two-dimensional kinematic maps of systematic velocity (e.g., due to bulk rotation of the galaxy) and velocity dispersion, typically out to 1 R_{eff}. These data were combined with high-resolution HST imaging of the gravitational-lens configuration and modelled in a fully self-consistent way. Although the results are in remarkable agreement (in general within the errors) with previous results based on simpler analyses, a much more detailed and three-dimensional census was obtained from the selected 16 ETGs. The total mass density profiles (Figure 3) could be compared with the stellar mass density under the assumption of two different stellar IMFs (Chabrier and Salpeter).

The main results that have come out of the VIMOS studies are that ETGs genuinely have total density profiles very close to isothermal, but also that there is intrinsic scatter between density profiles of order 10 %, consistent with studies in the nearby Universe. A small but interesting correlation is found between the density slope and the stellar mass density, which may be a result of their formation (e.g., adiabatic contraction). Another major result is that, for a fixed IMF along the mass sequence, the deviation between the total mass-density profile and that for the stars increases rapidly. Assuming the IMF is not varying (this question will be addressed later), this implies that the dark-matter content of ETGs within 1 R_{eff} is not only non-negligible but can even dominate for the most massive systems, with velocity dispersion $\sigma > 300$ km/s.

The inferred increase in dark matter content in the inner parts of ETGs is consistent with models where feedback increases for increasingly more massive ETGs, either through supernova or active galactic nucleus feedback (Hopkins et al., 2006). However, it should be kept in mind that a similar increase can also be caused by a change in the IMF for low-mass stars (< 0.5 $M_{\odot}$; van Dokkum &

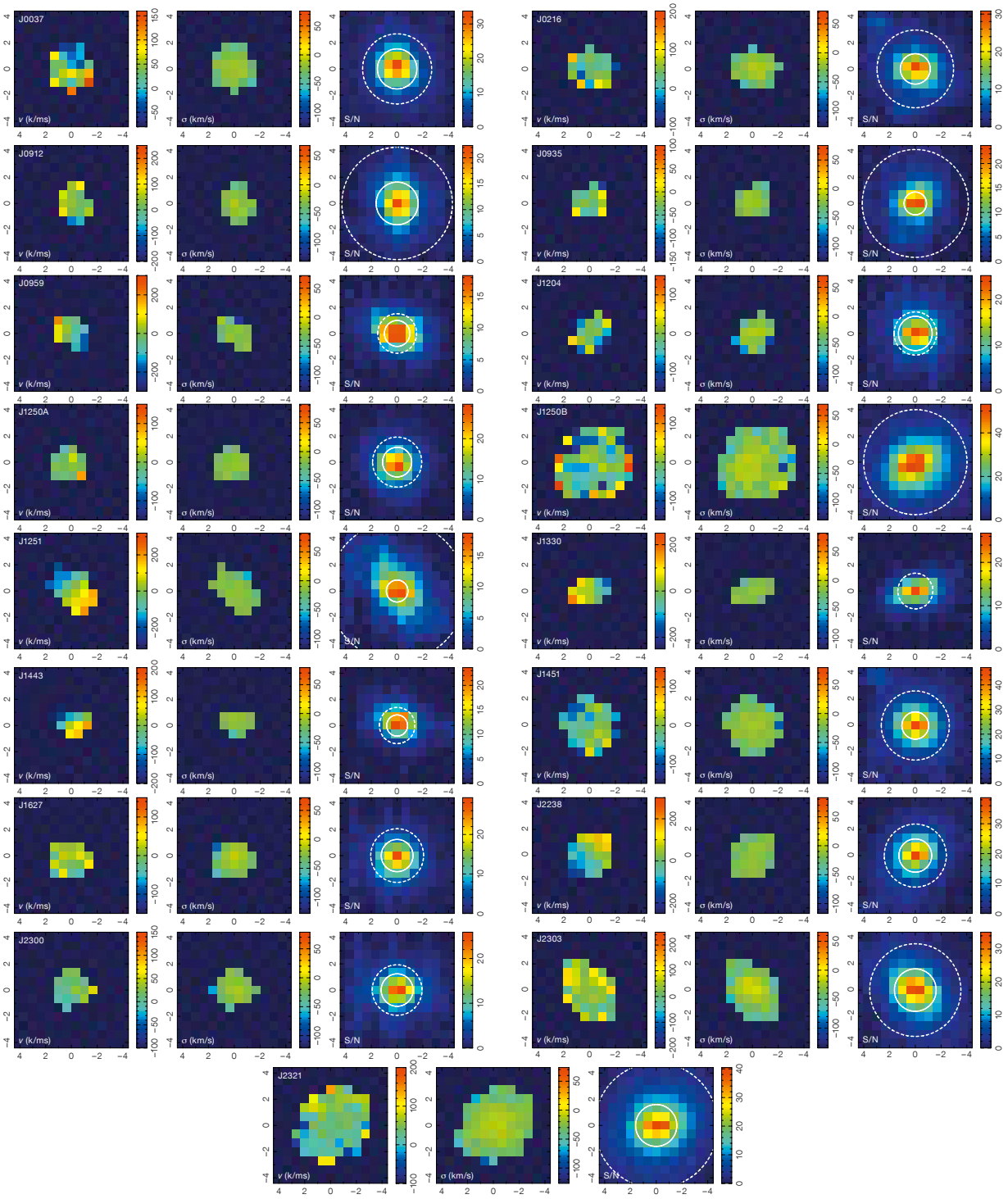

Figure 2. Kinematic maps for 17 SLACS lens systems as derived from VIMOS/IFU observations. For each system, the left panel shows the systematic velocity (with respect to the mean redshift of the lens galaxy), the middle panel the velocity dispersion and the right panel the signal-to-noise (S/N) ratios of the spectra in the stacked datacube. Kinematic measurements were obtained for spectra with S/N > 8 (per 0.65 Å pixel). From Czoske et al. (2012).

Conroy, 2010). This could indeed work for the lower-mass ETGs as can be seen in Figure 3, because the shapes of the stellar and total density profiles are relatively similar up to a constant within 1 R_{eff}. Steepening the low-mass end of the IMF could increase the stellar mass content of these galaxies to a level that dark matter is no longer needed, but in general this requires an IMF that is steeper than the Salpeter IMF. In many cases, however, scaling of the stellar mass profile does not match the total density profile, reflecting the fact that a steepening of

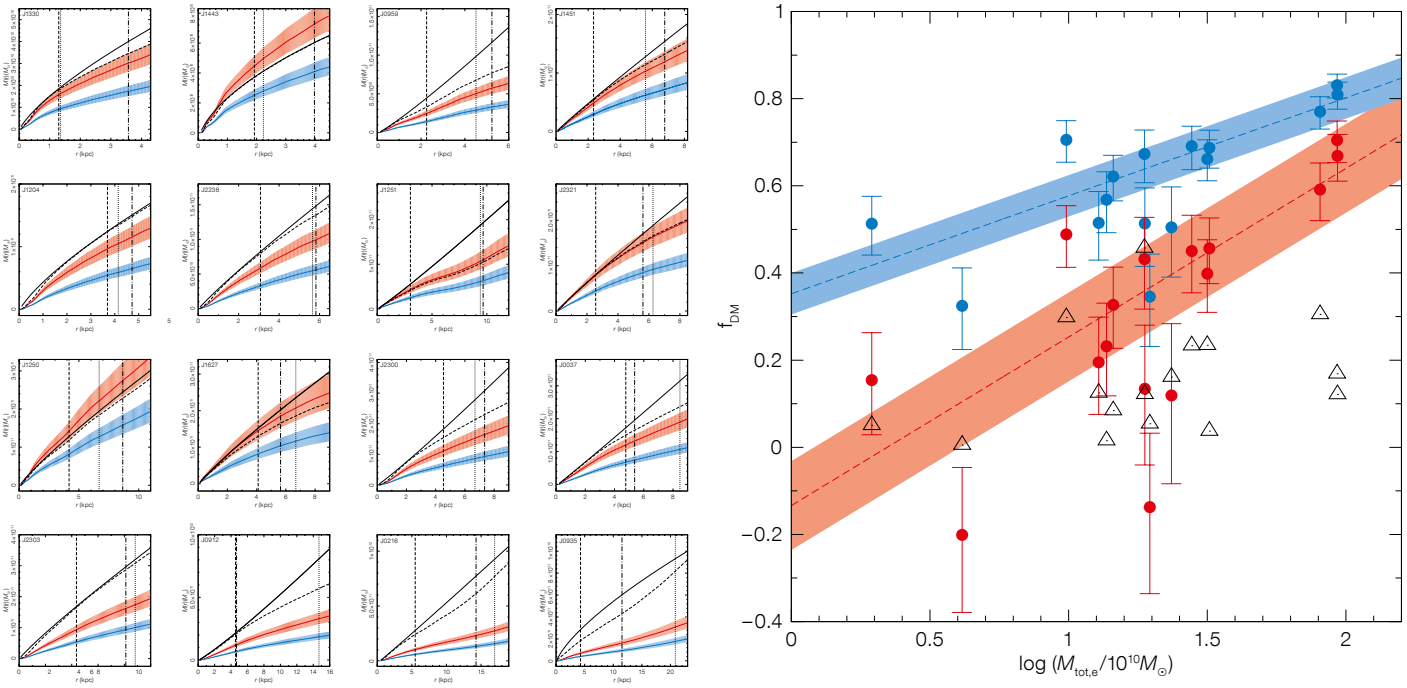

Figure 3. Left: Spherically averaged mass distributions for the 16 early-type galaxies in the SLACS/VIMOS sample, arranged by increasing galaxy mass. The total mass profiles, as derived from the lensing/kinematics analysis, are shown by solid black lines. Stellar mass profiles have been derived for two different IMFs: Salpeter (red) and Chabrier (blue). The dashed black line rescales the luminous mass profile to its maximum value consistent with the total mass distribution (the maximum-bulge hypothesis). Right: Dark matter fractions (f_{DM}) *versus* total mass enclosed within the three-dimensional effective radius for the 16 early-type galaxies in the sample, computed for Salpeter (red) and Chabrier (blue) IMFs. Lower limits for the dark matter fractions were obtained from the maximum-bulge hypothesis (open triangles). From Barnabè et al. (2011).

the IMF cannot be the sole cause of the change in M/L in ETGs. In fact, models with constant M/L can also be excluded for many other lens ETGs for which kinematic data are available, showing the strength of combining these two techniques. However, some degeneracies between stellar and dark matter mass remain.

Stellar populations and the initial mass function: XLENS with X-shooter

Our ability to measure the stellar IMF of these galaxies is one final piece in the puzzle posed by disentangling the fraction of the total mass in ETGs that is contained in dark matter. Again, the combination of lensing and dynamics gives very interesting clues. In Treu et al. (2010) it was found that a full analysis of 53 SLACS ETGs indicates that a Salpeter IMF fits the data best and that "light" IMFs (e.g., Chabrier, Kroupa) can be excluded. This agreed well with the later result by, for example, van Dokkum & Conroy (2010) that the spectra of ETGs seem to show absorption-line equivalent widths typical for low-mass stars and thus are only consistent with more bottom-heavy IMFs. A complementary analysis by Auger et al. (2010) based on their full structure seems to confirm that light IMFs are inconsistent with the kinematics of these ETGs.

Another tantalising result from SLACS was that the IMF seems to steepen with galaxy mass, although this was only found at the 2σ confidence level (Treu et al., 2010). In order to investigate this effect in greater detail we started the XLENS survey, which follows up a subsample of ten lenses with X-shooter covering the full ultraviolet to near-infrared (UV–NIR) wavelength range in order to measure the equivalent widths of several absorption lines (Na I, FeH, TiO_2, etc.) that are especially sensitive to low-mass stars. Based on a pilot programme, Spiniello et al. (2011) combined kinematic constraints from X-shooter data with lensing data of the Horseshoe lens system (Figure 4) as well as spectral energy distribution (SED) fitting to disentangle the stellar and dark matter distributions. Although lighter IMFs are harder to exclude due to degeneracies between the stellar and dark matter halo mass distributions, IMFs as steep as Salpeter (slope 2.35) were allowed. Also mass-function slopes steeper than 3.0 were excluded, based simply on the total enclosed mass within the Einstein radius of the system as well as the velocity dispersion profile (Spiniello et al., 2011).

New X-shooter data on the sample of ten systems continues to be obtained. First results were presented in Spiniello et al. (2012) based on one extremely interesting XLENS system (Figure 5) that shows very deep Na I and TiO_2 lines, which are both regarded as potential indicators of a population of low-mass stars (< 0.3 $M_{\odot}$). Naively therefore, this system should have a very steep IMF, which can however be excluded with high confidence for slopes exceeding 3.0. Combined with a larger sample of spectra from the SDSS (Figure 5), it was also shown that these lines deepen with increasing stellar velocity dispersion, suggesting some mild steepening of the IMF, in agreement with the work of Treu et al. (2010). Theoretical work by, for example, Hopkins (2012)

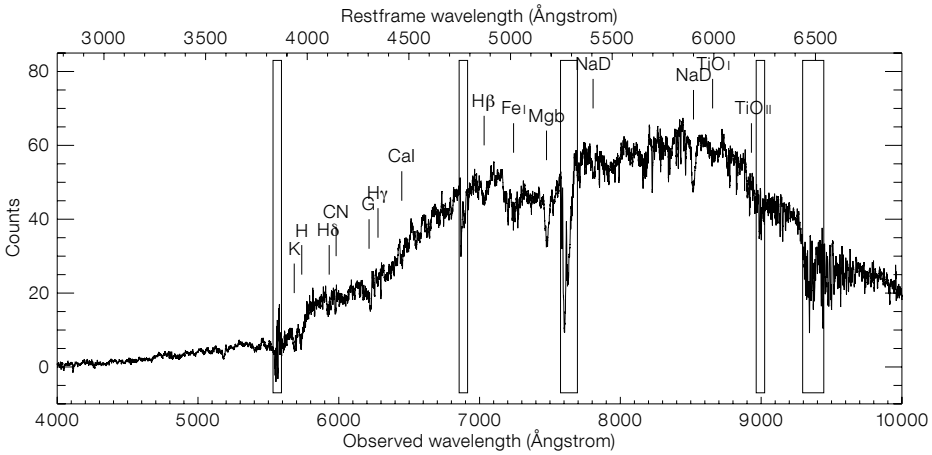

Figure 4 (above). Left: HST image of SDSS J1148+1930 (The Cosmic Horseshoe). Right: X-shooter spectrum of SDSS J1148+1930, covering the UVB and VIS arms. Several spectral features are marked, as are the positions of telluric absorption features and sky lines (boxes). From Spiniello et al. (2011).

Figure 5 (below). Index–index plots of ~250 ETGs from the SDSS, colour-coded by velocity dispersion. Lines that are sensitive to low-mass stars ([MgFe] (Gonzalez, 1993), TiO_2, NaI) tend to deepen with increasing velocity dispersion, indicative of a steepening of the low-mass IMF slope with galaxy mass (panels b and c). Various IMF slopes are plotted (C = Chabrier). The bottom-right panel (d) shows the correlation between the NaI and TiO_2 indicators, displaying a modest steepening of the IMF from Salpeter (slope of 2.35) to an IMF with a slope slightly less than 3.0. From Spiniello et al. (2012).

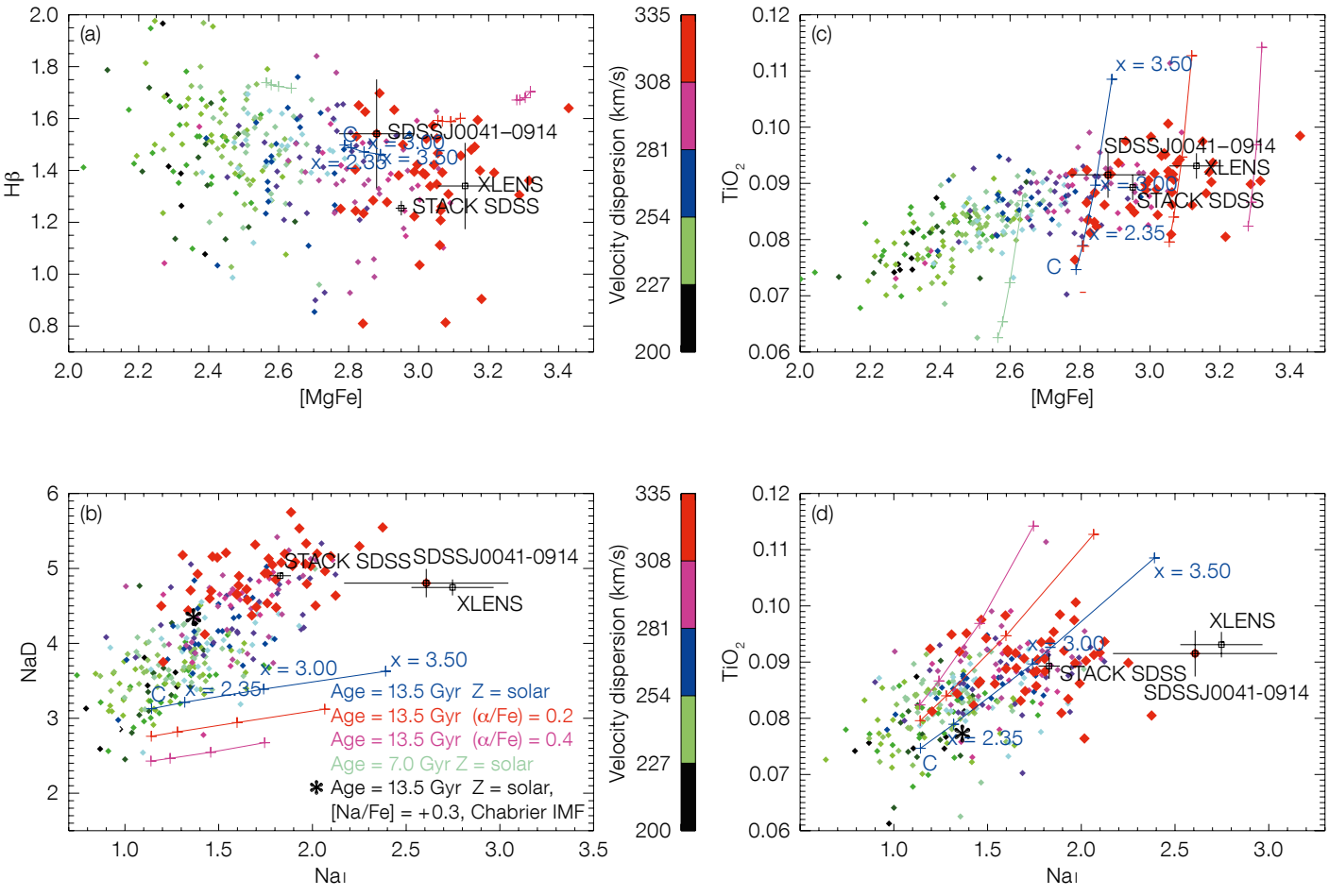

seems to be able to explain this result based on arguments of gas density during star/galaxy formation, but a detailed comparison between observations and theory remains to be done.

Future work

Accurate knowledge of the total mass of a galaxy is essential for disentangling the distributions of stellar and dark matter within it, as it breaks many of the degeneracies in mass models based on stellar kinematics. The technique of combining kinematics and gravitational lensing has been used extensively by the SLACS collaboration to arrive at a number of interesting results on the mass profiles of galaxies, limits on their dark matter content, as well as on the Fundamental Plane and the stellar IMF, as discussed in this article. More recently this analysis has been further extended by including constraints on the stellar IMF from broadband stellar SEDs and spectra.

Two-dimensional kinematics obtained with VIMOS on the VLT in combination with gravitational lensing has been shown to be powerful at modelling the mass distributions in elliptical galaxies beyond the local Universe. The next generation of integral field spectrographs both at the VLT and the E-ELT will further push the limits of applicability of this technique and allow the study of the evolution of the structure of ETGs over a fair fraction of the age of the Universe.

X-shooter will continue to play a crucial role as it allows full ultraviolet to near-infrared spectral coverage in one go; this is critical because the data provide not only the kinematics (from lines in the optical) but also equivalent widths of absorption lines in the infrared that are indicators of low-mass stars and hence can constrain the slope of the IMF. Much work is currently being done in these studies worldwide and we expect to be able to make a much stronger statement in the near future, based on these X-shooter data on a substantial sample of ETGs from SLACS, concerning the contribution of stars (i.e. their IMF) to the mass of ETGs. These results should also shed more light on the tilt of the FP, as well as on their formation history (and feedback) within massive dark matter haloes.

With the recent discovery of ~ 50 more SLACS lenses — extending the mass range down to ~ 150 km/s systems, well below the knee of the mass function of ETGs — we expect even more discoveries in the coming years that will allow a complete census of the internal structure, formation and evolution of ETGs and the successful SLACS saga to continue.

References

Auger, M. et al. 2010, ApJ, 721, L163
Barnabè, M. & Koopmans, L. V. E. 2007, ApJ, 666, 726
Barnabè, M. et al. 2011, MNRAS, 415, 2215
Bolton, A. S. et al. 2006, ApJ, 638, 703
Bolton, A. S. et al. 2007, ApJ, 665, 105
Bolton, A. S. et al. 2012, arXiv:1201.2988
Czoske, O. et al. 2012, MNRAS, 419, 656
Gonzalez, J. J. 1993, PhD Thesis, Univ. California, Santa Cruz
Hopkins, P. F. et al. 2006, ApJS, 163, 1
Hopkins, P. F. 2012, MNRAS, 423, 2037
Koopmans, L. V. E. & Treu, T. 2002, ApJ, 568, L5
Koopmans, L. V. E. et al. 2006, ApJ, 649, 599
Koopmans, L. V. E. et al. 2009, ApJL, 703, L51
Lagattuta, D. J. et al. 2012, MNRAS, 424, 2800
Spiniello, C. et al. 2011, MNRAS, 417, 3000
Spiniello, C. et al. 2012, ApJ, 753, 32
Treu, T. & Koopmans, L. V. E. 2002, ApJ, 575, 87
Treu, T. et al. 2010, ApJ, 709, 1195
van Dokkum, P. G. & Conroy, C. 2010, Nature, 468, 940
Vegetti, S. et al. 2012, Nature, 481, 341
Warren, S. J. et al. 1996, MNRAS, 278, 139

ESO/SOAR/NASA

This false colour picture of the galaxy cluster ACT-CL J0102–4915 combines *R*-, *i*- and *z*-band images taken with FORS2 on the VLT, *griz*-band images from the SOAR Telescope and X-ray observations of the hot gas from NASA's Chandra X-ray Observatory. The galaxy cluster is probably the most massive, hottest, most X-ray luminous and brightest Sunyaev-Zeldovich effect cluster currently known at a redshift greater than 0.6 and so was named *El Gordo*. See Release eso1203 for more details.

An ALMA Survey of Submillimetre Galaxies in the Extended Chandra Deep Field South: First Results

Mark Swinbank[1]
Ian Smail[1]
Alex Karim[1]
Jackie Hodge[2]
Fabian Walter[2]
Dave Alexander[1]
Frank Bertoldi[3]
Andy Biggs[4]
Niel Brandt[5]
Carlos De Breuck[4]
Scott Chapman[6]
Kristen Coppin[7]
Pierre Cox[8]
Alice Danielson[1]
Helmut Dannerbauer[9]
Alastair Edge[1]
Rob Ivison[10,11]
Thomas Greve[12]
Kirsten Knudsen[13]
Karl Menten[2]
James Simpson[1]
Eva Schinnerer[2]
Julie Wardlow[14]
Axel Weiss[2]
Paul van der Werf[15]

[1] Institute for Computational Cosmology, University of Durham, United Kingdom
[2] Max-Planck-Institut für Astronomie, Heidelberg, Germany
[3] Argelander-Institut für Astronomie, Bonn, Germany
[4] ESO
[5] Pennsylvania State University, University Park, USA
[6] Institute for Astronomy, Cambridge, United Kingdom
[7] Dept. of Physics, McGill University, Montréal, Canada
[8] IRAM, Saint Martin d'Hères, France
[9] Institut für Astronomie, Universität Wien, Austria
[10] UK Astronomy Technology Centre, Edinburgh, Scotland
[11] Institute for Astronomy, University of Edinburgh, Scotland
[12] University College London, United Kingdom
[13] Onsala Space Observatory, Chalmers University, Sweden
[14] Dept. of Physics and Astronomy, University of California Irvine, USA
[15] Leiden Observatory, the Netherlands

Sensitive ALMA submillimetre maps of a sample of 122 870 µm selected submillimetre sources from our survey of the Extended Chandra Deep Field South are presented. The combination of sensitivity and resolution of ALMA allows us to precisely pinpoint the submillimetre emission from these galaxies to an accuracy of < 0.3 arcseconds. In two ALMA submillimetre galaxies (SMGs) we serendipitously detect bright [C II] 157.4 µm emission, yielding redshifts of 4.4. This blind detection rate within the 7.5 GHz bandpass of ALMA is consistent with the previously derived photometric redshift distribution of SMGs and suggests a modest, but not dominant (< 25 %), tail of 870 µm selected SMGs at $z > 4$.

Background

A significant fraction of the obscured star formation at redshift $z > 1$ arises from the most luminous galaxies: ultraluminous infrared galaxies (ULIRGs) with bolometric luminosities of $> 10^{12}$–10^{13} $L_{\odot}$ and implied star formation rates (SFR) of > 100–1000 $M_{\odot}$/yr. Their very low space densities means ULIRGs are a negligible element of the star-forming population at $z \sim 0$, contributing < 1 % of the total SFR density. However, the situation at high redshift is very different: the first deep, single-dish bolometer surveys in the 870 µm atmospheric window uncovered a significant population of dusty starbursts (e.g., Smail et al., 1997), with SFRs > 1000 $M_{\odot}$/yr. These galaxies are some of the brightest sources in the submillimetre waveband and so are frequently called submillimetre galaxies.

This 870 µm high-redshift population may host up to half of the star formation occurring at $z \sim 2$ (Chapman et al., 2005; Wardlow et al., 2011) and may be linked to the formation of massive local elliptical galaxies (Genzel et al., 2003; Swinbank et al., 2006). Moreover, the highest-redshift SMGs ($z > 4$), have also been linked to the formation epoch of massive, "red and dead" galaxies at $z \sim 2$ which are now being found in large numbers (e.g., Whitaker et al., 2012). The progenitors of these $z \sim 2$ red and dead galaxies must have formed the bulk of their stellar populations at $z > 4$ and the necessary SFRs ~ 100–1000 $M_{\odot}$/yr correspond to the bright submillimetre galaxy population. If true, then SMGs are a key evolutionary stage for the evolution of massive galaxies at all epochs, and so determining their true redshift distribution and contribution to the star formation density are basic parameters that are needed to constrain galaxy formation models (Baugh et al., 2005). Indeed, since they lie on the rapidly diminishing, exponential tail of the mass function, massive galaxies at all epochs can provide strong tests of galaxy formation models as they are often the most challenging systems for galaxy formation models to reproduce.

However, measuring the redshifts for a complete and unbiased sample of SMGs is not trivial: the poor resolution of single-dish submillimetre telescopes, ~ 18 arcseconds, means that there are many possible counterparts responsible for submillimetre emission. SMGs have therefore to be identified through correlations between their submillimetre emission and that in other wavebands where higher spatial resolution is available, usually the radio and/or mid-infrared (e.g., Ivison et al., 2007). These identifications are probabilistic as they rely on empirical correlations that have both significant scatter and which may evolve with redshift. In submillimetre surveys, typically 30–50 % of SMGs lack robust counterparts in the radio or mid-infrared and these may represent either an unidentified tail of high-redshift SMGs, or galaxies whose submillimetre emission is relatively bright compared to the radio/mid-infrared. The latter includes SMGs with colder than average dust temperatures, which may include the isolated, gas-rich disc galaxies. Thus these biased identifications may miss precisely those SMGs that are critical for testing the models.

To circumvent this problem requires identifying the submillimetre emission directly using submillimetre interferometers, but until recently their sensitivity has been too low to locate large numbers of SMGs (Smolčić et al., 2012). However, with the commissioning of the Atacama Large Millimeter/submillimeter Array (ALMA), we can now construct the large samples of precisely located SMGs needed to unambiguously study their properties and test galaxy formation models.

The ALMA LESS (aLESS) survey

We have recently undertaken an ALMA Cycle 0 study of the 126 submillimetre sources from the 870 μm LABOCA survey of the Extended Chandra Deep Field South (the LESS survey of Weiss et al., 2009) conducted with the Large APEX Bolometer Camera (LABOCA) on the Atacama Pathfinder Experiment Telescope (APEX). Despite the short integration time per source (~ 2 min), our ALMA maps are typically ~ 3 times deeper (σ_{870} ~ 0.4 mJy) than the original LABOCA survey and critically the angular resolution is more than an order of magnitude higher, with a full width at half maximum (FWHM) of 1.4 arcseconds.

This combination of sensitivity and resolution precisely locates the SMGs directly (see examples in Figure 1), pinpointing the source(s) responsible for the submillimetre emission (to within < 0.3 arcseconds), without recourse to statistical radio/mid-infrared associations. Whilst a large number of the radio and/or mid-infrared counterparts from previous statistical associations are confirmed, in a significant number of instances the previous counterparts have been shown not to be SMGs. Our ALMA maps turn up new counterparts to previously unidentified submillimetre sources, as well as multiple SMG counterparts to LABOCA sources in a number of cases (Hodge et al., 2012). For the first time, this ALMA study provides us with a unique and unbiased sample of SMGs with direct identifications from the submillimetre with which we can study the multi-wavelength properties in an unbiased manner (Simpson et al., 2012; Smail et al., 2012). Animations of these ALMA observations of the Extended Chandra Deep Field South can be viewed[1].

We use the sources detected in these maps to derive the first reliable counts of faint SMGs free from the effects of confusion. These counts agree broadly with those derived from lower resolution single-dish surveys, demonstrating that the bulk of the submillimetre sources are not caused by the blending of emission from several, significantly fainter sources (Karim et al., 2012) However, we find an exception: all of the brightest submillimetre sources in the LESS sample (with $S_{870\,\mu m}$ > 10 mJy) actually consist of emission from multi-ple SMGs, each with 870 μm fluxes of 3–4 mJy, significantly steepening the 870 μm counts above ~ 8 mJy (Karim et al., 2012).

The highest redshift SMGs

As an initial step in our analysis of the ALMA data of the LESS SMGs, we also exploited the frequency coverage of our observations to search for emission lines in the datacubes. In two SMGs, aLESS61.1 and aLESS65.1 we identify the redshifted [C II] 157.4 μm emission line, indicating redshifts of 4.419 and 4.445 respectively (see Figure 2 and Swinbank et al., 2012). Both of these SMGs are very faint at all other wavelengths: both have radio (1.4 GHz) 3σ upper limits of < 25 mJy and are blank in the Herschel maps at 250, 350 and 500 μm; i.e. they are so-called 870 μm peakers. Although based on only two sources, the blind detection rate of [C II] in the 7.5 GHz (Δz = 0.12) bandpass of ALMA is consistent with the previously derived photometric redshift distribution of SMGs (Wardlow et al., 2011) and

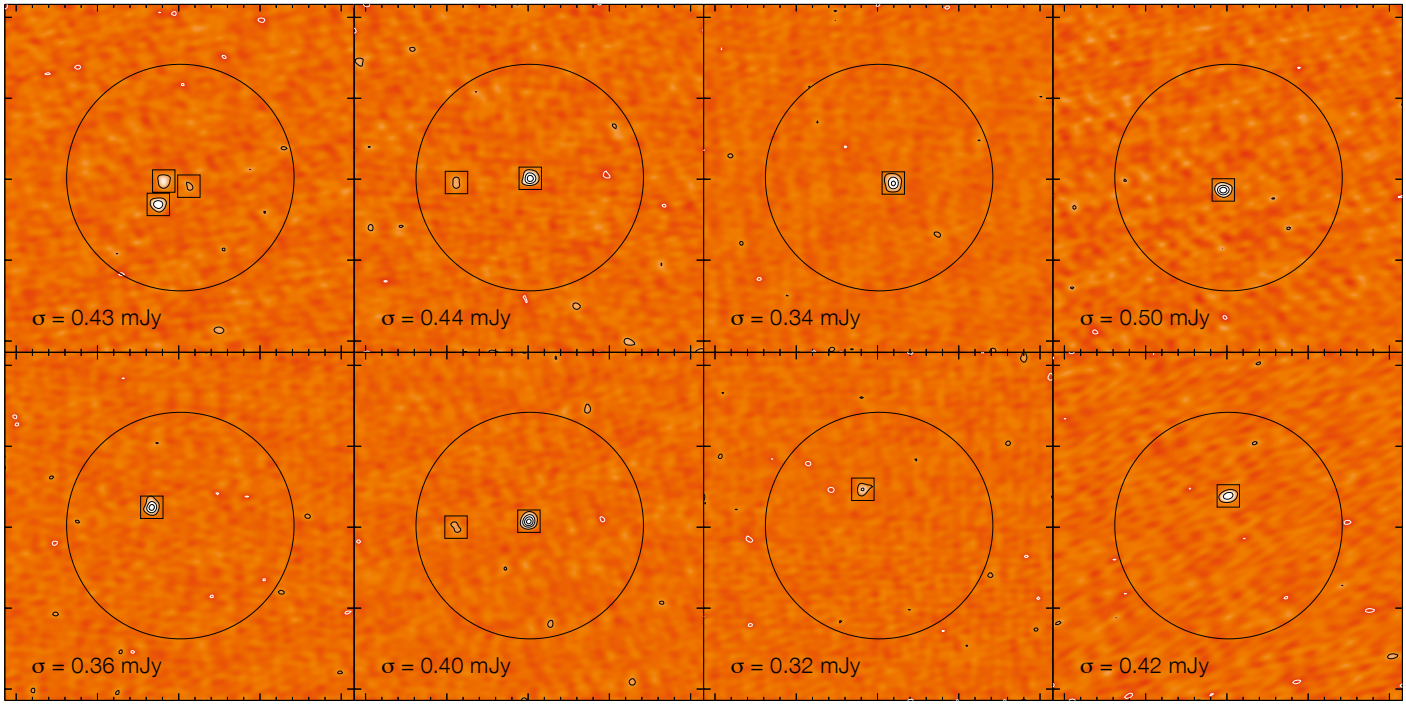

Figure 1. Examples of 345 GHz (870 μm) ALMA maps of eight of the SMGs in our ALMA LESS sample. In each map we identify all of the SMGs (with signal-to-noise > 4σ) by large squares. The contours on each map start at 4σ and are incremented by 2σ (and the 1σ value is given in the bottom left corner of each panel). We also show the primary beam (circle). Each map is 40 arcseconds across. The ALMA data unambiguously locates the SMG counterpart(s) to a precision of < 0.3 arcseconds and to flux limits of ~ 1.5 mJy.

suggests a modest, but not dominant, (< 25 %) tail of 870 μm selected SMGs at $z > 4$.

Since the [C II] emission line is the dominant cooling line within the interstellar medium (the [C II] emission line can comprise ~1% of the total bolometric luminosity of a galaxy), we can use the data to investigate the properties of the interstellar medium (ISM) in the galaxies. In local luminous-infrared galaxies, the ratio of $L_{[C\,II]}/L_{FIR}$ is approximately constant at ~1%, but decreases to < 0.1% in local ULIRGs (Figure 3, left). However, the [C II] detections in high-redshift ULIRGs and active galactic nuclei (AGNs) have shown that the [C II] emission can be as bright as in local, low luminosity galaxies. This has been interpreted as due to the lower ionisation field arising from more widely distributed star formation activity within these systems, in contrast to the compact nuclear star formation seen in low-redshift ULIRGs. From our ALMA observations, the ratio of $L_{[C\,II]}/L_{FIR}$ in these SMGs is also much higher than seen for similar far-infrared luminous galaxies in the local Universe (Figure 3, left). We attribute this to the more extended gas reservoirs in these high-redshift ULIRGs. In aLESS65.1 the [C II] emission shows extended emission on > 3 kpc scales.

We also use the volume probed by our ALMA survey to investigate the bright end of the [C II] luminosity function (Figure 3, right). Our ALMA observations cover the

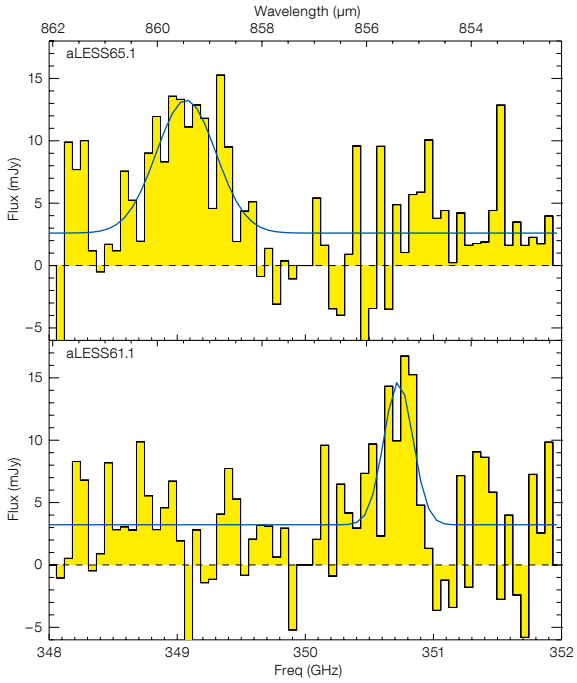

Figure 2. ALMA spectra of aLESS65.1 and aLESS61.1, extracted at the position of the peak submillimetre emission from the SMGs. From the spectra, we identify the [C II] 157.4 μm emission lines in the upper sideband which we attribute to [C II] emission at $z = 4.419$ and $z = 4.445$ for aLESS61.1 and aLESS65.1, respectively.

[C II] emission over a redshift range of $\Delta z = 0.12$ at $z = 4.4$ (a co-moving volume of 2.9×10^5 Mpc^3). Finding two galaxies in this volume with bright [C II] emission indicates an increase > 1000 times in the number density of luminous [C II] emitters from z ~ 0–4.4 (Figure 3). This is equivalent to a [C II] luminosity evolution of a factor ~ 3–4 times between $z = 0$ and 4.4, consistent with the evolution in the far-infrared luminosity function over the same redshift range.

Figure 3. Left: The ratio of the [C II] to far-infrared luminosity ($L_{[C\,II]}/L_{FIR}$) as a function of the far-infrared luminosity for aLESS61.1 and aLESS65.1 compared to local star-forming galaxies and ULIRGs. This figure shows that the ratio of $L_{[C\,II]}/L_{FIR}$ for high-redshift ULIRGs is a factor ~10 times higher given their far-infrared luminosities compared to those at z ~ 0. Right: The [C II] luminosity function at $z = 4.4$ from our survey compared to $z = 0$. For the $z = 4.4$ luminosity function, we assume that all of the [C II] emitting galaxies in the $\Delta z = 0.12$ volume covered by our observations were detected and so these calculations yield only a lower limit on the volume density of high-redshift [C II].

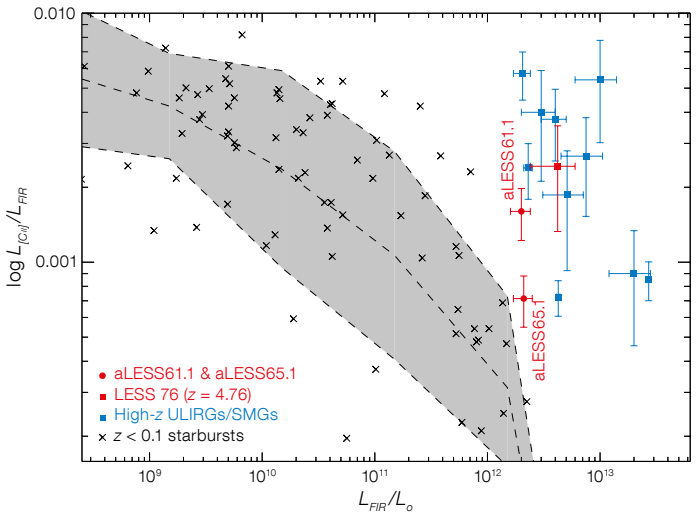

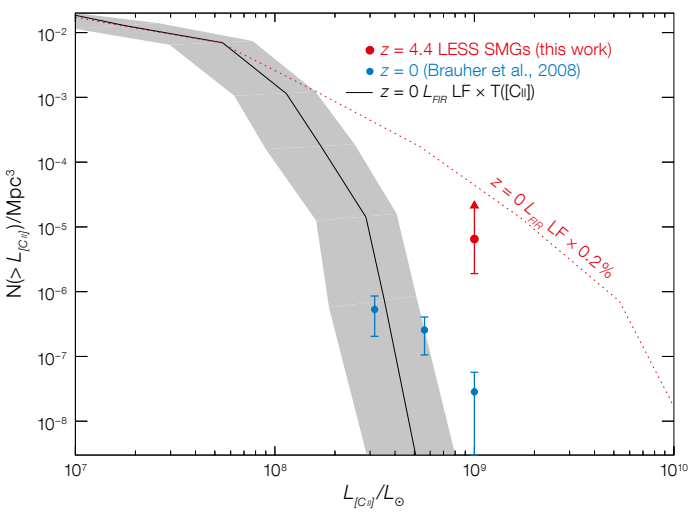

Prospects

These early results show that ALMA can trivially identify large samples of SMGs in short exposure times, measure blind redshifts through the detection of fine structure lines and spatially resolve the dust and gas within the galaxies on ~ kpc scales. Constructing large and unbiased samples of SMGs with ALMA in a single well-studied field are crucial to investigate the unbiased redshift distribution and the nature of these galaxies. Topics such as the triggering mechanisms for their immense starburst activity, their stellar and gas masses and dynamics can be addressed, and hence the evolution of a population which have been proposed as the formation epoch of today's massive galaxies — the luminous ellipticals.

References

Baugh, C. et al. 2005, MNRAS, 356, 1191
Brauher, J. et al. 2008, ApJS, 178, 280
Chapman, S. et al. 2005, ApJ, 622, 772
Genzel, R. et al. 2003, ApJ, 584, 633
Hodge, J. et al. 2012, MNRAS, in prep.
Karim, A. et al. 2012, MNRAS, submitted
Ivison, R. et al. 2007, MNRAS, 380, 199
Narayanan, R. et al. 2009, MNRAS, 400, 1919
Simpson, J. et al. 2012, MNRAS, in prep.
Smail, I. et al. 1997, ApJ, 490, 5
Smail, I. et al. 2012, MNRAS, in prep.
Smolčić, V. et al. 2012, ApJS, 200, 10
Swinbank, M. et al. 2006, MNRAS, 371, 465
Swinbank, M. et al. 2012, MNRAS, submitted
Wardlow, J. et al. 2011, MNRAS, 415, 1479
Weiss, A. et al. 2009, ApJ, 707, 1201
Whitaker, K. E. et al. 2012, ApJ, 745, 179

Links

[1] Fly-through animations of the ALMA observations: http://astro.dur.ac.uk/~ams/ALMAmovie/

ESO/B. Tafreshi (twanight.org)

A recent image showing some of the growing number of ALMA antennas on Chajnantor pointing towards the Milky Way. See Picture of the Week 28 May 2012.

Chemical Properties of a High-*z* Dusty Star-forming Galaxy from ALMA Cycle 0 Observations

Tohru Nagao[1,2]
Roberto Maiolino[3]
Carlos De Breuck[4]
Paola Caselli[5]
Bunyo Hatsukade[2]
Kazuya Saigo[6]

[1] The Hakubi Center for Advanced Research, Kyoto University, Japan
[2] Department of Astronomy, Kyoto University, Japan
[3] Cavendish Laboratory, University of Cambridge, United Kingdom
[4] ESO
[5] School of Physics and Astronomy, University of Leeds, United Kingdom
[6] East Asian ALMA Regional Center, National Astronomical Observatory of Japan, Japan

The chemical properties of galaxies provide strong constraints on galaxy evolutionary scenarios, but diagnosing the chemical properties of high-*z* dusty galaxies by means of optical and near-infrared spectroscopy has been challenging. We have therefore focussed on far-infrared fine-structure emission lines in high-*z* dusty galaxies, whose detection is feasible with ALMA. From ALMA Cycle 0 observations, we have detected [N II] 205 µm emission in a submillimetre galaxy at *z* = 4.76 whose [C II] 158 µm emission has been already detected in our previous APEX observations. The measured flux ratio of [N II] 205 µm/[C II] 158 µm implies solar metallicity in this galaxy, suggesting a significant chemical evolution even at *z* = 4.76 when the cosmic age was only ~1.3 billion years.

One of the main goals of modern astronomy is to understand the whole picture of galaxy evolution. However, the early phases of galaxy evolution in the early Universe are still poorly understood, partly because detailed observations of faint high-*z* galaxies are very difficult even with largest aperture telescopes available, such as the Very Large Telescope (VLT). Particularly at $z > 3.5$, the most important restframe optical emission lines are redshifted beyond the near-infrared atmospheric windows and therefore diagnosing the physical and chemical properties of galaxies is difficult (see, e.g., Maiolino et al., 2008). In addition, galaxies in their growth phase are often enshrouded by a huge amount of dust, which makes the restframe optical diagnostics unusable for such interesting populations of galaxies.

Therefore we have focused on the millimetre wavelength band, where we can examine spectra of galaxies without suffering from serious dust extinction effects. More specifically, some far-infrared emission lines, which can be used for diagnosing the physical and chemical properties of galaxies (e.g., Nagao et al., 2011), are redshifted into the submillimetre and millimetre bands at high-*z*. Therefore millimetre spectroscopy is, in principle, a promising tool to diagnose rapidly growing high-*z* dusty galaxies. However, such observations are very challenging because the diagnostic fine-structure emission lines are expected to be very faint. Recently we observed LESS J033229.4-275619 (a submillimetre galaxy [SMG] at $z = 4.76$, hereafter LESS J0332) with APEX and detected its strong [C II] 158 µm emission (De Breuck et al., 2011). This SMG hosts a heavily obscured active galactic nucleus (AGN) according to Gilli et al. (2011), but its effects on the emission line spectrum are expected to be small. This object is an interesting target because its star formation rate is very high, reaching ~1000 $M_{\odot}$ yr^{-1} (Coppin et al., 2009). However, until recently it has been impossible to detect any other fine-structure lines in this SMG due to the lack of sensitivity of previous facilities, thus preventing us from investigating in detail the properties of LESS J0332.

ALMA observations of LESS J0332

Within this context ALMA allowed us to make a major step forward. In order to assess the chemical properties of LESS J0332, we proposed to observe its [N II] 205 µm emission whose expected flux is only a few percent of the [C II] 158 µm emission. The observations were intermittently carried out from October 2011 to January 2012 with the band 6 receivers and 18 antennas. The redshifted [N II] 205 µm emission was successfully detected with a high significance (signal-to-noise of ~8) at the expected frequency, 253.9 GHz (Figure 1). In Figure 2 the resulting ALMA [N II] 205 µm spectrum is compared with the APEX [C II] 158 µm spectrum, showing that the measured [N II] 205 µm flux is only ~4 % of the [C II] 158 µm flux. It is surprising that such a faint [N II] 205 µm emission was detected with only 3.6 hours of integration with ALMA, while the [C II] 158 µm observation required 14.5 hours of integration with APEX. This demonstrates the amazing sensitivity of ALMA, even in Cycle 0.

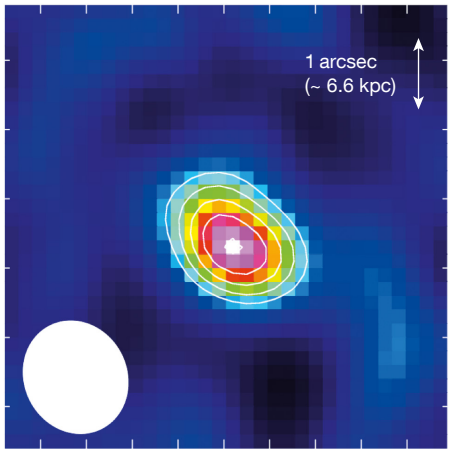

Figure 1. The ALMA image of the [N II] 205 µm emission from LESS J0332 (from Nagao et al., 2012). The size of the white arrow is equal to one arcsecond, equivalent to approximately 6.6 kpc at the distance of LESS J0322. The white ellipse at the left bottom shows the ALMA spatial resolution for the observation.

In order to assess the chemical properties of LESS J0332, we compared the observed flux ratio of [N II] 205 µm/[C II] 158 µm with predictions from photoionisation models. The comparison shows that the chemical composition of the gas clouds in LESS J0332 is close to the Solar value, i.e., $\log(Z_{gas}/Z_{sun}) = 0.0 \pm 0.4$. This is a surprising result, given the fact that we are observing a rapidly evolving SMG at $z = 4.76$, where the cosmic age was only ~1.3 billion years. Since SMGs are thought to be progenitors of local massive galaxies, our observational result suggests that massive galaxies had completed their chemical evolution much earlier than less massive galaxies. This is consistent with the "downsizing" evolutionary picture recently suggested for galaxies, i.e., mas-

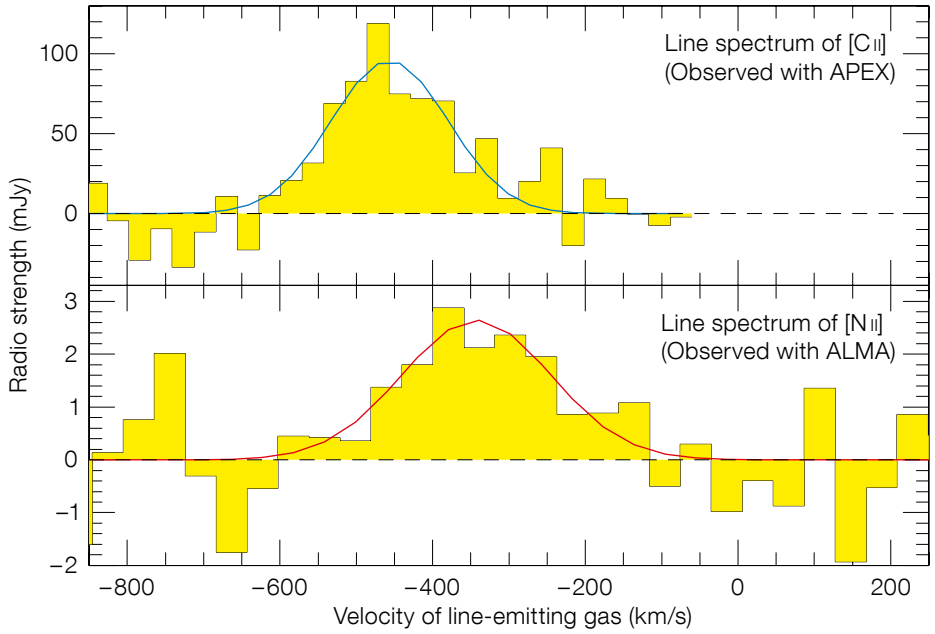

Figure 2. The APEX spectrum of the [C II] 158 μm emission (from De Breuck et al., 2011) is compared to the ALMA spectrum of the [N II] 205 μm emission (from Nagao et al., 2012) from LESS J0332.

sive galaxies underwent more evolution in earlier epochs than less massive galaxies. Note that the early metal enrichment in massive systems has also been inferred through observations of high-*z* active galactic nuclei such as quasars and radio galaxies (e.g., Nagao et al., 2006a, 2006b; Matsuoka et al., 2011).

The obvious next step is to obtain tighter constraints on the chemical properties of LESS J0332 to discriminate between different galaxy evolutionary scenarios. The current large uncertainty in the inferred metallicity is due to the fact that we have measured only two fine-structure lines, [C II] 158 μm and [N II] 205 μm. Additional observations of other lines such as [O I] 145 μm would give further constraints on the physical properties of the gas clouds in LESS J0332 and, accordingly, reduce the metallicity uncertainty.

The internal structure of the chemical properties in this SMG is also an interesting issue, because different evolutionary models of galaxies predict different redshift evolutionary scenarios of the spatial metallicity distribution (see, e.g., Cresci et al., 2010). When completed, ALMA will achieve a sensitivity and a spatial resolution significantly better than the current (already amazing) capabilities. Future ALMA observations of high-*z* SMGs, including LESS J0332, will shed additional light on the early evolutionary phase of massive galaxies.

References

Coppin, K. et al. 2009, MNRAS, 395, 1905
Cresci, G. et al. 2010, Nature, 467, 811
De Breuck, C. et al. 2011, A&A, 530, L8
Gilli, R. et al. 2011, ApJ, 730, L28
Maiolino, R. et al. 2008, A&A, 488, 463
Mannucci, F. et al. 2009, MNRAS, 398, 1915
Matsuoka, K. et al. 2011, A&A, 532, L10
Nagao, T. et al. 2006, A&A, 447, 157
Nagao, T. et al. 2006, A&A, 447, 863
Nagao, T. et al. 2011, A&A, 526, A149
Nagao, T. et al. 2012, A&A, 542, L34

ESO/S. Rossi

One of the ALMA 12-metre-diameter European antennas is shown being moved on the antenna transporter during testing at the ALMA Operations Support Facility. See Picture of the Week 16 July 2012 for more information.

The laying of the foundation stone of the new extension to the ESO Headquarters building was commemorated in a ceremony on 11 June 2012. Applying their hammers are (from left to right): the mayor of the town of Garching, Ms Hannelore Gabor, HQ extension project manager, Christoph Haupt, the President of the ESO Council, Xavier Barcons, and the ESO Director General, Tim de Zeeuw. Among the documents placed in the foundations was a copy of the June 2012 *Messenger*; see Announcement 12044 for more information.

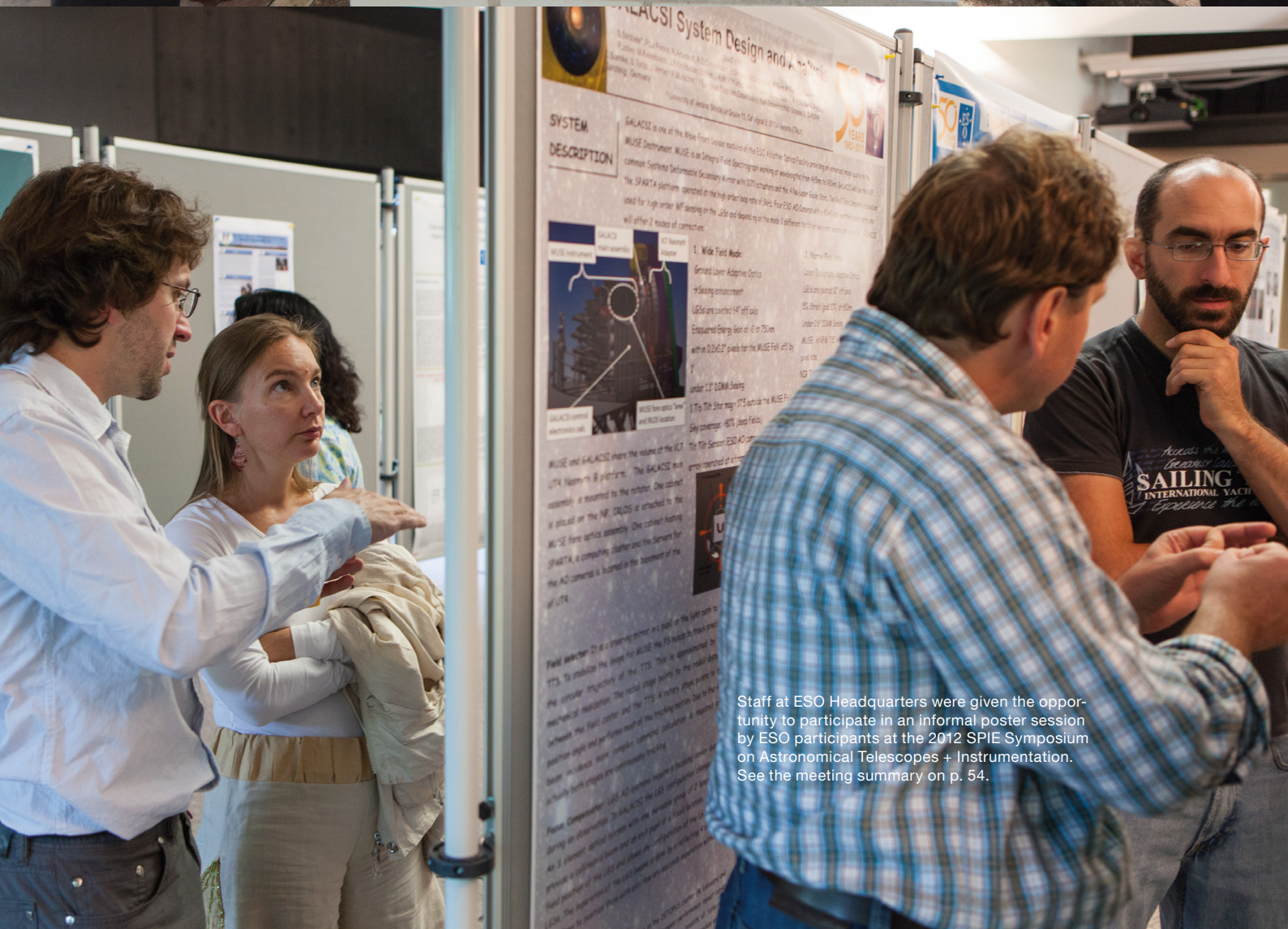

Staff at ESO Headquarters were given the opportunity to participate in an informal poster session by ESO participants at the 2012 SPIE Symposium on Astronomical Telescopes + Instrumentation. See the meeting summary on p. 54.

Report on the

ALMA Community Days: Early Science in Cycle 1

held at ESO Headquarters, Garching, Germany, 25–27 June 2012

Suzanna Randall[1]
Leonardo Testi[1]
Evanthia Hatziminaoglou[1]

[1] ESO

Early Science operations began in September 2011 and ALMA is now more than half way through Cycle 0 and continues to gather data of remarkable quality. The first scientific results based on ALMA data include some very interesting findings and the number of ALMA publications is rapidly increasing. From the start of Cycle 1 at the beginning of 2013, the array will be offered to the astronomical community with enhanced science capabilities. The 2012 ALMA Community Days, summarised here, were held just a few weeks before the Cycle 1 proposal submission deadline and were designed to optimally prepare the European ALMA Community for Cycle 1 proposal submission.

ALMA, the Atacama Large Millimeter/submillimeter Array, is a global collaboration involving Europe, North America, East Asia and the host country Chile. The array is located on the Chajnantor Plateau in northern Chile at an altitude of 5000 metres, and when fully completed will comprise at least 66 high-precision antennas equipped to observe in the 30 GHz to 1 THz frequency range. ALMA has already started to produce transformational results from Early Science Cycle 0 programmes and will continue to be the world's leading observatory at millimetre and submillimetre wavelengths over the coming decades.

Until the end of construction (foreseen for 2013) ALMA is being operated in Early Science mode, where part of the time available is used for approved projects from the astronomical community, but completion and commissioning of the telescope take priority. Nearly 1000 observing proposals from the ALMA Community were received for Early Science Cycle 0, with an average oversubscription factor approaching ten. The highest ranked projects were scheduled for execution in the period from September 2011 through to the end of 2012. The science capabilities offered for Cycle 0 were rather limited, and comprised only sixteen 12-metre antennas, very limited spectroscopic flexibility, and baselines shorter than ~400 metres. Nevertheless, the data quality is already unmatched by similar (sub)millimetre facilities at the same angular resolution, and the first scientific publications clearly reveal ALMA's potential as construction nears completion.

In Cycle 1, the science capabilities offered to the community will be greatly enhanced compared to Cycle 0, and will include 32 antennas in the main 12-metre array as well as nine 7-metre antennas in the Atacama Compact Array (ACA) and two 12-metre antennas for the Total Power (TP) array. The frequency bands offered will be the same as in Cycle 0 – Band 3 (84–116 GHz, ~ 3 mm), Band 6 (211–275 GHz, ~ 1.3 mm), Band 7 (275–373 GHz, ~ 850 μm) and Band 9 (602–720 GHz, ~ 450 μm). More flexibility in combining continuum and high spectral resolution observations will be offered, and antenna baselines will reach up to ~ 1 kilometre.

In order to introduce the community to the Cycle 1 capabilities, a 2–3 day workshop was organised at ESO Garching with the aim of optimally preparing the European ALMA user community for proposal preparation in Cycle 1. The format was similar to that of the previous ESO ALMA Community Days held in April 2011 in preparation for Cycle 0 (see Randall & Testi, 2011). The first day of the workshop featured a variety of technical presentations giving an overview of the ALMA project, Cycle 1, and the user support available, as well as scientific presentations showing the first ALMA results. The rest of the workshop was dedicated to hands-on tutorials for the two main pieces of software used for proposal preparation: the ALMA Observing Tool (OT) and the ALMA Simulator Tools.

The ESO ALMA Community Days were part of a coordinated effort by the European ALMA Regional Centre (ARC) network to organise tutorials and webinars for users across the ESO Member States. We welcomed around 80 registered participants mostly from Europe, but also from as far afield as Australia. Interestingly, more than half the participants described themselves as novices in radio/submillimetre interferometry, indicating the broad interest in ALMA science. This fully supports the design goal of ALMA, which from the outset was conceived as a general community facility with strong emphasis placed on easy-to-use tools and widespread user support.

Technical information

Intended as an introduction to ALMA, the first morning's presentations started off with an overview of the ALMA construction status and the role of the European Science Advisory Committee (ESAC). This was followed by a recap of the first year of ALMA science observations and a breakdown of the science capabilities in Cycle 1.

The audience were then walked through the tools and processes important for observing with ALMA, starting with the ALMA Science Portal[1]. This web interface provides all the relevant information and software tools, and allows registered users access to the Helpdesk facility as well as information on their ALMA projects. The software tools pertinent to proposal preparation, the ALMA Simulator Tools and the ALMA Observing Tool, were introduced in preparation for the practical hands-on tutorials of the following days. While the simulators are used to get a feel for the image that ALMA will obtain of an object, taking into account the array configuration and time spent on source, the ALMA OT is used to prepare and submit the actual proposal. It captures all the technical information necessary to execute the observations and determines the setup of the array and the correlator for accepted projects. The proposal review process was then outlined, followed by a description of Phase 2 processes for highly ranked projects and the quality assurance and data delivery measures taken for executed observations in Cycle 1.

In the afternoon of that same day, the technical talks focused on user support provided by the European ALMA Regional Centre. The European ARC together with its counterparts in North America and East Asia presents the inter-

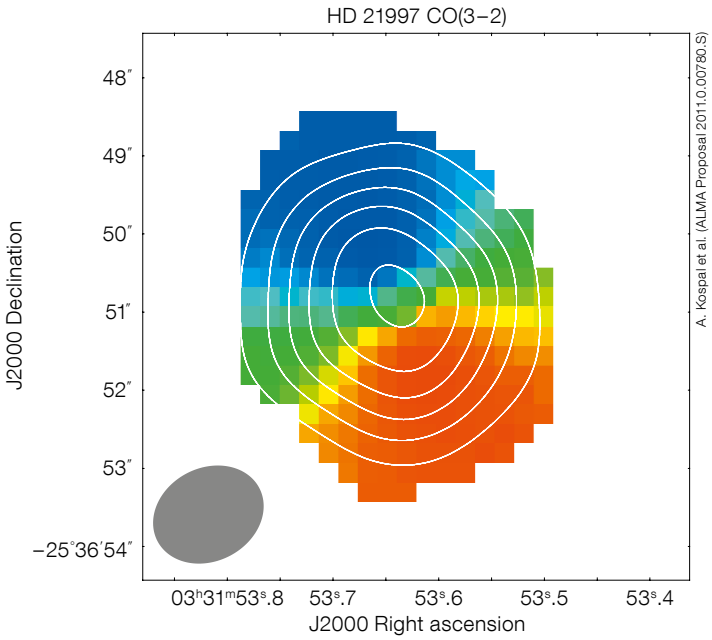

Figure 1. Map of the integrated CO line intensity (white contours) and the velocity field (background image) of the debris disc HD 21997 as seen by ALMA. The gray ellipse in the bottom left corner shows the synthesised beam.

face between the Joint ALMA Observatory in Chile and the astronomical community. It consists of a coordinating ARC hosted at ESO and seven ARC nodes distributed across Europe that between them provide a variety of services for European ALMA users, including face-to-face support, Phase 2 support, software development, data reduction and quality assurance, as well as the organisation of community events[2]. The ARC also runs the Helpdesk facility, which is the official point of contact for questions or comments specific to ALMA. Additional services offered by the ARC include the development of advanced data modelling software such as the ARTIST software, which was also presented.

The day of presentations was concluded by an outlook on the long-term development of ALMA science capabilities. In the medium term, it is expected that the array will be equipped with Band 5 (~187 GHz) receivers, originally developed in Europe as part of an EC-FP6 funded ALMA Enhancement Project. Another development within the next four years or so will be the capability to phase ALMA for incorporation into the mm-VLBI (millimetre-Very Long Baseline Interferometry) network (see the following report on the mm-VLBI workshop on p. 50). On a longer timescale, there are plans to equip the array with the low frequency Band 1 (~40 GHz) and Band 2 (~80 GHz) receivers. The possibility of supra-THz interferometry is also being studied, along with possible upgrades of the existing ALMA components.

First ALMA science results

Some spectacular scientific results based on both Cycle 0 projects and Science Verification ALMA data were presented by invited members of the European ALMA community in the science session. Matthias Maercker (ESO/Argelander Institut für Astronomie) presented an analysis of the shell structure of the asymptotic giant branch star R Scl (see front cover). The ALMA carbon monoxide (CO) observations allowed the mass loss of the star in the quiescent phase between thermal pulses to be reliably measured for the first time, leading to a reconstruction of the mass loss history in the ~2000 years since the last thermal pulse event.

Moving far beyond the realms of the Galaxy, Axel Weiss (Max-Planck-Institut für Radioastronomie) then described his redshift study of strongly lensed submillimetre galaxies from a Band 3 spectral scan. The use of ALMA as a stand-alone redshift pinpointer for submillimetre galaxies (alleviating the need for radio continuum cross-identification and subsequent expensive optical spectroscopy follow-up) was dramatically demonstrated. The quick ALMA spectral scans enabled the detection of at least one molecular line in 90 % of the submillimetre selected galaxies and two lines (allowing an unambiguous redshift determination) in 50 % of the sample. The emerging picture is a redshift distribution for submillimetre galaxies extending well beyond the $z \sim 2$–3 cutoff imposed by the selection effect caused by the centimetre radio continuum sensitivity in the past.

Agnes Kospal (ESA/ESTEC) was a little closer to home with her analysis of the molecular gas in the debris disc system HD 21997. ALMA's sensitivity makes it possible to observe the molecular gas abundance and kinematics in this young debris disc, allowing the study of the early phases of disc dissipation (see Figure 1). Switching back to extragalactic astrophysics, Cinthya Herrera (Institut d'Astrophysique Spatiale) combined ALMA Science Verification and VLT-SINFONI data to trace the Antennae galaxies merger. The combination of data from the two major ESO facilities in the infrared and submillimetre allowed the first detection of a compact and very massive molecular cloud, most likely a precursor for extragalactic Super Star Clusters. Moving to the Solar System, Thibault Cavalié (Laboratoire d'Astrophysique de Bordeaux) showed impressive maps of Saturn's 2011 storm as seen by Herschel and ALMA (see Figure 2). These data probe into the planetary atmosphere and can be used to constrain the physical and chemical models for gaseous giants.

Finally, an overview of the Science Verification data taken to date was presented, including the stunning Band 3 mosaics of the grand design spiral M100 and of the central regions of Centaurus A. The first released Band 9 data on IRAS 16293 were also shown.

Hands-on software tutorials

For the practical software tutorials the participants were split into two groups according to their experience with radio/submillimetre interferometry. While the advanced tutorials were designed to be more compact and last only one day, the

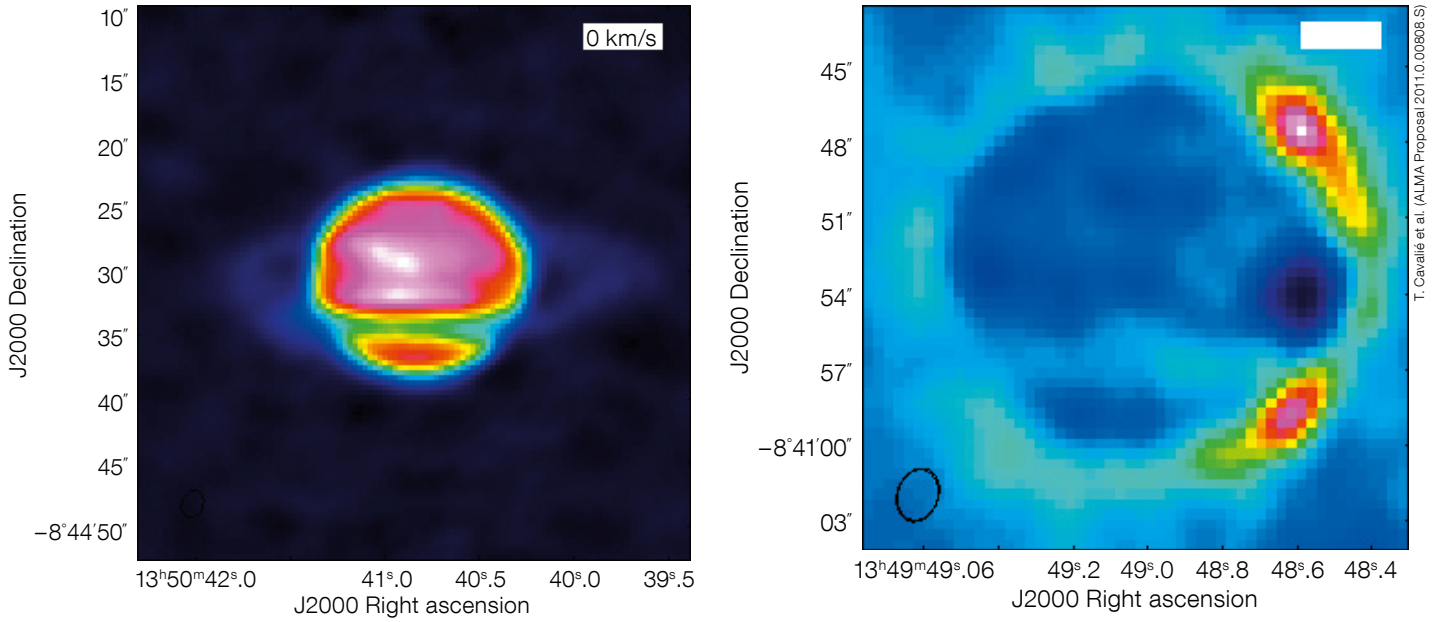

Figure 2. Left: ALMA continuum image of Saturn. The rings can also be seen (east and west of the planetary disc in emission, and in front of the planet absorbing part of its emission). The data were obtained in ALMA Band 6. Right: CO emission at the velocity of Saturn's Great Storm 2011 remnant (now a huge stratospheric warm vortex). While CO was detected in emission along the entire atmospheric limb, the vortex can easily be discerned as the brightest spot on the map (located at ~ 40 degrees northern latitude).

novice tutorials continued into the third day of the workshop, allowing more time. Each group was tutored in the use of both the Simulator Tools and the ALMA OT and started off with a short presentation/demonstration of the tool followed by periods of individual work assisted by tutors (see Figure 3). The novice tutorials included an extensive introduction to submillimetre concepts, the spectral setup and the basics of interferometry, whereas the advanced sessions focused more on the changes since Cycle 0. In total, around 60 participants chose to attend the tutorials.

The feedback received on the Cycle 1 ALMA Community Days was generally very positive, and several of the participants already expressed interest in a similar Cycle 2 workshop. Tutorial material and presentations are available in electronic form on the conference website[3].

Acknowledgements

We would like to thank Christina Stoffer and the ESO Garching IT Helpdesk for their practical support. We gratefully acknowledge the help of Luca Cortese and Roberto Galvan-Madrid. The tutorials on the second day would not have been possible without the tutors: Andy Biggs, Alan Bridger, Bartosz Dabrowski, Evanthia Hatziminaoglou, Liz Humphreys, Stefanie Mühle and Suzanna Randall (OT), as well as Steve Longmore, Anaelle Maury, Rosita Paladino, Anita Richards, Eelco van Kampen and Martin Zwaan (Simulators). Finally, we would like to thank all the speakers for putting so much work into their presentations. The workshop was sponsored by ESO and Radionet, who provided travel support to a number of speakers and tutors.

References

Randall, S. & Testi, L. 2011, The Messenger, 144, 39

Links

[1] ALMA Science Portal: www.almascience.org
[2] More information on the ARC at: http://www.eso.org/sci/facilities/alma/arc.html
[3] Community Days 2012 website: http://www.eso.org/sci/meetings/2012/alma_es_2012/program.html

Figure 3. The workshop participants busy at the practical tutorial sessions.

Report on the ESO Workshop

mm-wave VLBI with ALMA and Radio Telescopes around the World

held at ESO Headquarters, Garching, Germany, 27–28 June 2012

Heino Falcke[1]
Robert Laing[2]
Leonardo Testi[2]
Anton Zensus[3]

[1] Radboud University Nijmegen and ASTRON, Dwingeloo, the Netherlands
[2] ESO
[3] Max-Planck-Institut für Radioastronomie, Bonn, Germany

Very long baseline interferometry at millimetre/submillimetre wavelengths (mm-VLBI) offers the highest achievable spatial resolution at any wavelength in astronomy and the inclusion of ALMA into a global network will bring unprecedented sensitivity. The workshop on mm-VLBI reviewed the broad range of science topics, from imaging the event horizon of the black hole at the centre of the Galaxy, through masers in the Milky Way and distant galaxies to jets in radio galaxies. Plans were laid to develop a science case and a European organisation to promote mm-VLBI including ALMA.

The huge potential of very long baseline interferometry (VLBI) at millimetre and submillimetre wavelengths is that it enables the highest resolution imaging currently possible at any wavelength in astronomy. The spatial resolution of an interferometer in radians is given by the ratio of the observing wavelength to the separation of the telescopes. For a wavelength of 1 mm and a separation of 9000 km, this resolution is about 20 microarcseconds. Using ALMA as a phased array to form part of a global VLBI network will offer unprecedented sensitivity at very high angular resolution. This capability will allow the shadow of a black hole, the relativistic jet flows in active galactic nuclei (AGN) and the dusty winds near stellar surfaces to be imaged; and it may potentially even improve measurements of the Hubble constant.

While ALMA is nearing completion and the first observing cycle is under way, astronomers are already thinking ahead along these lines. To discuss the opportunities from a European perspective, over 65 scientists gathered at ESO Headquarters in Garching to attend a one and a half day workshop on mm-wave VLBI with ALMA and other telescopes. In the following report on the workshop, the names of speakers are given in square brackets in the text and all of their talks are linked to the conference webpage[1].

The reason why the millimetre-wave region is so important for ultra-high-resolution imaging is that heterodyne receivers can still be used and quantum effects do not yet limit our ability to do interferometry, as they do at shorter wavelengths. The addition of ALMA offers a leap in sensitivity, thus making many more and weaker sources accessible to ultra-high-resolution studies and greatly improving image fidelity for the brighter objects. Only sources with flux densities above several hundred milliJansky (mJy) have been observable so far; this threshold could be reduced by more than an order of magnitude if ALMA were to be included.

The phasing up of ALMA as part of a VLBI array had been envisaged from the beginning of the project and is incorporated into the system design, but had been deferred on cost grounds, and in the interests of completing the instrument for stand-alone operation. The ALMA Development Steering Committee is now considering a proposal by a team of institutions led by the MIT Haystack Observatory in the USA to upgrade the ALMA correlator and to create the operational infrastructure needed for the efficient phasing of all antennas [Doeleman, Baudry]. This would effectively allow the array to be used as a giant single dish in parallel to its normal interferometric mode. Recording ALMA data and correlating it with those of other (sub)millimetre telescopes would then provide the standard ALMA data products as well as super-high resolution images from the VLBI mode.

ALMA's wide frequency range (35–950 GHz, once all of the planned receiver bands are completed) will enable a broad range of VLBI science to be pursued by astronomers in Europe and around the world. It was therefore timely to bring together interested European astronomers to discuss their scientific interests and ambitions for this new ALMA observing capability. The meeting followed immediately after the Garching ALMA Community Days. The first part of the meeting included reviews of current activities and achievements in mm-VLBI, including the Event Horizon Telescope Collaboration, currently being run by Haystack Observatory, and the Global Millimeter VLBI Array coordinated at the Max-Planck-Institut für Radioastronomie in Bonn. The second part concerned the potential science that will be enabled by a VLBI array including ALMA (Figure 1). The final discussion centred on upcoming developments worldwide. Following

Figure 1. Scientists from all across Europe discussing mm-wave VLBI science with ALMA in the ESO auditorium.

on from the meeting, a science case will be developed, incorporating the ideas presented and discussed.

Approaching the event horizon

One major science case that has been driving the development of sub-mm VLBI has been the possibility of imaging the innermost parts of accretion discs and jets around supermassive black holes and in particular imaging the shadow of the event horizon in the black hole at the Galactic Centre [Falcke, Doeleman]. The shapes and sizes of the shadow and the photon ring surrounding it (e.g., Figure 2) are precisely predicted by Einstein's theory of general relativity (GR), so this observation would provide tests not only of the black hole paradigm but also of GR in its strong-field limit.

The Galactic Centre, Sgr A*, is the most favourable source for this experiment, since the angular size of its black hole shadow on the sky is the largest known and has optically thin millimetre- and submillimetre emission on event horizon scales. Most importantly, the mass of this source has been determined accurately by near-infrared imaging of the stars in the central region of the Milky Way. Ultimately, the mass constraints will improve even further with near-infrared interferometry, especially the GRAVITY project (Eisenhauer et al., 2011). There will be extremely interesting synergies between ALMA VLBI and VLTI in the area of strong-field GR studies [Eisenhauer].

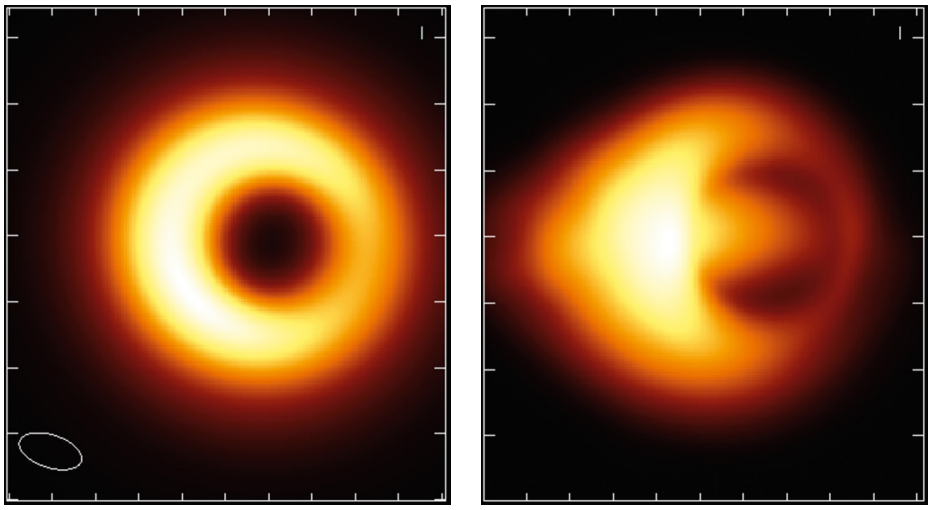

Figure 2. Simulated images at 345 GHz of the black hole in the Galactic Centre using a VLBI array involving ALMA and other telescopes. The input model is based on general relativistic magneto-hydrodynamic simulations of plasma around a Kerr black hole from Mościbrodzka et al. (2009). Left: Face-on orientation; Right: Edge-on orientation. The black hole shadow and photon ring are much more difficult to detect, but still visible in the edge-on case. Figure updated from Falcke et al. (2011).

Powerful jets

The other source of great interest in this respect is the black hole in the central galaxy of the Virgo cluster, M87. This black hole is a thousand times further away, but also a thousand times more massive then Sgr A*, so their event horizons are comparable in angular size. In M87, the radio emission is undoubtedly produced by a relativistic plasma jet (Figure 3). Recent mm-VLBI observations [Krichbaum, Hada] indicate that this jet forms on the scale of a few Schwarzschild radii, thus imposing extreme constraints on all possible models for jet formation. VLBI at 230 GHz and above should ultimately reveal the region where the jet is formed, thereby addressing one of the fundamental problems of astrophysics: jets and discs are ubiquitous in astronomical objects ranging from young stars to supermassive black holes.

Moreover, the study of relativistic jets with VLBI has recently received additional attention in connection with observations of blazars made by the Fermi satellite. Multi-wavelength campaigns suggest that bright gamma flares are directly connected to outbursts and component ejections seen at millimetre wavelengths.

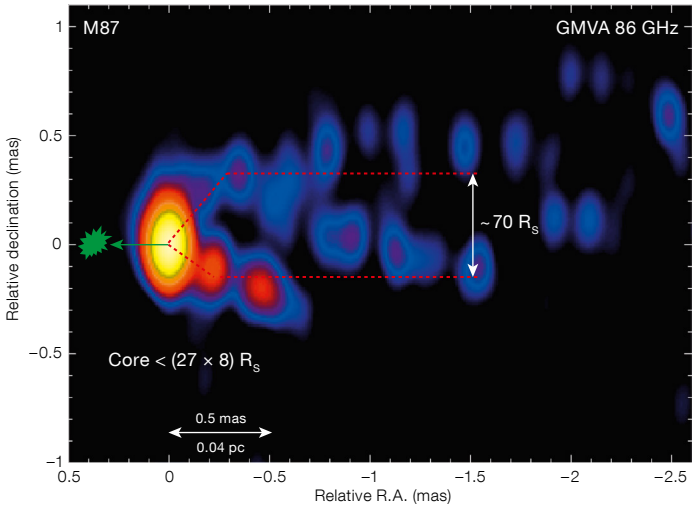

Figure 3. Left: 86 GHz VLBI image of the jet in M87 (from Krichbaum et al., 2007). The jet extends down to some tens of Schwarzschild radii (Hada et al., 2011). Right: A 43 GHz VLBA image from Walker et al. (2008), clearly revealing the limb-brightened structure also seen at 86 GHz.

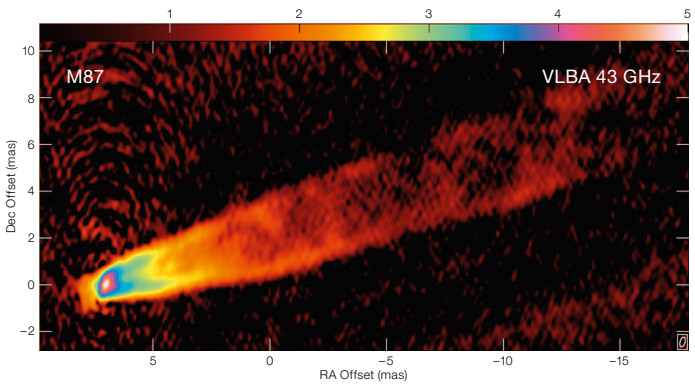

Surprisingly, these flares seem to come from rather large distances from the black hole, i.e., regions that can still be imaged by mm-VLBI even in more distant sources, where the event horizon is too small to resolve [Giroletti, Orienti].

Masers in stars, star-forming regions and AGN

Another fascinating science driver at millimetre wavelengths is high-brightness line emission. Many of the lines commonly detected by ALMA are produced in extended and diffuse regions with low brightness temperatures and are not detectable at high spatial resolution. This changes, however, when one looks at maser emission or at absorption lines towards compact continuum sources [Impellizzeri].

Well-known examples of maser sources occur in evolved stars, where H_20 and SiO masers provide impressively detailed tracers of the dynamics of the molecular and dusty winds blown away from the old star into the interstellar medium [Colomer, Richards]. Quite a number of maser lines of water and other molecules have frequencies above 35 GHz. (A list of maser transitions relevant to VLBI is given in the contribution by E. Humphreys linked to the conference web page). Some of these transitions are expected to come from the most excited molecules close to the stellar surface (Figure 4). Precise astrometry of masers [Brunthaler] is also needed in the Galactic Centre, where the accuracy of the basic reference frame for calculating stellar orbits is limited by errors in cross-referencing the radio and optical reference frame using SiO masers.

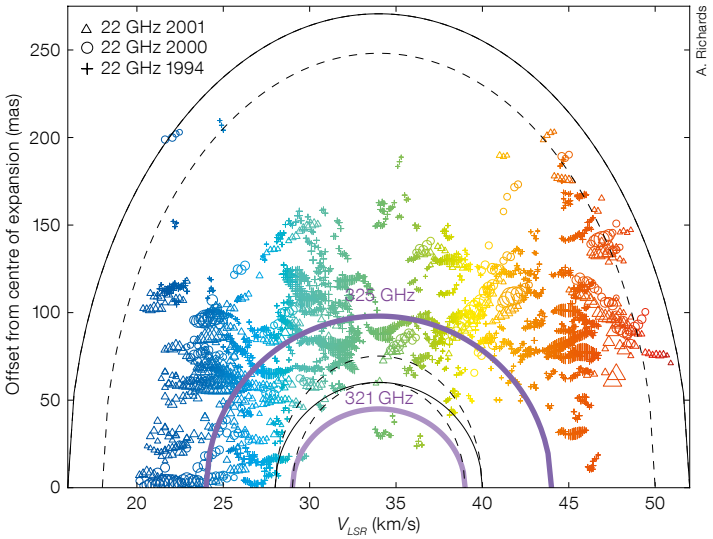

Figure 4. Position–velocity plot showing the observed 22 GHz water vapour emission from the oxygen-rich AGB star IK Tau (colour-coded by velocity), together with the predicted locations of water maser emission at 321 and 325 GHz from models by Malcolm Gray.

Masers are also seen in star-forming regions and young stellar objects, particularly in regions excited by shocks [Goddi]. They may trace radial infall as well as outflow. Again VLBI allows precise measurement of the dynamics of these processes.

A foretaste of the potential of high-resolution maser observations at millimetre wavelengths has been given by the first ALMA test observations of 321 and 658 GHz water masers with two-kilometre baselines (Figure 5). The observations are part of the initial tests on the longer baselines and demonstrate the use of compact spectral line sources for calibration. The targets chosen for these initial tests are well known high-mass star-forming regions, which contain bright maser sources, and analysis of the test data is still in progress. These early results clearly show the potential of ALMA and, in the future mm-VLBI, for high angular resolution imaging of bright maser sources. Additional tests are currently being planned targeting masers

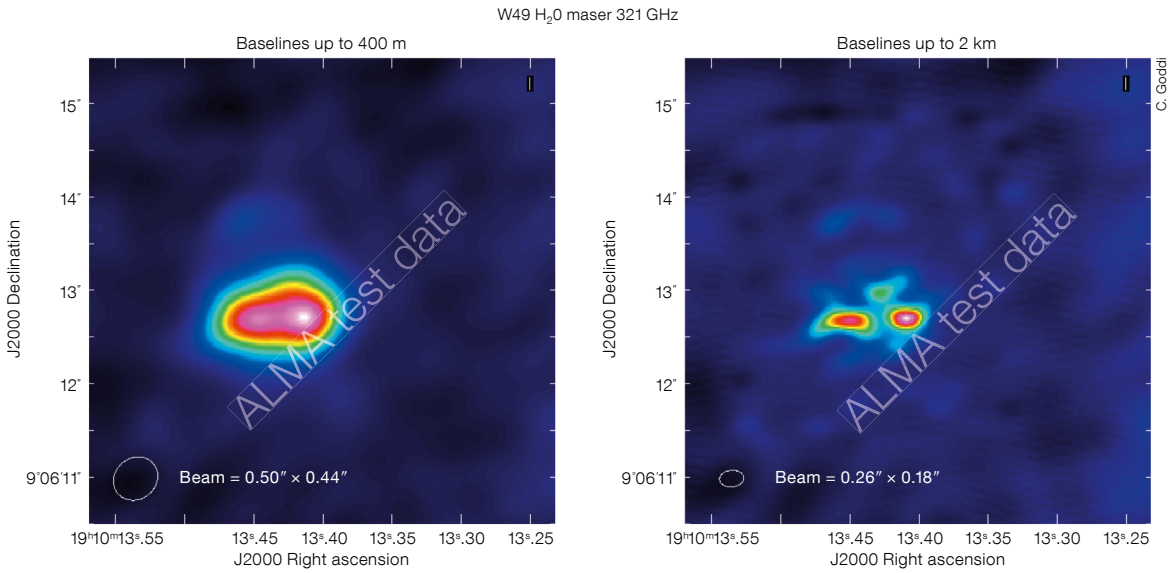

Figure 5. ALMA test observations of water-maser emission from W49N at 321 GHz. Left: baselines up to 400 metres, with a beam of 0.55 by 0.44 arcseconds. Right: baselines up to 2 kilometres with a beam of 0.26 by 0.16 arcseconds.

in late-type stars. A full characterisation of submillimetre maser sources across the sky may also generate an alternative network of (bright) phase calibrators for high frequency observations.

Extragalactic maser sources are also known [Humphreys]. A famous example is the nearby active galaxy NGC 4258, where a warped molecular disc surrounds the central supermassive black hole. VLBI proper motion observations of 22 GHz water masers in the disc have been used to obtain a precise geometric distance to this galaxy, making it a crucial component of the extragalactic distance ladder. Currently the water maser cosmology project is extending this technique to larger distances, thereby providing an independent measurement of the Hubble constant and a direct determination of black hole masses (important for the black hole mass–velocity dispersion relation). Observations of higher frequency water maser transitions (e.g., 183 or 321 GHz) have the potential to improve our understanding of the accretion disc physics and geometry. Particularly intriguing is the speculation that super-masers might exist. In those systems the millimetre-wave emission could be more intense than the well known 22 GHz line and perhaps detectable to greater distances.

Pulsars, microquasars and gamma-ray bursts

Finally, there are many other compact sources that are potential targets for mm-wave VLBI. In particular, transient sources such as supernovae, gamma-ray bursts and microquasars should be very interesting, since the highest frequencies probe the earliest phases of any eruption.

At first sight, pulsar science is an unexpected field for ALMA, since the radio spectra of pulsars are usually very steep. Nevertheless, there is some indication of spectral flattening at millimetre wavelengths and a phased ALMA should be able to observe pulsed emission [Kramer]. Of particular interest would be searches for pulsars in the Galactic Centre, where low-frequency pulses suffer from huge dispersion and scattering, to the extent that they become undetectable. An optimally located pulsar could, e.g., measure the black hole mass to one part in a million and provide independent tests of GR.

Organisational challenges

VLBI inherently requires many telescopes to operate together. While the ALMA phasing project is under way, other millimetre telescopes will also be needed to act as part of a global array. Existing activities at 3 mm (the Very Long Baseline Array and the Global Millimeter VLBI Array) and at 1 mm (the Event Horizon Telescope project) have laid the groundwork for future coordinated observations. Some of the most outstanding science goals, like imaging the black hole shadow, are unlikely to be achieved with just a few baselines. As ALMA reaches full operation, there will be financial pressures to close down existing facilities, but on the positive side, new facilities are emerging such as the Large Millimeter Telescope (LMT) in Mexico [Hughes] and the Long Latin American Millimeter Array (LLAMA) in Argentina [Cseh]. In Europe, the Northern Extended Millimeter Array (NOEMA) project, an upgrade of the Institut de Radioastronomie Millimétrique (IRAM) Plateau de Bure Interferometer is going ahead [Bremer] and large single dishes (IRAM 30-metre, Effelsberg, Sardinia Radio Telescope, Yebes, Onsala and Metsähovi) will play an important role at 3 and 7 mm wavelengths. In the USA, the Very Long Baseline Array (VLBA) is crucial, as well as the Combined Array for Research in Millimeter-wave Astronomy (CARMA) [Brinkerink], the Submillimeter Telescope (SMT) and Submillimeter Array (SMA) at higher frequencies.

Overall the meeting demonstrated that European astronomers have a broad range of science interests beyond the initial key projects that will be addressed by a phased ALMA facility alone and in coordinated mm-VLBI observations. This might, for example, be organised following the established examples of the European VLBI Network (EVN) supported by the Joint Institute for VLBI in Europe (JIVE) [van Langevelde], as well as the Global Millimeter VLBI Array. The inclusion of ALMA and the extension to higher frequencies will bring a very substantial improvement in data quality, but also an extra level of complexity, such as a yet-to-be achieved form of dynamic scheduling to take account of changing weather conditions.

The community's enthusiasm about the groundbreaking possibilities offered by mm-VLBI with ALMA was clearly evident during the workshop: some of the expected science results may indeed become transformational. There was general agreement at the conclusion of the meeting that, from a European perspective, the ultimate goal of the planning process should be a facility accessible to the general user, with time made available through open competition.

On the way towards this goal, the scientific needs of the user community for mm-VLBI with ALMA need to be compiled as a necessary input to the approval process for the ALMA phasing project. Some of the technical challenges of this project are being addressed by the international multi-partner phasing-project led by the Haystack Observatory: the task for the nascent European ALMA VLBI user community is to organise itself to prepare for the successful use of this exciting new capability.

The meeting was co-sponsored by ESO and Radionet3, an EU Integrated Infrastructure Initiative to coordinate access, development and training for radio astronomy facilities in Europe[2].

References

Eisenhauer, F. et al. 2011, The Messenger, 143, 16
Falcke, H. et al. 2011, IAU Symp., 275, 68
Hada, K. et al. 2011, Nature, 477, 185
Maitra, D. 2011, IAU Symp., 275, 82
Krichbaum, T. et al. 2007, *Exploring the Cosmic Frontier: Astrophysical Instruments for the 21st Century*, 189
Mościbrodzka, M. et al. 2009, ApJ, 706, 497
Walker, R. C. et al. 2008, *Extragalactic Jets: Theory and Observation from Radio to Gamma Ray*, ASP Conference Series, 386, 87

Links

[1] Workshop webpage: http://www.astro.ru.nl/mmVLBI2012
[2] Radionet3: http://www.radionet-eu.org

Some Reflections on the SPIE 2012 Symposium on Astronomical Telescopes + Instrumentation

Jeremy Walsh[1]
Compiled from contributions*

[1] ESO

A very brief summary of the 2012 SPIE Symposium on Astronomical Telescopes + Instrumentation, held in July in Amsterdam, is presented from the viewpoint of ESO contributions.

The 2012 SPIE meeting on Astronomical Telescopes + Instrumentation (1–6 July 2012)[1] was even larger than the last meeting in 2010 in San Diego (see Casali, 2010) with around 2300 attendees. It is thus almost impossible to present a comprehensive overview of such a huge meeting consisting of 12 separate conferences, as well as courses and exhibitions. Instead a few reflections collected from some of the ESO participants are presented.

Not surprisingly ESO staff played a strong role in the meeting with more than 100 attending, many involved in the programme committees and a number chairing. Mark Casali was Symposium co-chair and four of the conferences had ESO chairs — Françoise Delplanke for the Optical and Infrared Interferometry III conference, Suzanne Ramsay for Ground-based and Airbourne Instrumentation for Astronomy IV, Enrico Marchetti for Adaptive Optics Systems III and Fernando Comeron for Observatory Operations: Strategies, Processes and Systems IV. In addition, the speaker at the conference dinner was Jason Spyromillio, who talked on how big telescopes can also make big trouble (for engineers at least). One of the plenary speakers was also Thijs de Graauw from the Joint ALMA Observatory.

The conference on Observatory Operations is closest to ESO's core task of running a ground-based observatory. This year time domain astronomy had an increased emphasis, motivated by the growing numbers of robotic telescopes and networks producing enormous amounts of data on a nightly basis, and mainly geared towards the identification of various types of transients. In the current context of global financial difficulties, maintaining the excellence of operations and of support to the community in an environment of increasingly tight resources was a common underlying theme. The measurement of scientific effectiveness of facilities through bibliometrics and their importance as a part of the observatory operations chain is viewed as increasingly important at observatories, including La Silla Paranal.

The Ground-based and Airbourne Instrumentation for Astronomy conference featured VLT instruments heavily, including overviews of the ESO instrumentation programme. Separate presentations of instruments under construction such as KMOS, MUSE and SPHERE, those in plan, such as ERIS, ESPRESSO, MOONS and 4MOS, and current instruments undergoing upgrade, such as VISIR and CRIRES, were given. There were extensive poster sessions on multi-object instruments and planet finders. The instrument programmes for the three Extra Large Telescopes (European Extremely Large Telescope [E-ELT], Giant Magellan Telescope [GMT] and Thirty Meter Telescope [TMT]) were presented as well as several of the individual instrument concepts for the E-ELT.

The Adaptive Optics Systems conference, not surprisingly, was very heavily attended with more than 260 contributions. The most exciting results are coming from the multi-conjugate adaptive optics (MCAO) systems demonstrating exceptional image sharpness over fields up to 80 arcseconds. The VLT Adaptive Optics Facility (AOF) is currently the most complex system under development and was well represented. The realms of astronomical science where AO makes the greatest mark from Solar System science to extragalactic were presented, not forgetting the Galactic Centre. The plans for AO for the three ELTs were featured and a new development of MCAO for ELTs using natural guide stars was outlined.

The conference on Optical and Infrared Interferometry strongly featured the existing VLTI instruments among those of the other ground-based interferometry facilities and their critical subsystems. There were also presentations of the VLTI visitor instrument Pionier and the two second generation VLTI instruments GRAVITY and MATISSE. While space interferometry featured less strongly than in previous years, sparse aperture masking showed an impressive boost in capabilities and science results. Future prospects for interferometric facilities and data reduction software were intensively discussed (during almost a full day) and the, now regular, award of the prize in the Interferometric Imaging Beauty Contest was presented.

Given the important role of the SPIE Astronomical Telescopes + Instrumentation meetings in presenting so many aspects of ESO's core activities and to give those who could not attend a flavour of some of the ESO presentations, an informal poster session was organised at ESO Headquarters on 17 July (see Figure on p. 46). Twenty-four posters were shown and the presenters were available for discussion. The topics covered all ESO activities from detectors, laser systems, adaptive optics, fibres, instrument and E-ELT component designs, instrument software control, to operating performance monitoring and bibliometrics. The poster session was well attended and appreciated by those who did not attend the meeting, and by a few who were at the SPIE meeting, but might understandably have missed something.

The next SPIE meeting will be held in Montreal, Canada in 2014.

* Contributions from Fernando Comeron, Françoise Delplancke, Enrico Marchetti and Suzanne Ramsay.

References

Casali, M. 2010, The Messenger, 141, 40

Links

[1] SPIE 2012Astronomical Telescopes + Instrumentation: http://www.spie.org/x13662.xml

Report on the Symposium

30 Years of Italian Participation to ESO

held at the Pontificia Università Lateranense, Rome, Italy, 2–3 July 2012
as part of the European Week of Astronomy and Space Science (EWASS 2012) meeting

Vincenzo Mainieri[1]

[1] ESO

On 24 May 1982 Italy joined ESO, becoming the eighth Member State. In the past 30 years the participation of Italy in all of ESO's endeavours has been substantial in all respects: people; fundamental industrial contributions in the construction of telescopes and infrastructures; collaboration of institutes in the development of instrument components; and science programmes. The aim of the symposium was to review critically these past achievements and discuss Italian participation in future ESO projects.

After a welcome address by the ESO Director General, Tim de Zeeuw, the programme started with a historical review by Giancarlo Setti, which illustrated the reasons why Italy did not join at the time of ESO's foundation in 1962, and described the key players, scientists as well as politicians, and the favourable circumstances that contributed to Italy becoming a Member State 20 years later. The importance of access to ESO facilities for the Italian astronomical community was stressed by Monica Tosi, as well as the significant success rate of Large Programme proposals with Italian principal investigators (PIs). The rest of the first morning was dedicated to the contribution of Italian industry to ESO projects. Massimo Tarenghi described the contributions connected with the New Technology Telescope (NTT) and the Very Large Telescope (VLT), while Stefano Stanghellini covered the involvement in the European Atacama Large Millimeter/submillimeter Array (ALMA) antenna design and construction.

In the afternoon session there were invited talks on some highlights of extragalactic scientific results obtained by Italian astronomers using ESO facilities (presented by Elena Pian, Adriano Fontana, Laura Pentericci and Giovanni Cresci), proceeded by a review talk from Alvio Renzini on high impact scientific papers led by Italian astronomers. The access to ESO observing facilities has been highly beneficial for the scientific community in Italy and has resulted in a large number of outstanding scientific results and publications: 24 out of the 100 most-cited papers from the Paranal Observatory, and 23 out of the 100 most-cited papers from the La Silla Observatory have an Italian astronomer as first author. The first day included also a one-hour discussion forum where representatives of different ESO directorates (Martino Romaniello, Sandro D'Odorico and Bruno Leibundgut) answered questions related to operations, instrumentation and ESO policies.

The second day was opened by a review talk by Sandro D'Odorico on the Italian contribution to ESO instrumentation. The review showed how there has been an increasing involvement of Italian institutes in the past 30 years: from the first contributions to La Silla instrumentation (e.g., SUSI2 and WFI), to the involvement in several first generation (UVES, VIMOS, FLAMES, FINITO and AMBER) and second generation (X-shooter, SPHERE, ESPRESSO) VLT instruments. This positive trend continued in recent years with a strong participation from Italian institutes in E-ELT instrument studies. An important Italian contribution was also in the field of instrument control software, mostly led by the Astronomical Observatory of Trieste, and Paolo Santin gave a review talk on this longstanding and fruitful collaboration with ESO.

One of the aims of the meeting was to discuss the involvement of the Italian astronomical community in future ESO projects. In the framework of the E-ELT there were four talks on instrument studies with significant contributions from Italian institutes: CODEX (Stefano Cristiani), SIMPLE (Roberto Maiolino), MAORY (Paolo Ciliegi) and QuantEYE (Roberto Mignani). The afternoon session of the second day started with a review talk by Giuseppe Bono quantifying the impact of ESO facilities on Italian astronomical research. With a particular focus on the field of stellar astrophysics, it was recognised that access to VLT instruments has had a tremendous impact on the scientific output of the Italian astronomical community. An overview of the VST project was given by Paolo Vettolani and first scientific results based on Guaranteed Observing Time (GTO) presented in two contributed talks (Nicola Rosario Napolitano and Enrichetta Iodice). Paolo Vettolani, INAF Scientific Director, illustrated also the plan for the involvement of INAF in future ESO projects. Finally, the last session of the meeting started with a review talk by Leonardo Testi on ALMA science, followed by several contributed talks highlighting important scientific results obtained with ESO facilities in the field of metal-poor stars (Elisabetta Caffau), globular clusters (Raffaele Gratton) and star formation (Matteo Correnti, Fabrizio Massi, Carlo Felice Manara).

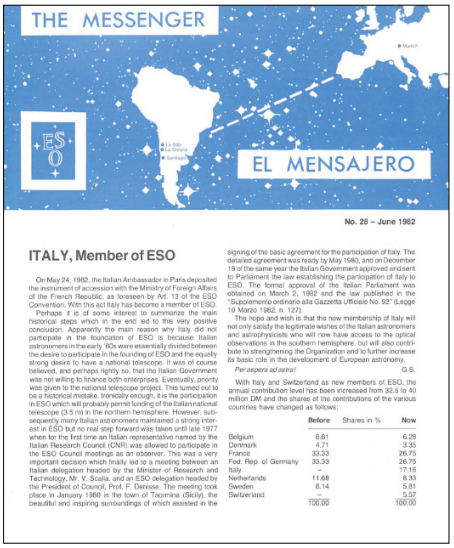
THE MESSENGER

EL MENSAJERO

No. 28 – June 1982

ITALY, Member of ESO

The proceedings of the meeting will be published in the online version[1] of *Supplements of the Memorie della Società Astronomica Italiana* and the presentations are available on the symposium webpage[2].

Acknowledgements

I wish to personally thank the members of the SOC (Magda Arnaboldi, Claudio Cumani, Sandro D'Odorico, Bruno Leibundgut, Alessandro Marconi, Gianni Marconi, Nando Patat, Francesca Primas and Martino Romaniello) and the EWASS2012 LOC (Giuliana Giobbi and Livia Giacomini) for their help in organising this symposium.

Links

[1] Online proceedings to be published: http://sait.oats.inaf.it/Supplementi.htm
[2] Symposium webpage: http://www.eso.org/sci/meetings/2012/ewass2012.html

ESO 50th Anniversary Activities

A number of products are available as part of ESO's 50th anniversary celebrations. More details of the 50th anniversary activities are available on the web page[1].

Books

Claus Madsen's book, *The Jewel on the Mountaintop — The European Southern Observatory through Fifty Years*, has been produced especially for ESO's 50th anniversary. It contains 560 pages of ESO history with stories about the people behind the organisation and 150 historical photos and illustrations[2].

An illustrated 264-page coffee-table book, *Europe to the Stars*, has also been released for the 50th anniversary[3], resplendent with 300 of the best hand-picked images from ESO's large collection of more than 100 000 images from ESO telescopes.

Documentary film

A 63-minute HD blu-ray film is being released in conjunction with *Europe to the Stars*, taking a graphical journey behind the scenes of ESO. The narration is in English and subtitles are available in 20 languages, including some not covered by ESO member states[4]. This DVD will be distributed with the December issue of *The Messenger*.

Exhibition

Awesome Universe is a public exhibition celebrating 50 years of ESO's exploration of the southern sky. It is presented in Europe and around the world. Dozens of venues have already hosted this exhibition, such as the Museu de Ciencias Naturais PUC Minas in Brazil and the Sternwarte Reutlingen, Germany, and many more will do so over the next few months. A full listing of exhibition venues is available[5]. The exhibition catalogue will be available at the venues and may also be downloaded or ordered in hardcopy[6].

Links

[1] 50 years of ESO web page: http://www.eso.org/public/outreach/50years.html
[2] C. Madsen, *The Jewel on the Mountaintop*, Wiley-Wiley-VCH. Price: €49.90 from http://www.wiley-vch.de
[3] G. Schilling, L. L. Christensen, *Europe to the Stars*, Wiley-VCH. Price: €34.90 from http://www.wiley-vch.de
[4] *Europe to the Stars — ESO's first 50 years of exploring the southern sky* (blu-ray DVD) available from http://www.eso.org/public/shop/product/cdrom_europe_stars_bluray/. Price: €5.99, with a reduction for bulk orders.
[5] Listing of all the *Awesome Universe* exhibition venues: http://www.eso.org/public/events/special-evt/awesome-universe/venues.html
[6] *Awesome Universe* exhibition catalogue: http://www.eso.org/public/products/books/eso50_exhibition_catalogue/

Fellows at ESO

Myriam Rodrigues

Like many astronomers, I've had the amazing chance to realise a child's dream: "When I grow up, I want to be an astronomer!"

Everything started 20 years ago, when a family friend working in a condensed matter lab took me into the lab for a couple of days. At the time, condensed matter physicists were excited by a new toy, invented a few years earlier: the scanning tunnelling microscope. I was just seven years old, but I still remember perfectly the huge instrument filling the room and a little TV with some kind of purple spheres on the screen. "These are atoms," they said, "and these are molecules," pointing to another screen close to another huge piece of machinery. I came back to school, totally convinced that I wanted to be a particle physicist and feeling like a new Messiah preaching new-found truth to my schoolmates: "Matter is made of molecules and molecules are made of atoms, how cool is that?!"

I would have probably become a particle physicist if the star-studded night sky at my grandmother's village in Spain had not brought the poetry of astronomy to me. On summer nights, the children used to go to the "movie theatre": a field with a clear horizon. Lying on the warm ground, with a pack of sunflower seeds (the Spanish version of popcorn) in hand, we used to gaze at the sky for hours: the Milky Way, shooting stars, the constellations. The link between these two passions fused a few years later, when I discovered in a kid's science book an incredible invention: spectroscopy! It is possible to make the atoms of stars and nebulae speak! I was definitely decided: I wanted to study galaxies using spectroscopy. Some years ago, I read a quote from Annie Jump Cannon that remains carved in my mind. She expressed beautifully what had been on my mind all those years: "They are not only lines for me; each new spectrum opens the door to a new wonderland. It is as if the distant stars have acquired the gift of speech and started to tell us their physical conditions and constitution."

I studied physics at the Instituto Superior Tecnico at Lisbon. Unfortunately there

Myriam Rodrigues

was no research on distant galaxies at the astronomy department and I started to look for a place to do my undergraduate research project on galaxy evolution. I finally decided to send an email directly to François Hammer of the Paris Observatory to ask for an undergraduate project. A few months later, I left the sunny skies of Lisbon to start a Masters in astrophysics at the Paris Observatory and one year later began a PhD on galaxy evolution in the team of François Hammer.

My main research topic is the study of the interstellar medium and stellar populations of intermediate-mass galaxies at intermediate redshift. This galaxy population appears to be the likeliest progenitor of the present-day spiral galaxies and their properties therefore provide strong constraints on galaxy evolution models. During my PhD I started working on the characterisation of the interstellar medium — metallicity, star formation rate (SFR), gas fraction and presence of star-formation-driven outflows — of distant galaxies from integrated spectroscopy from FORS2 on the Very Large Telescope. I also worked on the estimation of their stellar populations using broadband spectral energy distributions from the ultraviolet to the infrared combined with Lick indices and SFR.

I applied for the ESO-Chile Fellowship moved by the same child's dream. The small child in me was categorical: there is only one place in the world where you can be an astronomer. This place is the Very Large Telescope at the Paranal Observatory, surrounded by the driest desert and the darkest sky in the world.

And here I am, writing this article from my room at the Paranal Residencia. I started my ESO-Chile Fellowship two years ago and I am a support astronomer at Unit Telescopes 1 and 2. I have learnt a lot in these past two years about observation strategies, operations and instrumentation. Being a support astronomer has allowed me to be a more complete astrophysicist by seeing the complete chain of the science. I always find that moment when a new frame appears gradually on the screen fascinating. At this exact moment, the incomprehensible light arising from the sky above our heads is caught in the pixels of the detector and becomes science.

That's it! This is the story of a stubborn daydreamer.

Rubén Sánchez-Janssen

When I was a child, I was all about dinosaurs and outer space. But I guess that, having grown up in the Canary Islands and with an engineer dad who works on infrared astronomical instrumentation, the odds were uneven. I think I made *The Decision* to become an astronomer during a cold February night in the late 80s, after a visit to the IAC80 telescope in Tenerife with my father. Of course I had no clue what the job was really about, but became absolutely fascinated by the quietness of the telescope control room at those after midnight hours. What really touched me, though, was the image of a galaxy that the astronomers had just obtained. That whole big collection of stars existed somewhere out there, and they got to observe it in much greater detail than I could have ever imagined!

So that was it. I pursued that winter night's dream and years later obtained a degree in Astrophysics at the Universidad de La Laguna. This was followed by a PhD at the Instituto de Astrofísica de Canarias on the effects of the environment on the evolution of galaxies in nearby clusters. My enchantment with telescopes not only persisted, but increased with the years of experience. I was therefore excited when I got the opportunity to join ESO as a Fellow in Chile and work at the VLT. I landed in Santiago on a cold and rainy day in mid-

Rubén Sánchez-Janssen

August 2009, a mere month after my PhD defence. I had spent my entire life on a small Atlantic island, and was expecting some rough times ahead and a period of adjustment. It took me less than a week to realise that this new place 9 000 kilometres away was easily to become my second home.

At ESO I've continued my research on galaxy evolution as a function of mass and environment, and established new collaborations with colleagues at Vitacura, at other Chilean institutions and from abroad. During my functional duties as a Fellow I have supported observations at the Paranal Observatory, with a particular commitment to VLT/UT3 and its suite of instruments. More specifically, I've been the VIMOS Fellow during the recent instrument upgrade project, which has allowed me to become involved in the re-commissioning activities together with a great team of engineers and astronomers.

Paranal is a place that everyone should visit at least once. You reach the mining city of Antofagasta and start travelling deeper into the heart of the Atacama Desert. One rock, five rocks, 377 rocks, 6 765 rocks ... and nothing else but rocks. And then, out of the blue, the telescopes' silhouettes out in the distance, like giants in a modern Quixote's wildest delirium. Sunsets from the telescope platform are one of the greatest privileges of observatory life, when the desert is painted in red and shadows play with hills and mountains. Afterwards, from dusk to dawn, it's the time of the astronomer.

I look in my rear view mirror and realise my time at ESO has gone by fast. I have just started the fourth and last year of my Fellowship, and the future awaits. I still like dinosaurs. But above all, I love my job.

Loredana Spezzi

Thinking back, I was around the age of six when I first thought about "knowing more about stars" (the word "astronomy" was not yet part of my vocabulary).

I grew up in Sicily and during my childhood I spent innumerable summer nights sitting with my father on our terrace, trying to fight the heat (typically 40 degrees) and enjoying the view of the Milky Way on a clear night in the south of Italy. During those nights I exhausted him with the never-ending questions that children of that age ask about all the inexplicable details of this world. One of the more recursive ones was: "Dad … tell me about the Universe!" and "Dad…tell me more about the Universe!" I repeated it over and over again and, after a few summers, my father (who studied medicine) had no more news for me and redirected me to illustrated astronomy books. The interest stayed with me and the illustrated books became university textbooks, when at the age of 19 I decided to study physics, foreseeing a future career in astrophysics (and not knowing exactly what was the deal!).

And so the amazing "trip" started: I graduated in Physics and I obtained a PhD in Astrophysics at the University of Catania. After that, I had the privilege to be a postdoctoral fellow in two of the top European institutes for astronomy and space science: first the European Space Agency (ESA-ESTEC at Noordwijk in the Netherlands) and now at ESO-Garching.

The "trip" turned out to be long, not always easy and it is not yet over! I am still looking for the "final destination", but in the meanwhile the little six-year old "me" is quite satisfied. Not only does she "know a lot about stars", but she is even trying to understand how and why they are up there! Translated into the language of an adult astronomer, this means that my current research is devoted to the investigation of the properties of young low-mass stars and brown dwarfs and their circumstellar discs, both in our Milky Way and in the Magellanic Clouds. These studies aim at clarifying the star formation mechanism, its dependency on specific star-forming conditions (such as metallicity, the presence of strong radiation fields, etc.) and, in particular, to identify the specific conditions leading to the formation of planets in circumstellar discs and to assess how frequently they occur. My approach is mainly observational. I make extensive use of both imaging and spectroscopic data from ESO ground-based telescopes and satellite observatories (HST, Spitzer and Herschel).

Of course, the ten years I have spent so far in the astronomy world have given me much more than the pleasure of satisfying the whim of a six-year old girl. I have lost count of the many breathtaking places that I have visited during the several observing trips, conferences, meetings and, even more importantly, I have lost count of the many outstanding people I have met. Some of them have been my mentors, supervisors and advisors, and they have transmitted to me a fund of human and professional experiences that will stay with me until the end of my career. Many others are colleagues, sharing with me the good and the bad of this job. Finally, many of them are people with no connection with astronomy whatsoever. I crossed their paths just because I was following mine, but they have become immeasurable lifetime friends.

Loredana Spezzi

Personnel Movements

Arrivals (1 July–30 September 2012)

Europe	
Baltayne Korompay, Katalin (H)	Paid Associate
García Dabó, César Enrique (E)	Software Engineer
Gray, Peter Murray (AUS)	Project Engineer
McLay, Stewart (GB)	Software Engineer
Nielsen, Bitten (DK)	Student

Chile	
Alvarez, Nicolas (RCH)	Electronics Control Engineer
Müller, Andre (D)	Fellow
Ober, Claudia (RCH)	Contract Officer
Rodriguez, Francisco (RCH)	Press Officer
Vasquez, Sergio (RCH)	Student

Departures (1 July–30 September 2012)

Europe	
Arbogast, Dina (D)	Adminstrative Assistant
Bressert, Eli (USA)	Student
Daemgen, Sebastian (D)	Student
Goddi, Ciriaco (I)	Fellow
González Gutiérrez, Juan Esteban (RCH)	Fellow
Heckel, Isabell (D)	Adminstrative Assistant
Julbe Lopez, Francesco (E)	Software Engineer
Kempf, Andreas (D)	Electronics Engineer
Krajnovic, Davor (HR)	Fellow
Kümmel, Martin (D)	Scientific Data Analyst
Lagadec, Eric (F)	Fellow
Moerchen, Margaret (USA)	Fellow
Kissler-Patig, Markus (D)	E-ELT Project Scientist
Smiljanic, Rodolfo (BR)	Fellow
Wieland, Gerd (D)	Senior Contract Officer
Yaitskova, Nataliya (RUS)	Applied Scientist

Chile	
Hills, Richard (GB)	ALMA Project Scientist
Lucas, Robert (F)	Astronomer ALMA Commissioning
Manjarrez, Guillermo (MEX)	Student
Parra, Ricardo Andrés (RCH)	Mechanical Engineer
Rawlings, Mark (GB)	Operations Staff Astronomer
Vanderbeke, Joachim (B)	Student

Construction of the extension to ESO Headquarters was begun at the beginning of this year and has now reached the second floor, as shown in this recent image. More details of the building concept can be found in a *Messenger* article (135, p. 2) and in Release eso1215.

ESO, the European Southern Observatory, is the foremost intergovernmental astronomy organisation in Europe. It is supported by 15 countries: Austria, Belgium, Brazil, the Czech Republic, Denmark, France, Finland, Germany, Italy, the Netherlands, Portugal, Spain, Sweden, Switzerland and the United Kingdom. ESO's programme is focused on the design, construction and operation of powerful ground-based observing facilities. ESO operates three observatories in Chile: at La Silla, at Paranal, site of the Very Large Telescope, and at Llano de Chajnantor. ESO is the European partner in the Atacama Large Millimeter/submillimeter Array (ALMA) under construction at Chajnantor. Currently ESO is engaged in the design of the European Extremely Large Telescope.

The Messenger is published, in hard-copy and electronic form, four times a year: in March, June, September and December. ESO produces and distributes a wide variety of media connected to its activities. For further information, including postal subscription to The Messenger, contact the ESO education and Public Outreach Department at the following address:

ESO Headquarters
Karl-Schwarzschild-Straße 2
85748 Garching bei München
Germany
Phone +49 89 320 06-0
information@eso.org

The Messenger:
Editor: Jeremy R. Walsh;
Design, Layout, Production:
Jutta Boxheimer;
Layout, Typesetting: Mafalda Martins;
Graphics: Roberto Duque
www.eso.org/messenger/

Printed by G. Peschke Druckerei GmbH, Schatzbogen 35, 81805 München, Germany

ISSN 0722-6691

Contents

Front cover: A remarkable early observation by the Atacama Large Millimeter/submillimeter Array (ALMA) taken in Cycle 0 reveals a spiral structure in the molecular material around the asymptotic giant branch (AGB) star R Sculptoris. While shells of cool gas have been detected around AGB stars before, the additional presence of a spiral feature, detected in CO(J=3-2) emission at 345 GHz with ALMA (Band 7) interior to the main shell, is revealed for the first time (shown here in the emission velocity slice around the stellar velocity). The spiral pattern can be explained by a binary companion orbiting the central star with a period of about 350 years and winding up the escape of the wind from the AGB star. This investigation was led by Matthias Maercker, ESO Fellow at the ALMA Regional Centre Bonn node, and more details can be found in Release 1239.